



UNIVERSITY OF TWENTE.

Faculty of Engineering Technology

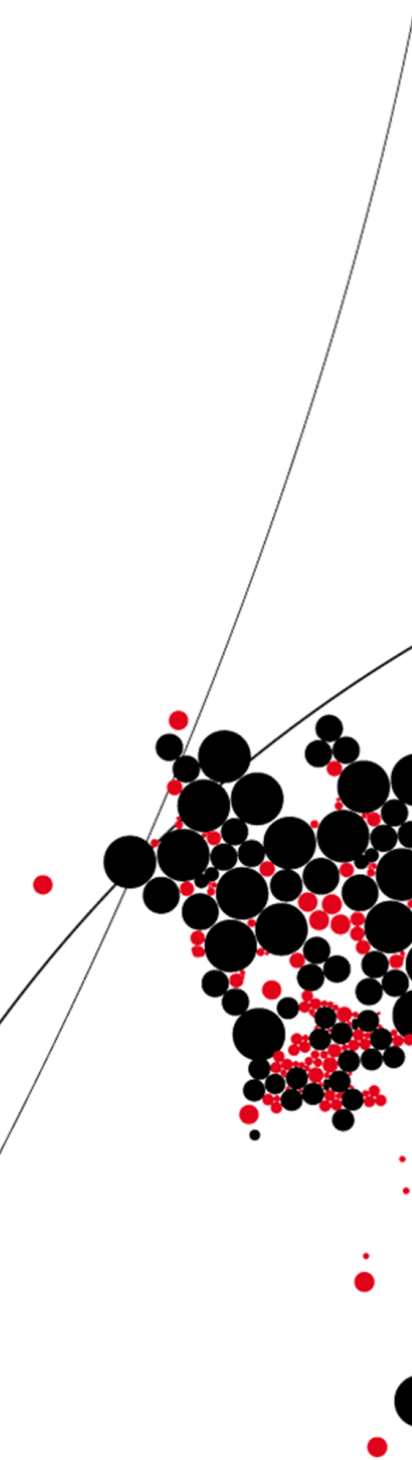
electrostatics for mobile glass cleaning robots

master thesis

E.G. Nethe, *s2122960*

Master Mechanical Engineering

Thesis from June 2020 to February 2021 (40EC)
February 2021



Supervisor:

Prof.Dr.Ir. Matthijn B. de Rooij

University of Twente
Faculty of Engineering Technology
Horst Complex N106
P.O. Box 217
7500 AE Enschede
The Netherlands

Co-Supervisor:

Dr. Liangyong Chu

University of Twente
Faculty of Engineering Technology
Horst Complex N114
P.O. Box 217
7500 AE Enschede
The Netherlands

Contents

1	Summary	4
2	Introduction	6
2.1	The background	7
2.2	Technical state of electrostatic actuators	10
2.3	Surface charges and cleaning	14
3	Principles of electrostatics	15
3.1	Mathematical treatment of static electric charges	15
3.1.1	Coulomb's law	15
3.1.2	Energy and forces in a parallel plate capacitor	17
3.1.3	Attractive forces on dipoles	20
3.1.4	Forces in parallel capacitors with multiple dielectric layers	23
3.2	Material properties for electrostatics	29
4	Categorizing the physically available options	33
4.1	Electrophoretic attraction (parallel capacitor)	33
4.2	Dielectrophoretic attraction	34
4.3	Residue charge electrophoretic attraction	36
5	The effect of the attraction gap on the achievable force	40
5.1	Procedure	40
5.2	Results and conclusions regarding cleaning robots	42
6	Design criteria for an in-contact solution	44
6.1	Summarized guidelines	44
6.2	Risks for in-contact electroadhesives on cleaning robots	45
6.3	An approach to optimizing an interdigital electrode adhesive for glass	46
6.4	Applying in-contact adhesion to cleaning robots	49
7	Design criteria for attraction over an air gap	51
7.1	Choice of adhesion technology	51
7.2	Aspects of residual surface charge	52
8	Plasma aided surface cleaning	55
8.1	The combination of surface attraction and surface cleaning	55
8.2	Plasma treatment of surfaces in general	56

8.3	Testing plasma aided cleaning	56
8.4	Results from plasma aided cleaning test	60
9	Final conclusions	63
9.1	Usability of the attraction forces for cleaning robots	63
9.2	Usability of surface charge treatment for the cleaning process	64
9.3	Ideas and recommendations for further research	65
A	Details of experiments on attraction forces over an air gap	67
A.1	Build of experimental setup to test non-insulated and insulated electrodes	68
A.2	Analysis of the conducted experiments and resulting forces	70
A.2.1	First experiment: Non-insulated electrodes	71
A.2.2	Second experiment: Semi-insulated electrodes	73
A.2.3	Third experiment: Fully-insulated electrodes	74
A.2.4	Comparison of experimental results with simulations	78
A.2.5	Fourth experiment: In-contact, insulated electrodes	82
A.3	Summary of results	86
B	Details of research on in-contact electroadhesives	87
B.1	Current state of the art of dielectric attraction	87
B.2	Distance dependency of dielectric attraction forces	92
B.3	Forces achieved with in-contact dielectric attraction	93
C	Simulation of known electroadhesives	95
C.1	Simulation of electroadhesive from reference [17]	95
C.2	Simulation of electroadhesive from [22]	98
D	Optimizing an in-contact electroadhesive for glass	100
D.1	Optimizing the electric field distribution	100
D.2	Prohibiting breakdown in the vicinity	103
E	Experiments for residue surface charge attraction	105
E.1	Surface charging of glass	105
E.2	Attraction forces on a contaminated glass surface	107
F	Detailed steps taken for plasma aided cleaning test	109
F.1	Method of preparing contaminated samples	109
F.2	Specifying contaminated and non-contaminated states	111
F.3	Characterization of piezobrush PZ3 plasma treatment	114

G Mathematical derivation and examples of increased gradeability 115

1 Summary

This thesis brings together the field of cleaning robots for glass-roofs, solar-arrays and windows with the field of electrostatics. Primarily it is investigated how electrostatic attraction forces can be applied to increase the traction of cleaning robots on the slanted glass surfaces that they work on. In the course of the research, as an additional asset for this technology, the effect of the residual surface charge created by the use of cold plasma on the cleaning process is considered and looked into in a further section.

First the reader is introduced to the functioning of these cleaning robots and the current concepts of electrostatic actuators. Next the necessary theory of electrostatics and electrostatic forces is treated, shortly delivering the mathematical background and an understanding for the effect of electrostatic attraction.

Using this knowledge the physically available options are worked out. This delivers three independent designs that open up two design directions that are useful for this project. Both are treated in separate sections thereafter. The first one concentrates on an in-contact adhesion solution while the other looks into enabling an attraction force over a distance of multiple millimeters.

Before these two are treated in detail a series of experiments is conducted and backed by simulations in COMSOL to evaluate the impact of the surrounding air with and without a larger air-filled gap.

Then the first option that concentrates on an in-contact electroadhesive solution is treated in detail. The evaluation is based on the results that have been acquired and published in literature and is supplemented by simulations. A design optimized for the attraction of glass is developed. After that the second option, which is to generate an attraction force over a gap, is investigated, since such a design is superior in regard to multiple technical aspects for cleaning robots, as is further explained in the introduction. This is done in a more experimental approach, as not much work on this topic was found. A suggestion for a demonstration setup for this design is described.

Both options are found to have their benefits and their disadvantages. In short the better researched in-contact adhesion - in contrast to the non-contact attraction - is found to inherently be capable of producing higher attraction forces that are at a useful level for these robots, while it is far more vulnerable to contamination and wetting, which are both involved in the cleaning process on glass roofs and solar arrays. The restrictively low limit to the attraction forces over an air-filled gap may explain the limited research on this topic.

Apart from the attraction effect of electrostatic charges, in a further section their

effect on the cleaning process is also analysed. For this, contaminated samples are prepared to mimic the contaminated surface of glass-roofs and solar-arrays. The ease of removing this contamination with and without being treated with charges is then compared.

In total this report gives insight into the field of electrostatics and electrostatic attraction devices specializing on applying these to the described cleaning robots or other applications where temporary adhesion is required in combination with a cleaning operation.

2 Introduction

A growing industry is that of industrial glass-roof and solar-array cleaning robots. Also smaller versions are coming onto the market for cleaning windows in the private sector. These machines all have in common that they must maintain secure traction on the smooth and contaminated slanted surface that they are cleaning.

There are multiple ways to approach this, as is outlined in the next section. This thesis looks into utilizing electrostatic forces to increase the traction.

The field of electrostatics is a broad one and according to the book "Electrostatics and its applications" by A.D. Moore [2] it has a history dating all the way back to at least 600 B.C., when the Greeks took note of an electrostatic effect: They observed that amber when rubbed could attract small and light objects. They had found the triboelectric effect, as it is called today. Nevertheless in its details the field of electrostatics seems to remain a poorly understood phenomenon. Remarks on this are found in many places, such as "[...] many of the phenomena [...] are still not adequately understood!" in [2] from nearly fifty years ago and - even though a lot has happened since then - one still comes across formulations such as: "Currently, there is still a lack of comprehensive and in-depth understanding of the EA [electroadhesive] phenomenon", in "Electroadhesion technologies for robotics: A comprehensive review" by J. Guo et al. [15], which is a recent paper from 2020, in the context of advanced modelling for example.

A sub-area in the field of electrostatics that has been described extensively, however, is the principle of electrostatic forces, that is the attraction and repulsion between charged particles of any kind. The basis of this is defined by Coulomb's Law, also termed the second law of electrostatics, that is named after its discoverer Charles-Augustin de Coulomb.

In this thesis many fragments of experimental insight from literature and from own experiments backed by the theory of electrostatic attraction are brought together to discuss to which extent this technology holds possibilities for a section in industry in which electrostatics have to my knowledge not yet been applied in any form. As I have spent a year working for a leading German company in this industry,[37] I have been able to gain some insight in the daily practices and problems that occur. The following two sections describe the problem in detail and the current state of electrostatic technology that is available for this purpose. In a final section the idea of surface-charge aided cleaning is introduced.

2.1 The background

The window-glass and solar-array cleaning robots are mobile, remotely controlled machines that use some form of drive such as caterpillar tracks or wheels to maneuver across the surface that is to be cleaned. On industrial machines the surface is typically scrubbed using rotating brushes and often clear water, while smaller window cleaners try to achieve a reasonable cleaning effect even without using water. An example of an industrial cleaning machine is depicted in figure 1. These machines are seldom designed specifically for a single type of roof or solar array. On the contrary the developers are trying to make them as versatile as possible for their products to reach a broad range of customers.



Figure 1: An example of a roof and solar cleaning robot

A major limit to the use of these machines is the maximum slope that they are able to safely maneuver on. Typically the maximum allowed slope is 25° . In regions further from the equator such as central and northern Europe, however, solar arrays are often placed at steeper angles. It is therefore of interest to further improve the gradeability of these robots.

A lot of effort has been and is being put into increasing the traction of the drive system on the contaminated, often dusty and wetted surface. While the rotating brushes do create a slight lift and backward force during operation, the major parameter inducing slip is simply the tangential force due to the angle of the gravitational vector of the robots mass to that of the slanted surface as is shown in figure 2.

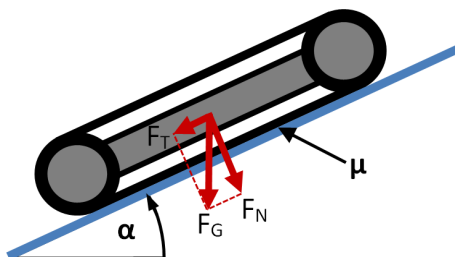


Figure 2: Schematic of a caterpillar driven robot on a slanted surface

Apart from optimizing the surface contact to achieve a higher and more reliable traction by improving the friction coefficient μ , it would also be advantageous to increase the normal force on the machine. At this point the idea of utilizing some form of attractive force comes in. On small machines, that are designed to only clean single window panes, vacuum has proven to be a viable solution that even enables them to work on vertical surfaces. For larger industrial machines approaches along these lines have been made, however with marginal success on the market. As larger surfaces are generally not continuous due to seams, frames and gaps between panels, solutions in the form of suction cups have proven to become very complex and therefore expensive, while being unreliable and energy consuming. Magnetic attraction would only be an option for ferromagnetic roof materials which undoubtedly exist, but only make up a minority of the cases and do not include solar arrays.

A new approach in this field is to utilize electrostatic forces. Electrostatic attraction is versatile as it appears in context with conductors and any dielectric insulating material such as plastics and - more relevant in this case - glass. In relatively dry air electrostatic effects that naturally occur such as standing hair, clinging foils or unpleasant electric shocks are perceptible to our senses and therefore commonly known. These "everyday" electrostatic effects are most often due to the triboelectric effect, which is the build up of surface charge on insulating materials due to friction. However for electrostatic attraction forces to become interesting for this endeavor they must be brought to a far higher level. This will for example require inducing higher charge densities.

Electrostatic actuators have been developed and successfully demonstrated in experiments. Examples are given in the next section. The previous and current development of electrostatic actuators concentrates on thin flexible foils that are brought into contact with the attracted surface. These foils then electrostatically adhere to the surface and generate tangential traction via the friction coefficient between the foil and the attracted surface. Experiments with light weight wall climbing robots on tracks have implemented these foils on the robots' drive tracks. However this industry of larger cleaning robots requires mechanically robust machines that are suited for outdoor use. Electrostatic foils on the driven caterpillar tracks with a form of high voltage electric input would become difficult to design in a robust way and likely complex to manufacture. As of today these robots are not mass produced and therefore the production technique of each component must be kept simple to be feasible. These requirements lead to the favouring of a fixed (non-moving) and solid (non-flexible) module that can be placed on the underside of the robots chassis and that could induce an attractive

force from a slight distance, over the more common approach of flexible in-contact electrodes incorporated within the drive system.

To later be able to evaluate the potential of this idea under set circumstances a few parameters will be chosen in the order of what is typical for this type of machine. The following measurements are also depicted on the left hand side of figure 3. Newer versions of industrial cleaning machines typically have a mass of around $50kg$ (e.g. the upcoming version of the black SOLAR facelift).[36] The two driven caterpillar tracks can be around $500mm$ in length and $100mm$ wide. The usable underbody area where an attraction device could be placed is around $400mm$ by $400mm$. The aim for the ground clearance of the underbody panel is set to $10mm$, as it must be able to pass over small irregularities such as window-pane or panel frames as well as angular differences between panels. At the lower end of the broad and growing range of glass cleaning robots are the devices that are designed to clean one glass pane at a time (e.g. EVOVACS W830).[13] These gadgets only weigh around $1kg$ and span an area of about $200mm$ by $200mm$ while they do not have the requirement to have a certain ground clearance.

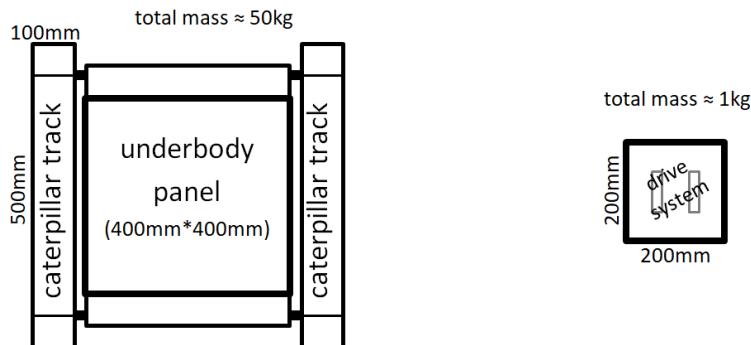


Figure 3: Underside schematic of: (left) an industrial-size caterpillar driven cleaning robot showing the area available for different forms of underside electrostatic attraction mechanisms, (right) small scale window pane cleaning robot

As a third option apart from either inducing an attractive force from a slight distance via a solid panel underneath the robot, or incorporating the electroadhesive within the drive tracks for contact adhesion, a solid panel beneath the robot that is designed for contact adhesion could be deployed, i.e. brought into contact with the glass surface, and powered up whenever the robot begins to slip. This third option solely functions as a mechanism to increase working safety on steeply sloped surfaces, rather than a technology to increase the gradeability of these robots.

The final objective of this thesis is to evaluate in how far the generated attraction

force stands in a relevant ratio to the inevitable forces acting on the robot. For this assessment it shall suffice to compare the generated attraction force to the gravitational forces induced by the robots mass. Other forces such as those caused by the brush, the water supply hose or vehicle acceleration will not be considered in this feasibility analysis.

2.2 Technical state of electrostatic actuators

The foundation of the idea that the use of electrostatic forces could lead to usable results for these industrial robots lies in published experiments, in which small robots use electroadhesive foils to cling to vertical walls or windows and even drive up them. An example is a caterpillar driven device demonstrated by H. Prahlad et al. and published in "Electroadhesive robots — wall climbing robots enabled by a novel, robust, and electrically controllable adhesion technology" [11] in 2008. Commercial electrostatic climbing robots were not found.

Electroadhesives make use of the mutual attraction of opposite charges. Applying a potential difference to a set of two adjacent conductors will result in a displacement of charges and lead to a certain level of charge separation. These separated poles generate strong electric fields in their vicinity that effect objects of both conducting and nonconducting materials, resulting in electrostatic forces between these. Oppositely charged objects will attract each other, mutually charged objects repel each other. The force of a charged object towards neutrally charged bodies is weaker but generally not equal to zero and most often attractive.¹ This is due to the attraction of opposite charges and their consequential displacement within the effected material, which - even though neutral in total - consists of both positively and negatively charged particles. These electrophoretic (in conductors) and dielectrophoretic (in dielectric insulators) effects will be treated in detail in the following sections.

Electroadhesives have been a subject of interest for some time as they feature multiple advantages compared to other adhesion technologies such as vacuum, magnetism, dry adhesion (gecko feet) or micro spines.[19][11] The advantages range from its versatile functioning on very different materials including conductors as well as insulators over being directly electrically controllable while having a low energy consumption all the way to its mechanical simplicity which is favourable for lite-weight applications and cost effectiveness. This has led to numerous developments for production facilities, robotics and some experiments for space industry. References to a number of

¹An exception is the apoelectric behaviour that can occur with strongly polarized particles under very specific conditions and leads to a repulsive force. This effect is briefly explained in [12], p.156 and [2], p. 349, but will not further be treated here because of its irrelevance.

these developments can be found in "Electroadhesion Technologies for Robotics: A Comprehensive Review" by J. Guo et al. [15].

However, the effect of electroadhesion also has its drawbacks. It yields comparatively low forces and is a complex phenomenon with tens of variables effecting the resulting forces (precisely 33 variables according to [16]). The many dependencies make it more challenging to optimize and also can have a problematic effect on the reliability if an influencing parameter has not properly been taken into account or understood. For example in the above cited paper by H. Prahlad et al. [11] it is mentioned that good electroadhesive forces could also be achieved on damp surfaces, while in the paper by J. Guo et al. [15] it is emphasized that an increase of humidity can reduce the adhesive force and in one of the conducted experiments (in appendix A.2.5) it is found that actual fluid water in the contact region can fully eliminate the electroadhesive force. Also an optimization may depend on a varying parameter, which as so often with any technology results in a certain design being more appropriate only for very specific circumstances. An example for this is given in the following paragraphs. As long as the relevant parameters are known and their effects understood they can be taken into account for the electroadhesive design.

Reported electroadhesives generally have a common basic setup. They feature sets of thin electrodes that are arranged alongside each other in a plane. Each of these electrodes is alternatingly connected to one of the two outlets of a high voltage supply. The voltage used is typically in the order of multiple kilovolts. All conducting surfaces are covered by highly breakdown resistant insulator-material to prohibit grounding or short circuiting. The arrangement that is essentially a thin electroadhesive foil is shown in figure 4.

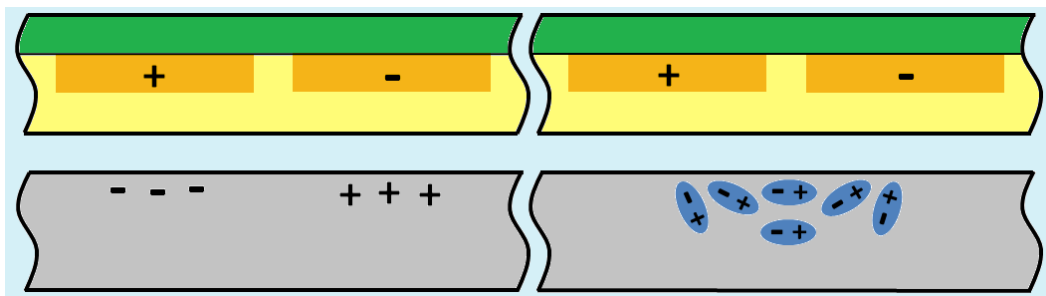


Figure 4: Cross-sectional schematic of a basic electroadhesive element consisting of electrodes (orange), carrier material (green) and insulator coating (yellow) attracting a substrate (grey) that can be either a conductor (left) or dielectric insulator (right) over an air gap (light blue)

An example for the optimization of such a device for certain circumstances is the

electrode pattern. J. Guo et al. published a paper in which a fairly detailed comparison of different patterns is presented [17] that will be treated later on. A few basic patterns are shown schematically in figure 5.

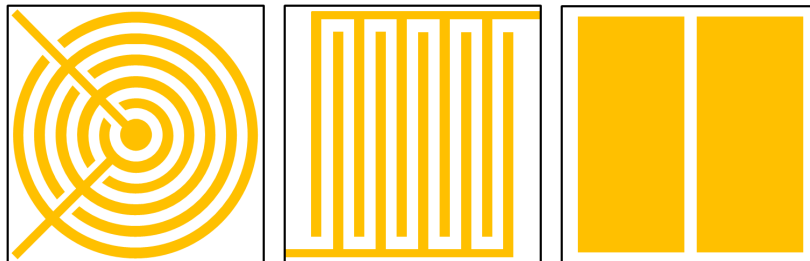


Figure 5: Schematics of a few possible electrode patterns for electroadhesion foils: concentric rings with alternating polarity, parallel digits with alternating polarity, simple two-plate format

As an example the very simple design on the right hand side of figure 5, that utilizes only two large electrode plates, will yield satisfactory results on a conducting substrate. On a dielectric material, however, it will be significantly inferior to the other designs where narrow electrodes become necessary. This topic - concerning electrode patterns and widths - will be treated in more detail in appendix B.1.

A few examples of how these foils have been utilised are displayed schematically in figure 6. The left hand design represents a simple wall-climbing robot design. As referenced above, an example for such a device is the caterpillar track design by H. Prahlad et al.[11]. The middle schematic resembles a grabber for pick and place tasks that also utilises flexible electroadhesive foils. An example for such a device is the versatile soft gripper developed by J. Shintake et al. [22]. Further designs are utilized in industry for placing technical textiles or silicon wafers with designs similar to the one depicted on the right hand side.

As mentioned above these electroadhesive foils are generally designed to function in close proximity (contact) with the surface that is to be attracted. However there are also examples where electrostatic forces are utilised over a distance. Experimental setups include electrostatic motors. In contrast to electromagnetic motors these rely on electrostatic forces and are therefor driven on comparatively high voltages. Among others an advanced approach to such a motor from the 1970s is displayed in [2], p. 144. It is a corona type electrostatic motor, meaning that it relies on a corona discharge from sharp-edged electrodes to charge the rotors surface. The electrostatic forces between the charged rotor surface and the stator plates let it rotate. At a length and diameter of approximately 5 inches and a supply voltage of 6kV it can produce 0.1hp

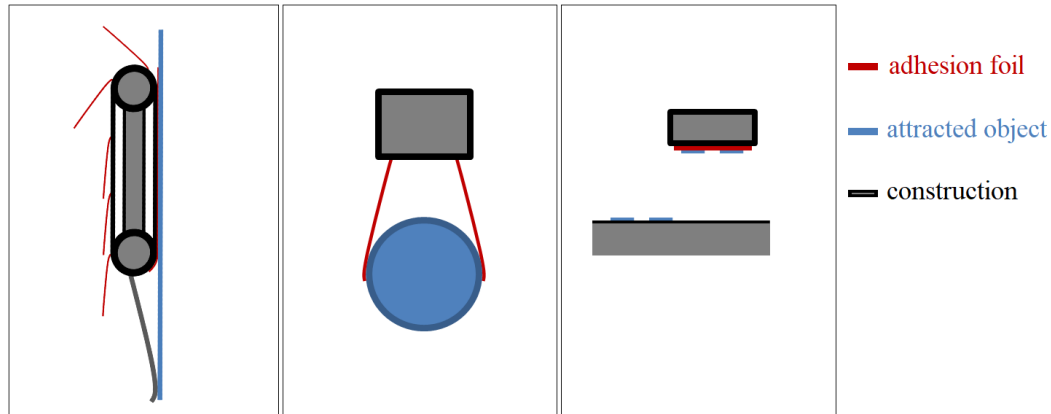


Figure 6: Schematics of existing applications of electroadhesion foils: (left) caterpillar driven climbing robot with a supporting tail to reduce peel-off torque, (middle) flexible grabber, (right) wafer pick and place head, adhesion foils in red

(around 75W) of mechanical power. The relatively low power density of such setups has prevented them from becoming commercially interesting.

An industrially used application of electric field forces over larger distances is that of particle separation and particle dispersion. Here electric charges are deposited on the surface of particles, such as ground minerals or paint droplets and an electric field is applied to direct their motion. A number of these applications are described in "Electrostatics and its applications" by A.D. Moore.

In how far these principles that enable the attraction over a larger separation distance can be applied to this project is analysed in section 7.

Concerning the availability of electroadhesive equipment the numerous reported uses seem to be deceiving. Electrostatic foils have - despite the many designs in published experiments and the apparent use in industry by companies claiming the implementation of electroadhesion in their material handling processes - not been found to be commercially available as such.

Other electrostatic equipment does exist on the market, such as electrostatic surface charging equipment utilizing corona discharge for charging or neutralizing surfaces in production processes as well as plasma generators that are used to partially ionize air and other gases for surface treatment and surface activation. Also high-voltage supply units are available with various characteristics.

Due to the above described circumstances any electrostatic adhesion device implemented in this project will have to be custom designed and produced for testing.

2.3 Surface charges and cleaning

The use of high voltages and resulting high electric fields for electroadhesion brings forth another interesting aspect when applied to the field of cleaning robots: It could lead to increased wettability induced by residing surface charges.

The process of treating surfaces with charges for increased wettability is a well established technique that is used to increase bonding of paints, adhesives and other surface coatings.[33] For high-level surface activation surfaces are exposed to for example corona discharge, ion beams, electron beams, ultraviolet radiation or a source of plasma.[27]

Both corona discharge and plasma treatment have the potential to be utilized for this electrostatic attraction application, specifically for the option of generating forces from a distance, as will be discussed in the respective section 4.3. But also exposing an insulating surface to high electric field intensities within air, which is just as much the case for in-contact dielectric electroadhesives, will lead to a more or less pronounced accumulation of charged particles on it (see section 5).

Such a surface charge treatment decreases the contact angle of droplets on the surface by increasing the surface energy and therefor helps to properly moisten the entire surface.

Charged particles that are applied at a sufficient energy level, such as by the surface charging techniques mentioned above, have the potential to break up organic bonds and therefor can directly replace chemical cleaning agents.[1] For slightly contaminated surfaces such a treatment with charged particles can even yield microscopically thorough cleaning by dispersing contaminating organic matter all together, giving this technique the term plasma cleaning.

In section 8 this appealing prospect for electrostatics on cleaning robots is reviewed.

3 Principles of electrostatics

This section captures the basic theoretical knowledge of the electrostatics needed for this project. These formulations will be used in the following sections to reason on the possibilities that electrostatics hold for generating attractive forces on the proposed setups.

3.1 Mathematical treatment of static electric charges

3.1.1 Coulomb's law

As long as electric charges are dealt with in a static manner their mathematical description becomes relatively straight forward.² The analysis conducted within this project largely concentrates on this static situation, as in the case of the electrically adhering module underneath a cleaning robot, during operation a quasi static setting is assumed to be realistic. The motion across the surface - continuously replacing the attracted area underneath the robot - will occur in the order of seconds, whereas within conductors charge flows freely and thus is applied within a time scale many orders smaller. In the case of charge buildup on the surface of insulators or the transport of charges through very high resistances, the effect of changes over time become of interest.

The basis of electrostatics is Coulomb's law, which although being a purely experimentally determined relationship is treated as if it were a proven result of mathematical derivation.³ The basic equation concerning the relation that was found by Coulomb between two charges Q_1 and Q_2 is:

$$F = \frac{Q_1 Q_2}{4\pi\epsilon r^2} [N] \quad (1)$$

where F is the force developed between these two charges, with r being the distance between the two charges and ϵ the permittivity of the space that the charges are located in. In empty space $\epsilon = \epsilon_0 = 8.85 \cdot 10^{-12} F/m$. In general epsilon is defined as $\epsilon = \epsilon_0 * \epsilon_r$, with ϵ_r being the unitless relative permittivity also termed dielectric constant of the material filling the space.

²The more general approach is based on Maxwell's equations. This set of differential equations is the basis for electromagnetic models such as those implemented in the simulation tool COMSOL, which will be used further on and for the solution of time dependant electromagnetic problems. Details on the formulation of these equations can be found for example in "Introduction to electrodynamics" by D.J. Griffiths. [6]

³This realization was stated by C.D. Hendricks in "Electrostatics and its applications".[2] Also the following derivations in this section are largely based on this reference.

To correctly describe the force-vector \mathbf{F} the equation can be extended to:

$$\mathbf{F} = \frac{Q_1 Q_2}{4\pi\epsilon r^3} \mathbf{r} \quad [N] \quad (2)$$

with \mathbf{r} being the vector distance between the charges.

Presumably this relation is the source of misconception to some extent, that electrostatic forces necessarily depend in a quadratic manner on the distance between two objects. While this is true for the relation between two point charges, for other geometries this is not the case. Clearly the geometry of two macroscopic objects will have a large influence on the overall resultant force between them. Integrating over this geometry leads to less distance sensitivity. This applies to surface force relations in general.

An easy to picture case for example are two oppositely charged, concentric, spherical shells, which - even though the charges are separated by a distance that is equal to the difference in radius of the two spheres - will have no resulting force on one another, as the overall electrostatic pull is equal in all directions. The case of two plane parallel surfaces, as it will be needed for this project, is shown in detail further on.

From the relation found in equation 2 the electric field \mathbf{E} that is generated by a single point charge Q at a distance r can be derived:

$$\mathbf{E} = \frac{Q}{4\pi\epsilon r^3} \mathbf{r} \quad [N/C] \text{ or } [V/m] \quad (3)$$

In the case of multiple point charges, the resulting field is the vectorial sum of the electric fields of all individuals:

$$\mathbf{E} = \mathbf{E}_1 + \mathbf{E}_2 + \mathbf{E}_3 + \dots + \mathbf{E}_n \quad (4)$$

and the force on a charge Q in an electric field \mathbf{E} is then:

$$\mathbf{F} = Q\mathbf{E} \quad (5)$$

However in this case the charge Q must be sufficiently small to not significantly effect the surrounding electric field \mathbf{E} .

To be able to separate opposite charges, or equivalently to move a charge against the force acting upon it in an electric field, an electric potential is required. If a certain potential V results in the transport of charge Q from one arbitrary object to another arbitrary object, resulting in one object holding the charge $+Q$ and the other object holding the charge $-Q$, then doubling the potential will result in twice the charge being transported. This is a simple linear relation that can be expressed as:

$$Q = CV \quad [C] \quad (6)$$

with C being the constant of proportionality. This constant depends on the geometry of the specific arrangement and on the materials that surround the charged objects. It is called the capacitance.

For certain symmetrical geometries it is possible to find analytical solutions for the capacitance using Gauss's law. An example for such a configuration is the above mentioned pair of concentric spherical shells on which the computation of the complete surface integral is simple.

Another analytically computable configuration is that of two plane parallel plates in the case that they are very large in area compared to their distance to one another. In this case symmetry and Gauss's law are used to argue that only the volume in between the two parallel plates need be taken into consideration. This setup is also known as a parallel capacitor and it is assumed that the electric field in between the two plates is uniform in direction and magnitude.[2] The solution to its capacity is then found to be:

$$C_{parallel_capacitor} = \frac{\epsilon A}{x} [F] \quad (7)$$

with A being the surface area of one plate and x the distance between the two plates.

3.1.2 Energy and forces in a parallel plate capacitor

The two oppositely charged plates of a parallel capacitor will attract each other. The force that is generated can be found via an energy balance. For this it is assumed that the system is conservative, i.e. that it does not contain any dissipative components. If the distance between the plates were to be altered, while a force is acting upon them, this would require a certain amount of energy to be transferred out of or into the system.

The electrical field that generates the force also is a source of stored energy. The portion of energy dw required to transfer the charge dQ from one plate to the other against a potential V can be expressed as:

$$dw_{el} = V dQ \quad (8)$$

If the charging process starts at zero charge and therefor at zero potential, then the energy required to charge the capacitor to a certain potential is:

$$w_{el} = \int_0^Q v dQ \quad (9)$$

while it is known that $V = Q/C$ (derived from equation 6), so that

$$w_{el} = \int_0^Q \frac{Q}{C} dQ = \frac{1}{2} \frac{Q^2}{C} [J] \quad (10)$$

This energy is termed the energy stored in the electric field.

Looking back at the capacitor with variable plate separation-distance, the energy stored in the electric field must increase if the plates are pulled apart (positive x direction) as work is put into the system. If the capacitor plates are isolated, this will result in an increase in potential. If the plates are connected to a constant potential source, it will result in a transfer of charge against the potential, thus resulting in an energy output from the system.

A small amount of mechanical work dw_{mech} is put into the system by a force displacing a plate by a distance dx , thus the amount of mechanical work equates to⁴:

$$dw_{mech} = F dx \quad (11)$$

In the case of isolated pre-charged plates the work that is mechanically put into the system by an external source is stored in the electric field, so that the energy balance is:

$$dw_{mech} + dw_{el} = 0 \quad \text{or} \quad dw_{mech} = -dw_{el} \quad (12)$$

which by inserting equation 11 becomes:

$$F dx = -dw_{el} \quad (13)$$

which can be rewritten to:

$$F = -\frac{dw_{el}}{dx} \quad (14)$$

As w_{el} can also depend on further variables other than x , the correct syntax in this case would be:

$$F = -\frac{\partial w_{el}}{\partial x} \quad (15)$$

The expression for the energy w_{el} stored in the plate system is given by equation 10, which by substituting C with equation 7 reads:

$$w_{el} = \frac{1}{2} \frac{Q^2 x}{\epsilon A} \quad (16)$$

This can now be used to substitute w_{el} in equation 15 to become:[2]

$$F = -\frac{\partial}{\partial x} \left(\frac{1}{2} \frac{Q^2 x}{\epsilon A} \right) = -\frac{1}{2} \frac{Q^2}{\epsilon A} [N] \quad (17)$$

This shows impressively how two plates with a given charge will generate a constant attractive force to one another, independently of the distance between the plates, as

⁴In this section all variables are represented as simple scalars rather than vectors, because field lines, motion and forces are all in parallel with the coordinate axis x .

long as the geometry supports the previously made assumption that the electric field is uniform in direction and magnitude.

The plate charge Q is typically applied via a given voltage supply. If for convenience it is favoured to have the expression for the force depend directly on the applied voltage, Q can be substituted by CV (equation 6) in which C can be replaced using the relation from equation 7 resulting in:

$$F = -\frac{1}{2} \frac{C^2 V^2}{\epsilon A} = -\frac{1}{2} \frac{\epsilon A V^2}{x^2} \quad (18)$$

or

$$F_{attr.} = \frac{1}{2} \frac{\epsilon A V^2}{x^2} \quad (19)$$

if we chose to omit the negative sign, because we will only be working with attractive forces in this context.

Now it may seem as though the force on the plates of a parallel capacitor does depend on the distance after all, even quadratically. It is however for parallel capacitors the equation 17, which is formulated with respect to the charge Q and is not distance dependent, that is the equivalent to equation 1 for point charges, which inevitably develop a distance dependent force.

If the supply voltage in equation 19 were to be kept constant on a parallel capacitor, while the distance between the plates is increased, the force would in fact drop quadratically. At the same time, the work put into the system mechanically would be transferred back out of the system electrically by a backflow of charge and therefore a decrease of charge on the plates.

Summarizing, equations 17 and 19 give the basic relation between the applied electrical charge and voltage to the developed electrostatic attraction force for two oppositely charged parallel planes of large extent compared to their separation distance.

The crucial factor here is the applied voltage. The question is, which voltage can be applied. Increasing it seems very 'attractive', as it would quadratically increase the attractive force at a given plate separation. However, there are material-based limits to this. The most known visible effect due to this limit would be electrical flashover such as lightning. Details on the properties of a few relevant materials are given in section 3.2. Basically though, for a given homogeneous material the maximum voltage, before a flashover occurs through it, scales linearly with its thickness. For the parallel capacitor that means the maximum applicable voltage scales linearly with the distance between the plates for a given material within the gap, therefore confirming the notion that the maximum force remains constant regardless of the plate separation. Since

$E = V/x$ the formulation

$$F_{attr.} = \frac{1}{2}\varepsilon AE^2 \quad (20)$$

most directly represents the relevant circumstances. In the context of planar parallel capacitors and electroadhesives it can also be useful to introduce the electrostatic pressure, which is the electrostatically generated attractive force per interface area:

$$f_{attr.} = \frac{1}{2}\varepsilon E^2 \text{ [N/m}^2\text{]} \quad (21)$$

With equations 20 and 21 the real correlation between the applied electrical component and the developed force (mechanical component) is given for $E \leq E_{max}$, with E_{max} being the breakdown strength of the materials exposed to the electric field E . Any attempt to increase the voltage and therefore the charge and the electric field above this limit will result in material failure and a loss of charge on the plates. Below this limit the force is constant for an unchanging electric field independent of the separation distance.

However, as mentioned above the concept of a force that is independent of the separation distance still has its limits: It is only valid so long as the plates' separation remains sufficiently small compared to the plates' area, to support the assumption that the electric field in between the two plates is uniform in direction and magnitude.

One may also wonder if the electric field created outside the capacitor induces opposite forces that pull the plates apart: Even for a capacitor that is far from infinite in its area this force is negligibly small and for a geometry that ideally fulfills the the assumption the outward force becomes zero.

3.1.3 Attractive forces on dipoles

The previous statements have concentrated on the more straightforward treatment of attraction forces of oppositely charged objects, which together with the repulsion of alike charges is an electrophoretic effect. A very important concept for electrostatic actuators in general, however, is the dielectrophoretic effect.

Dielectrophoresis describes the behaviour of non-charged objects in an electric field. It occurs with conducting as well as with dielectric, non-conducting materials and results in an attraction to the region of strongest electric field, regardless of the polarity. Therefore it does not occur within uniform fields.

The simplest case is that of a single polarized molecule - a so called dipole, as it is schematically depicted in figure 7 - in the electric field of a point charge such as an ion. The dipole has two equal but opposite charges located a short distance d from one another. This distance will generally be far smaller than the distance r to the

source of the electric field.

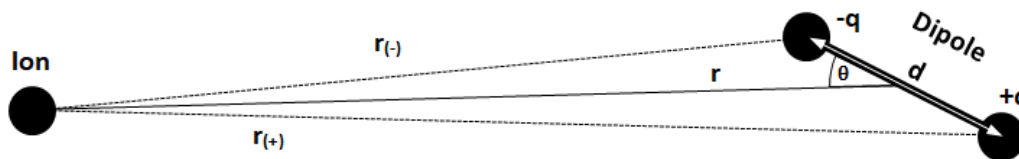


Figure 7: Possible orientation of a dipole to an ion

The charge which is opposite to that of the ion will be attracted while the similar charge will be repelled. This creates a moment on the dipole. If the dipole is free to rotate, this moment results in a reorientation so that the axis of the dipole points through the point charge, i.e. the angle θ becomes equal to zero or 180° , depending on the polarity of the ion. In this new position the largest attraction force occurs.

Also in atoms and molecules that are not polar in themselves an induced polarization, similar to that of van der Waals forces, can be enforced by a strong external electric field. Here it is a slight displacement of the electrons around the positive core of the atoms that results in dipoles orientated accordingly with the external electric field.⁵

That the overall force on the dipole is not identical to zero is a direct consequence of the distance dependency of the force acting between two point charges as it is specified in equation 2. In an electric field induced by the ion that is strong compared to the charges within the dipole the resulting force on the dipole will be:

$$\begin{aligned} \mathbf{F} &= \mathbf{F}_{\text{ion.dip}+} + \mathbf{F}_{\text{ion.dip}-} \\ &= \frac{Q_{\text{ion}}Q_{\text{dip}+}}{4\pi\epsilon r_{(+)}^3} \mathbf{r}_{(+)} + \frac{Q_{\text{ion}}Q_{\text{dip}-}}{4\pi\epsilon r_{(-)}^3} \mathbf{r}_{(-)} \end{aligned} \quad (22)$$

with

$$r_{(+)} = |\mathbf{r}_{(+)}| = \sqrt{|\mathbf{r}|^2 + \left(\frac{d}{2}\right)^2 + 2|\mathbf{r}|\left(\frac{d}{2}\right) \cos \theta} \quad (23)$$

$$r_{(-)} = |\mathbf{r}_{(-)}| = \sqrt{|\mathbf{r}|^2 + \left(\frac{d}{2}\right)^2 - 2|\mathbf{r}|\left(\frac{d}{2}\right) \cos \theta} \quad (24)$$

which are gained using the cosine rule.

These resulting forces in ion-dipole interactions are smaller than those between objects of opposite charge. Because of the small distance between the two oppositely charged poles of the dipole compared to the distance of the dipole to the field source,

⁵More information on types of polarization can be found in reference [2] chapter 14.2.5, that distinguishes between five effects.

their forces largely cancel each other out.

In the case of a particle that consists of a conducting material all charges are free to move within it. Thus, when subject to an electric field, the charges will reorganize within the particle, additionally inducing a rotation to align the longest dimension of the particle with the electric field if the particle is free to rotate. After the transport of charges the entire particle becomes a dipole in itself. Such a particle typically has far larger dimensions than a molecule, i.e. the ratio $\frac{d}{r}$ is larger, and the number of charges at each pole can typically be higher than within a molecule.

Not always are fixed dipoles - such as polar molecules - free to rotate. Their ability to follow the orientation of the electric field is material and temperature dependant among others. The average orientation of the dipoles within an object is a result of the energy for rotation available through the electric field as well as the thermal energy of the dipoles.

To get a notion of the relative distance dependency of the effects between charges and dipoles, a comparison of the relation of the potential energy in these interactions to their separation distance, as it is given in "Fundamentals of interfacial engineering" by R.J. Stokes et al. [34], is helpful:

- $E_{ion-ion} \propto \frac{1}{R}$
- $E_{ion-dipole} \propto \frac{1}{R^2}$
- $E_{dipole-dipole} \propto \frac{1}{R^3}$

Ion-Ion interactions could be called the point-charge equivalent to the macroscopic situation of oppositely charged plates or in the case of typical multi-electrode electroadhesives the attraction of a conductor by a multi-electrode actuator. Ion-dipole interactions correspond to the case of an electroadhesive actuator attracting a dielectric material. In the case of dipole-dipole interactions the energy is often less than the thermal energy and therefore it generally does not result in a reorientation of the dipoles to one another and no overall forces develop,⁶ which is equivalent to two dielectrics brought into proximity to one another.

The polarizability also depends on the frequency of the electric field, which is relevant at high frequency electric fields. While an alternating field will still result in the dielectrophoretic force to act in a single direction, the level of polarization of the dielectric is frequency dependent: It reduces at high frequencies as an effect of the inertia of the dipoles, as these have to reorientate by 180° for every alternation.[31]

⁶A detailed treatment of this topic is given in [34], chapter 2.2.

Even though it would seem the permittivity should also be a function of the absolute electric field strength, no documentation on such a dependency was found.

Summarizing, the resulting dielectric force depends on:

- the strength of the electric field,
- the divergence of the electric field (allowing for an overall force to occur on the dipole) and
- the polarization of the effected object (which can depend on the electric field's frequency, the materials involved and other conditions such as the temperature).

As a mathematical expression this reads for the simplified equilibrium case:[26]

$$\mathbf{F} = \left(p_x \frac{\partial}{\partial x} + p_y \frac{\partial}{\partial y} + p_z \frac{\partial}{\partial z} \right) \mathbf{E}_e = (\mathbf{p} \cdot \nabla) \mathbf{E}_e \quad (25)$$

where \mathbf{F} is the overall force on the dielectric object resulting from its polarization \mathbf{p} (the dipole vector that is a constant here) in the external electric field \mathbf{E}_e , with ∇ the nabla operator that in a dot product produces the divergence.

As long as \mathbf{p} and \mathbf{E} are treated as constants, i.e. \mathbf{p} is not a function of \mathbf{E} or time and \mathbf{E} is not changing over time, so that the above assumptions can be made, the problem becomes workable with equation 25. Values for the dipole moment \mathbf{p} can be obtained from the relative permittivity, which can be measured. For linear, homogeneous, isotropic materials this a typically known property for certain conditions. Once again this only holds for materials and parameter combinations in which the dipole moment and relative permittivity actually can be treated as constants. Cases in which this does not apply are for example high temperature variations when working with dielectric fluids, as higher temperatures generally reduce the relative permittivity due to the increased thermal energy in the molecules, or when working with varying high frequency electric fields.

The relative permittivity is also the value that a simulation model - such as the one that is used later on in COMSOL - requires to calculate the behaviour of dielectrics in an electric field. When dealing with dielectric attraction in this simplified manner, the previously given information should be a pointer to the many possible dependencies of the supposedly constant permittivity, that should be kept in mind.

3.1.4 Forces in parallel capacitors with multiple dielectric layers

When dealing with in-contact electrostatic attraction the dielectric insulation layers on the electrodes play a significant role in the forces that are generated between

the different components. These forces determine the effectiveness of the attraction device, as well as further properties such as attraction or repulsion between layers. This understanding is important to be able to locate the strongest forces within the multiple layer device, the interface forces between the device's layers and also how these influence the overall attractive force to the attracted object at varying interface gaps towards the object's surface.

This section explains where the forces on dielectrics appear in a uniform field and what effects they have for electrostatic attraction devices.

When a dielectric body is placed into a region with a uniform field it is not attracted by either pole, but the reorientation of the dipoles within the dielectric due to the electric field will lead to alterations in the surface charge, which is depicted in figure 8. A surface facing the positively charged field source will have a certain level of negative charge and visa versa. The surface charge originates from the reorientated, exposed dipole sides at the materials surface. Any such surface will feel an attraction to the opposite pole, thus generating surface forces on the macroscopic body. On a whole these will perfectly cancel each other out over the surface of the body, but nevertheless they result in stresses within the body.



Figure 8: (left) Idealized dipole orientation withing a dielectric placed in a uniform electric field, (right) macroscopically resulting low level surface charge.

To be precise figure 8 is only complete for a dielectric surrounded by empty space or some entirely non-polarizable medium. Any other medium surrounding it would generate its own surface charge and surface attraction forces at any boundaries or interfaces with other materials. Concluding from this a force is generated at any interface that has different relative permittivities on either side. An interface with the same permittivity on both sides has equal forces acting on it from either side, resulting in an overall force of zero, which is equivalent to cutting a block of homogeneous dielectric material and analyzing the forces on the newly created interface.

In other words; in an electric field that is uniform in direction a force is generated at any change in permittivity. This can be a step in permittivity at a material interface or a gradual change over the volume of an inhomogeneous material.

In an electrostatic attraction device these forces should be harnessed to generate the

strongest possible attraction. The next part describes how the individual forces within such a multi layer setup are calculated.

The just mentioned change in permittivity consequently produces a change in electric field intensity, where a higher relative permittivity will result in a weaker field. This relationship is displayed in figure 9. To be able to quantify the field intensities within such a multi layer configuration the concept of a displacement vector \mathbf{D} becomes a useful tool. It could be regarded as the magnitude of charge separation within the dielectric and is simply defined by:

$$\mathbf{D} = \varepsilon \mathbf{E} \quad (26)$$

Its useful property is that its normal component on the interface between two different dielectrics is equal on both sides.[40]⁷

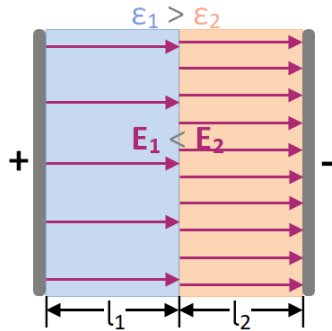


Figure 9: Multi-dielectric parallel capacitor with two dielectric layers with differing relative permittivities

The electric field intensities \mathbf{E}_1 and \mathbf{E}_2 are found via the following calculation that makes use of the relation in equation 26. In a uniform field E and D can be treated as scalars:

$$V = \Delta V_1 + \Delta V_2 = E_1 l_1 + E_2 l_2 = \frac{D}{\varepsilon_1} l_1 + \frac{D}{\varepsilon_2} l_2 = D \left(\frac{l_1}{\varepsilon_1} + \frac{l_2}{\varepsilon_2} \right) = D \left(\frac{l_1 \varepsilon_2 + l_2 \varepsilon_1}{\varepsilon_1 \varepsilon_2} \right) \quad (27)$$

where V is the total potential difference across the two opposing electrodes and all E , l and ε correspond to those in figure 9. This relation can be reorganized to:

$$D = \frac{\varepsilon_1 \varepsilon_2 V}{l_1 \varepsilon_2 + l_2 \varepsilon_1} \quad (28)$$

with which the electric field intensities E_1 and E_2 can now be supplemented to read:

$$E_1 = \frac{D}{\varepsilon_1} = \frac{\varepsilon_2 V}{l_1 \varepsilon_2 + l_2 \varepsilon_1} \quad (29)$$

⁷The following derivation of the electric field intensities was also found in this reference.

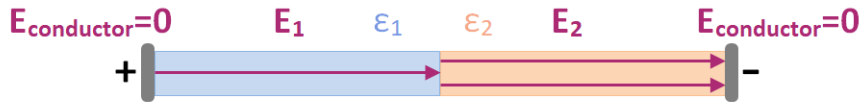
and

$$E_2 = \frac{D}{\varepsilon_2} = \frac{\varepsilon_1 V}{l_1 \varepsilon_2 + l_2 \varepsilon_1} \quad (30)$$

Now that the field intensities are known they can be used to calculate the forces acting on the interfaces. Each force calculation in itself is identical to the original calculation from equation 21. The inward facing surfaces of both electrodes are attracted in the direction towards the opposite electrode with a force that depends on the electric field intensity and permittivity that they are facing. These interfaces do not feel an outward bound force as the electric field within the conductor must be equal to zero.

In addition to the two electrode interfaces within a simple parallel capacitor further interfaces exist in a capacitor with multiple dielectric layers, which have electric field intensities unequal to zero on either side. Each of these additional interfaces between the dielectric layers is effected by two forces in opposite directions. The force on each interface can be obtained by calculating its attraction to each pole and subtracting the two forces from one another if they are represented by positive scalars, or by summing the two forces if their vectorial direction is taken into account. Again the force in either direction is calculated using equation 21 by inserting the electric field and permittivity in the respective direction.

An example is displayed in table 1 and explained in the following paragraphs. The displayed configuration is analogous to the one displayed in figure 9. The table underneath it presents the force equation applied to each interface and in both directions respectively. As a result of the differing permittivities of the materials that are in contact with the two electrodes, the two electrodes themselves do not experience an equal and opposite force toward each other.



acting forces	$f_1 \rightarrow$	$\leftarrow f_2$	$f_3 \rightarrow$	$\leftarrow f_4$	$f_5 \rightarrow$	$\leftarrow f_6$
equations	$=\frac{1}{2}\varepsilon_1 E_1^2$	$= 0$	$=\frac{1}{2}\varepsilon_2 E_2^2$	$=\frac{1}{2}\varepsilon_1 E_1^2$	$= 0$	$=\frac{1}{2}\varepsilon_2 E_2^2$
interface force	$f_{12} = \frac{1}{2}\varepsilon_1 E_1^2$		$f_{34} = \frac{1}{2}(\varepsilon_2 E_2^2 - \varepsilon_1 E_1^2)$		$f_{56} = -\frac{1}{2}\varepsilon_2 E_2^2$	

Table 1: Example of forces within a parallel capacitor with two dielectric layers

Even though the forces f_{12} and f_{56} on the inner interfaces of the two electrodes with their respective dielectrics differ from one another the overall sum of forces on the complete setup must be equal to zero. One may imagine the setup consisting of the two charged electrodes separated by two differing layers of dielectric material floating freely in space: If forces would only develop on electrode interfaces the setup would

accelerate in space without further input of energy, thus breaking the law of energy conservation. Here the statement comes into play, that in an electric field a force is generated at any change in permittivity, which was made in the explanation following figure 8. The remaining interface forces in between the different dielectrics - in this case f_{34} - must therefore cancel out the remaining force from the electrodes so that the sum does equate to zero.

Coming back to electrostatic attraction devices it is relevant for the forces developed by the mutual attraction of two facing and possibly dielectrically coated electrodes, which dielectrics are solids, i.e. which can transfer forces due to their stiffness, and which are fluid. The largest force occurs across the dielectric with the lowest permittivity. Where 'across' means the forces pointing inwards on the two interfaces of that dielectric layer. For example, if the configuration in table 1 is chosen to have two dielectrics 1 and 2 for which $\varepsilon_1 = 2\varepsilon_2$, then $2\mathbf{E}_1 = \mathbf{E}_2$, so that the force across dielectric 1 is half that across dielectric 2 (because \mathbf{E} is squared in the force equation). If dielectric 1 is solid and fixed to its adjacent electrode, while dielectric 2 is a fluid or vacuum, the attractive force will be twice that of a configuration in which dielectric 2 is the solid while dielectric 1 is the non-solid.

A further point of interest is the pressure on the interface between two layers of different material. For certain cases the following observations are useful to analyse which layers become attracted to each other and which tend to peel off if they are not appropriately fixed to the surface that they are applied to.

An interface pressure exists as long as the dielectrics involved have a permittivity larger than one and the surrounding medium that would potentially fill the appearing void at the interface between the two materials when they are separated is of lower permittivity than the separating dielectrics. In any case in the very first instance this 'medium' in the appearing void would be empty space. Only during actual separation could a surrounding medium such as air or water follow up and fill the emerging gap. As an example it is assumed that the two dielectrics in the configuration from table 1 are both solids and that each is fixed to its adjacent electrode, while the two dielectrics are only in loose contact with each other at the central interface. The interface pressure can be calculated by inserting a virtual third layer that is merely occupied by empty space, which naturally has a relative permittivity of $\varepsilon = 1$ (allowing the gap to fill with air would also remain at $\varepsilon \approx 1$). The force on the two new interfaces is calculated in the same way as the interfaces in table 1. If both dielectrics have a relative permittivity larger than one, then the strongest electric field will be across the new layer of vacuum resulting in an inward force on both sides of the vacuum layer. The sum of these two

force vectors (i.e. the difference between the absolute value of these two forces) equals the resulting force on the interface. The absolute value of the smaller of the two forces equals the pressure on the interface, that acts like a clamping pressure that holds the two material surfaces together.

If there is a surrounding medium with a higher permittivity than the medium that is currently occupying the gap, then this medium will be attracted into the gap. If the permittivity of the new medium in the gap is higher than that of one or both of the neighbouring dielectrics, the force on that interface will point outwards. These outward bound forces will however always be weaker than the compressing force over the whole setup from one electrode to the other, so that the two electrodes remain attracted to one another regardless of the dielectrics in between them. The outward bound forces at the interfaces of this region with the weakest electric field show that the setup will always strive to fill the space in between the electrodes with the highest permittivity available.

The sum of these two force vectors on either side of the gap is still the resulting force on the original (closed-gap) interface, but there is no pressure on the interface itself. The pressure is even "negative" (gap-opening) in the case that there is a medium with higher permittivity filling the "new gap". Only if the dielectrics on both sides of the "new gap" are solids, as well as all other layers involved up until the electrodes' surfaces, then the overall compressing force between the electrodes will keep this interface clamped and in contact. If any of the layers is a fluid with lower permittivity, then the "new gap" will grow and the less permittive dielectric will be displaced and replaced by the surrounding medium with higher permittivity. Also a solid dielectric layer will be subjected to these forces and if it is not adequately held in place, will be forced out by the replacing dielectric.

Summarizing, it is crucial to take note of thickness and permittivity of all involved layers to be able to derive the actual electric fields and therefor attraction force of the complete setup from one electrode to the other as well as the forces in between the layers that are important for the mechanical integrity of the multi layer configuration.

An afterthought: In the specific case of a single separation layer or separation gap that is large compared to all other layers involved, the thin in-between layers must not always be taken into account for the calculation of the overall force between two electrodes. Thin layers within a large total distance between the potential sources only have a small effect on the remaining electric fields. This is even more so if the thin layer has a high permittivity. This configuration is more typically the case for an attraction over an air gap, in which for example the electrode insulation coatings

represent comparatively thin dielectric layers. In such a case, in which the force between the coated electrodes is sought, the thin layers can be neglected in the force calculation between the two plates and the formula remains as simple as for a standard parallel capacitor (equation 21). This is because the force on the electrodes is the sum of the forces on both the interface of electrode to dielectric coating and the interface of the coating to the medium in the gap (here typically air). This sum will be equal to the force on the uncoated electrode, since the potential on the electrode and the electric field across the gap have not (significantly) changed by applying the thin coating.

3.2 Material properties for electrostatics

The properties that are most relevant for electrostatics applications are the electric conductivity, relative permittivity and dielectric breakdown strength.

Conductivity is the ease at which charges will move through a material when subjected to an electric field. It is measured in S (Siemens) with $S = \Omega^{-1} = A/V$, so it is the inverse of the electrical resistance that is measured in Ω (Ohm). As the concern here is electrostatics, the conductivity is mainly of interest to define whether a material is classified as a conductor or an insulator. Even in electrostatics charges have to be moved. Good conductors are for example any type of metal, which have a conductivity around the order of $10^7 S/m$, but also poor conductors such as non-purified water and therefor also damp materials are sufficiently conductive so that high voltages will lead to a significant flow of charges. Good insulators have a conductivity around $10^{-10} S/m$ or lower. Examples are glass ($S \approx 5 \cdot 10^{-12}$), plastics or very dry wood ($S \approx 3 \cdot 10^{-9}$).

The relative permittivity of a material is to some respect the materials ability to conduct the electric field. The permittivity of empty space is $\epsilon_0 = 8.85 \cdot 10^{-12} F/m$. The relative permittivity is a unitless factor to this number. For typical electrically insulating materials values for the relative permittivity range from 1 (for paper $\epsilon_r = 1.2 \dots 3.0$) to around 80, which is approximately the relative permittivity of distilled water. Specialized ceramics can have a relative permittivity of up to 50,000. Non-polar materials generally have a low relative permittivity, while materials with polar molecules will generally have a high relative permittivity. Conductors can be viewed as having infinite permittivity in the static case as their conductivity eliminates the electric field within them.

As electrostatics systems typically produce or even rely on high electric field intensities, the dielectric breakdown strength is an important property of the insulators that

are used. It is the maximum electric field intensity that an isotropic, homogeneous material can withstand without losing its insulating property and therefore has the unit V/m . The breakdown potential across a piece of insulating material therefore scales linearly with the material's thickness.

For gases the characteristics are different and Paschen's law specifies the breakdown potential. Paschen's law is based on the Townsend theory of charged particle avalanches. For any given pressure and type of gas there exists a minimum breakdown voltage at a certain distance called the Paschen minimum. A breakdown across a distance above or below this value will require a higher voltage. At atmospheric pressure the Paschen minimum for air is at a distance of approximately $7\mu m$ and requires around $330V$ (values vary slightly between sources) resulting in a breakdown strength in excess of $40kV/mm$. At increasing distances the breakdown strength first rapidly decreases until the relation becomes approximately linear for large gap lengths so that the breakdown potential again scales linearly with the distance. The typically quoted value for the breakdown strength of atmospheric air is $3kV/mm$. An empirical function for the breakdown voltage of atmospheric air that is valid for distances between $0.1mm$ and $200mm$ was derived by H. Lau by averaging the breakdown voltages found by several authors.[21] The derived function for the breakdown potential is:

$$V_{breakdown} = 24.4\rho d + 6.53\sqrt{\rho d} \quad (31)$$

which yields $V_{breakdown}$ in kV for a distance d in cm and with

$$\rho = \frac{p}{1013} \cdot \frac{293}{t + 273} \quad (32)$$

where p is the pressure in hPa and t is the temperature in $^{\circ}C$ so that $\rho = 1$ for standardized parameters.

Figure 10 displays V_{max} and derived from it E_{max} for air at standard pressure and temperature for gap lengths between $0.1mm$ and $15mm$. The displayed range is limited at its lower end by the validity of the used function ($> 0.1mm$) and on the upper end by what is relevant for this project. A graph of experimental results is given in "Electrical breakdown of gases" by J.M. Meek et al.. [21](p. 542)

Breakdown occurs when electrons that are normally not free to move within an insulator break loose by the influence of a strong electric field. Accelerated electrons will collide with neighbouring molecules and initiate an avalanche of free electrons if they are accelerated to a sufficient energy level before collision. Depending on the material and energies involved various wavelengths of light can be emitted during the collisions: The avalanche becomes visible as a flashover.

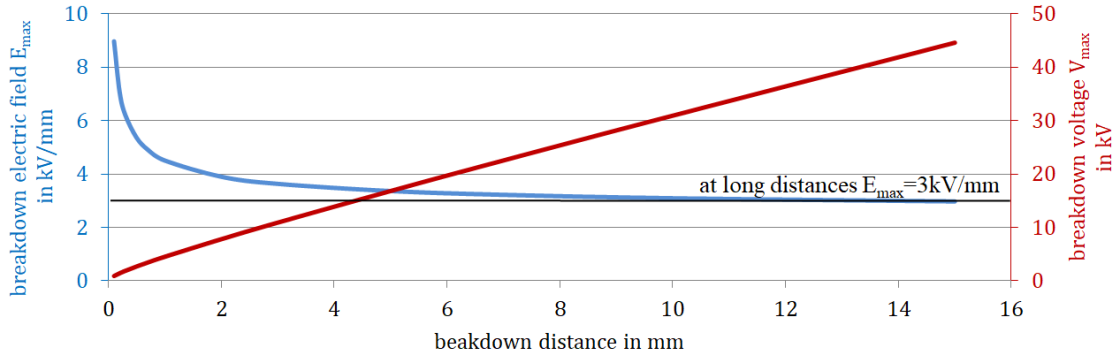


Figure 10: Diagram of breakdown electric field and voltage derived from equation 31 for air at $p = 1013hPa$ and $t = 20^\circ C$ and gap lengths from $0.1mm$ to $15mm$ (at distances below the Paschen minimum ($\approx 7\mu m$) the maximum voltage before breakdown increases again)

Some relevant materials for electrostatics systems and for this project are listed in table 2. Polyimide (PI) films are especially popular for the insulation of high voltages, because of their very high breakdown strength claimed to be as high as $315kV/mm$. [7] Also silicone which is of interest due to its elastic properties can have a relatively high breakdown strength, although it also depends on the material thickness and its strain: Values are stated to be approximately between $10...100kV/mm$. [5]

material	conductivity	rel. permittivity	dielectric strength
atmospheric air	$\approx 10^{-14}S/m$ (*) [8]	1.0006 [-] [9]	$\approx 3kV/mm$ [2]
drinking water	$0.005...0.05S/m$ [23]	-	-
deionized water	$\approx 5.5 \cdot 10^{-6}S/m$ [23]	81 [-] [9]	$65...70kV/mm$ [18]
glass	$\approx 5 \cdot 10^{-12}S/m$ [2]	5...16 [-] [9]	$9.8...13.8kV/mm$ [18]
PI (Kapton)	$5.6...7.1 \cdot 10^{-15}S/m$ [30]	3.1...3.55 [30]	$22...27.6kV/mm$ (**) [30]
vacuum(***)	-	$\equiv 1$	$\approx 50...70kV/mm$ [21][38]

Table 2: Some materials and typical properties relevant for this electrostatics application, (*) The conductivity of air is strongly dependent on the humidity and level of ionization, (**) Another company claims even $315kV/mm$ for their $12.7\mu m$ foil [25], (***) Vacuum is not a material and the values given are not vacuum material properties. It is nevertheless added to the table for a convenient overview. The dielectric strength applies to metallic electrodes.

Even in vacuum there is a limit to the electric field intensity before electric breakdown occurs, although here the mechanisms are different. Here breakdown is facilitated by

emissions from the charged surfaces and is therefore dependent on the surface- and material-properties of the electrodes. For multiple metals it has been found to be in the range of $50kV/mm$ ⁸ to $70kV/mm$ ⁹ which is not extraordinarily high if it is compared to the dielectric strength of electrically strong insulators.

However this breakdown in the form of field emission only directly applies to conductors. Naturally the electric resistance of dielectric insulators will prevent an unrestrained emission of charges up until their breakdown strength is reached. Therefore a charged conductor coated by an insulator is expected to show the emission characteristics of the insulating material. More specific data on the field emission from insulators, due to their low but nevertheless existing electrical conductivity, was not found.

⁸according to graphs presented in "Electrical breakdown of gases" by J.M. Meek et. al that can be found on p.130 [21]

⁹according to findings by Lee et al. quoted by V. Babrauskas in their paper on breakdown in very small gaps[38]

4 Categorizing the physically available options

This section uses the previously gained insight to characterize different possibilities for the electrostatic attraction that is to be realized for this application. It consists of three parts that shall serve as an overview, from which the design directions can be chosen before going into more depth.

4.1 Electrophoretic attraction (parallel capacitor)

This form of electrostatic attraction is the most simple and straight forward one. It directly utilizes the attraction between two oppositely charged conducting surfaces. While it is not a feasible solution for this project, because the substrate that is to be attracted is typically glass and therefore not a conductor, it will be detailed here for completeness and because it is a good introduction to give a feel for what is involved as a minimum to create an electrostatic attractor.

In the simplest case a high voltage supply is connected to two conducting plane parallel surfaces. A possible configuration is shown in figure 11. The edges of the attraction plate are rounded to reduce peaks in the electric field intensity induced by sharp corners and edges. At high potentials and electric field strengths this is necessary to avoid local corona discharges within the surrounding air or even local electrical breakdown of the insulator material. These two surfaces thereby form a parallel capacitor, for which the attractive force can easily be approximated analytically with the formula from equation 20, although it is not as precise as for an ideal parallel capacitor configuration, because the effective plate area can only be estimated. If the plane surface area of the attraction plate is used, the result will be slightly conservative as the larger grounded surface and the rounded plate edges will also slightly contribute to the attractive force. The accuracy of the formula also decreases with an increase of the ratio between separation distance and plate size.

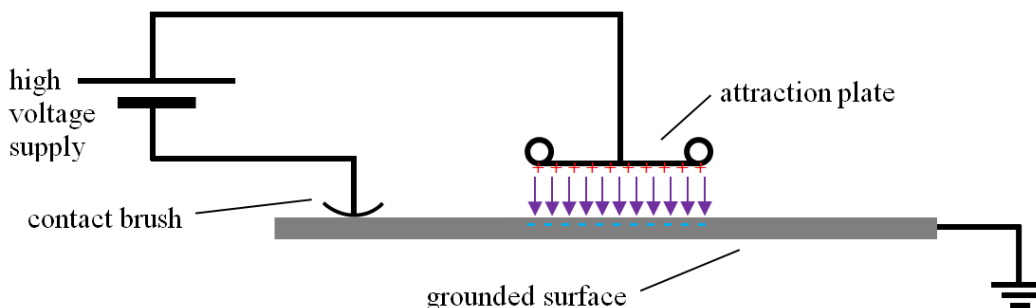


Figure 11: A possible configuration for a parallel capacitor style electrostatic attractor, the grounded surface represents a non-insulated metallic building skin.

For a given attraction plate area the major variable left to influence the resulting force is the electrostatic field intensity E in between the surfaces. As this region is inevitably filled with air, the properties of air will have a decisive effect on which forces can be sustained. Apart from the air in between the metallic surfaces an insulating coating can be applied on the electrodes which can introduce a layer with high breakdown strength. However breakdown can still occur within the air surrounding the insulation.

This leads to the conclusion that for larger gap distances of multiple millimeters the electrical breakdown strength of air of $E_{max_air} = 3kV/mm$ is the maximum electrical field that can be sustained between the electrodes, which gives a maximum limit to the possible attraction force that is achievable within air. Inserting this value into equation 21 yields the theoretical maximum attractive force per unit area for electrodes separated by multiple millimeters of air at atmospheric pressure:

$$f_{max_air} = \frac{1}{2}\epsilon E_{max_air}^2 = 39.8N/m^2 \quad (33)$$

If verified practically, this is a decisive value for all designs that build up an electrostatic attraction force over a distance of multiple millimeters within air and means that the force is hardly useful for heavy applications. More details on the effect of air and insulating layers are experimentally found and discussed in chapter 5. Therefore only systems that build up their attraction force over a very small air gap, at distances in which the breakdown strength of air becomes significantly larger, can produce higher forces. These can be multiple orders higher (see section 6.1).

4.2 Dielectrophoretic attraction

In contrast to the previously described setup this approach uses a multi electrode configuration, with the electrodes all positioned in one plane, to activate dielectric polarization in an attracted object. A simple overview of this configuration is given in figure 12. Therefore it does not require any electrical contact to the attracted body and can attract both dielectrics and conductors. Strictly speaking the attraction of a conductor with this method is not a dielectric effect: The multi electrode attractor will evoke a full separation of charges within the conductor (this is depicted in figure 4 in section 2.2), therefore it more closely represents the opposite charge attraction within a parallel capacitor. The multi electrode technique is the one most often addressed in the literature about electroadhesion, but only in the context of in-contact applications. This will be due to the fact that in non-contact situations the limiting breakdown strength of air makes its use far less attractive.

From the point of view of obtaining force solutions this is probably the most tedious

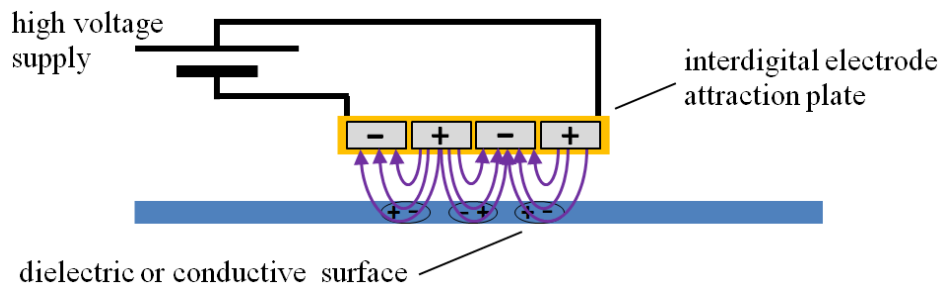


Figure 12: A simplified configuration of a multi electrode electrostatic attractor

in comparison to the other options, especially if the goal is to find the maximum possible force, as this not only depends on the intensity but also on the divergence of the electric field. To create the maximum possible divergence over the volume of the attracted object an optimized electrode pattern must be found. Section 6 and the respective appendices go into more detail on this. They show that dielectrophoretic attraction is slightly inferior to electrophoretic attraction regarding the achievable forces. Specifically in the case of attracting low permittivity glass with $\epsilon_r = 5$ it is found to be around $\frac{1}{4}$ of the force possible with electrophoretic attraction. At the same time, being used for in-contact electroadhesion, it does not have the low limit of $39.8\text{N}/\text{m}^2$ on the force that is otherwise given by the breakdown strength of air.

For the in-contact attraction of a dielectric such a multi-electrode adhesive is the only functioning option, as it alone is capable of inducing strong dielectric polarization within the attracted body.

For in-contact attraction of a conductor the multi-electrode electroadhesive is also the most practical approach, since it requires no electrical contact to the attracted object and produces approximately the same forces as the parallel capacitor approach, as once again it is an electrophoretic effect (appendix B.1).

However, for non-contact attraction of dielectrics the inferior force generation of the dielectric attraction further lowers the strict limit given by the low breakdown strength of air, so that residue surface charge electrophoretic attraction (section 4.3) becomes more attractive.

The knowledge of how the attraction force is influenced can be used to intelligently develop specific designs that can then be evaluated by simulation. For dielectric attraction the main additional parameter is the divergence of the electric field over the volume of the attracted object, which is governed by the electrode pattern and can be weakened by the insulating coating of the electroadhesive. Literature on this topic is treated in appendix B.1. The true effectiveness of a promising design can then be verified experimentally.

4.3 Residue charge electrophoretic attraction

A third and possibly novel approach - at least with respect to electroadhesives - is the use of surface charge. This configuration would consist of firstly a surface charging unit that deposits charge of one polarity on the surface of a non-conductive object and secondly an attraction plate that is charged with the opposite polarity. Figure 13 gives an impression of how this configuration would be set up. If the charge is only deposited at one side of the attraction plate, as it is depicted, then naturally the motion of the vehicle is limited to the direction that transports the newly charged region underneath the attraction plate. A more practical design would include surface charging elements in either direction of motion.

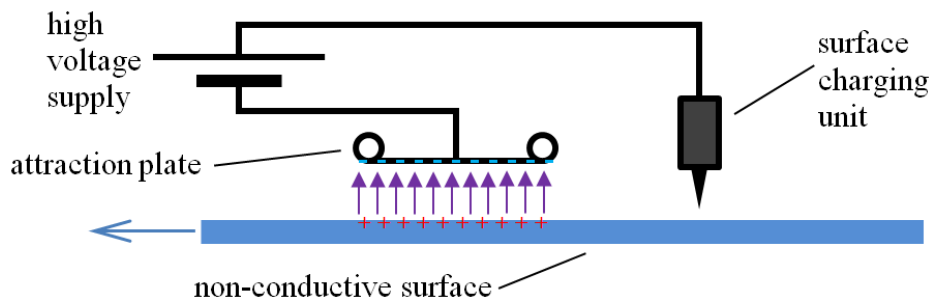


Figure 13: Basic configuration of a surface charge attractor

Surface charge can occur naturally due to friction or even sunlight on some materials. For friction between two surfaces to leave behind surface charge the two materials in contact must have differing affinity to electrons or negative charge in general. Relative values for many materials have been found empirically and are sorted to yield the so called triboelectric series. The further the two materials are apart within the triboelectric series the more effective they are at becoming charged by friction. A detailed list of materials and additional information is for example given by B.W. Lee et. al in their empirically acquired listing.[3] This effect is for example utilized in a Van de Graaff generator to produce a high voltage charge on an often spherical electrode. In a similar fashion a cylindrical brush or other soft material rotating at a high speed, that is brought into contact with the insulator surface could deposit charge on it (see left hand sketch in figure 14), if the right choice of material is made. The rotating cylinder additionally has to be able to give off its own charge to ground or to the attraction plate that is then charged oppositely to the rubbed surface. Apart from the technological simplicity of this approach it has multiple disadvantages such as the need for moving parts, generating friction and possibly unwanted forces as well as wear on the rubbing components. The friction and therefor inefficiency of this Van de Graaf

generator approach is also the reason why this principle is not popular anymore for the generation of high voltages. It has been replaced by influence machines and electric transformer circuits.

There are further methods of applying surface charge. Corona discharges will for example occur on sharp conductive tips that are - in relation to their near surroundings - connected to a high electric potential. Two possible configurations for this corona discharge are shown schematically in the central drawing of figure 14. The advantage is that once a high voltage source is on board additionally only relatively simple technology (the electrodes) is required. Once the electric field strength that becomes higher around small radii exceeds the breakdown strength of air a partial breakdown and discharge via charged air particles will occur from this tip. If this discharge is directed onto an insulating surface the charges can cling to it. Surface charging via corona discharge, however, also has its challenges for this project. It would work best if there was an oppositely charged electrode behind the surface which is to be charged (see left-hand option in the schematic). This would direct the discharge straight onto the surface. However for a robot traveling across a glass surface it is not feasible to require a further electrode to be placed behind the glass wherever the robot is. The design must work from the upper side of the glass only. An oppositely charged electrode near the discharge tips on the same side of the glass pane that is to be charged (see right-hand option in the schematic) is able to induce high enough electric field intensities to enable corona discharge, but likely results in a large amount of lost current, as the charged particles will be strongly attracted to the electrode rather than the surface that is meant to be charged. This could also reduce the density of surface charge that can be applied.

Another method is the use of partially ionized air or cold plasma. It is similar to the use of corona discharge in so far that it also relies on charged air particles to transport the charge to the insulators surface. The main difference lies in the method of producing the ions and transporting them to the surface. A schematic drawing is given in the right hand sketch of figure 14. Often a high frequency voltage is used to excite the air molecules around an insulated electrode to a level that some of them become ionized. This consequentially produces an overall neutrally charged plasma. This type of plasma is used in industry for the neutralization of surface charges in industrial processes and for the activation of surfaces for chemical treatment, surface coating and the application of adhesives.[33] For this purpose however a unipolar plasma is required, since its purpose is to apply a strong charge to a surface. Therefor the oppositely charged particles within the neutral plasma must be separated. An electrode

connected to a high potential DC supply will attract oppositely charge particles and accelerate similarly charged particles away from it.

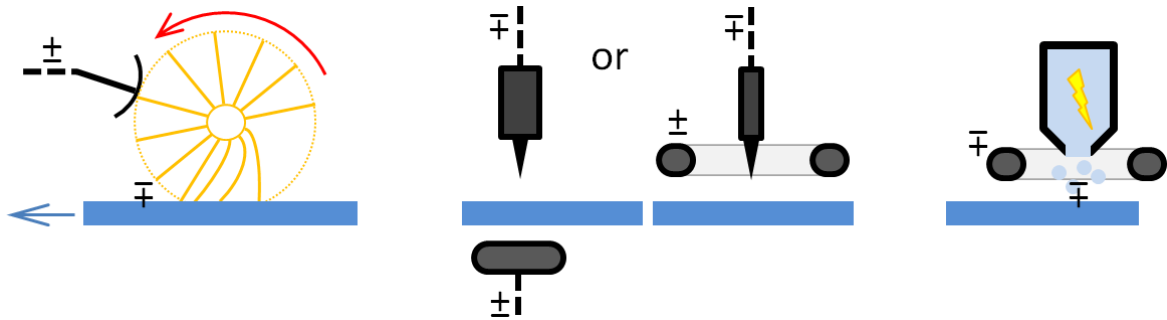


Figure 14: Sketches of different possibilities to generate surface charge on an insulator via: (left) friction, (middle) corona discharge, (right) cold plasma.

Both for corona discharge and plasma treatment the potential on the electrode that is designed to accelerate the charges onto the surface must be high enough to counteract the rising electric potential of the charging glass surface to enable further charging up to a required degree (also mentioned in a consensus study report on ion implantation by the National Research Council and others[28]). As long as its potential is high enough the acceleration can suffice to attach further charges to the already partially charged surface.

In their paper on generating surface charge for triboelectric nanogenerators[35] S. Wang et. al also report successful surface charging with an ionized air gun that has the option to alternately eject either polarity of charge.

A disadvantage of surface charge could be that it must linger for long enough. Naturally surface charge will slowly disperse by low level conductivity. Even a glass surface is a slight conductor, the conductivity of which is however strongly dependent on the humidity.[3] The topic of charge loss is shortly treated in section 7.

For continuous operation a balance between ejected charge that is deposited on the insulator surface and regained charge that is collected from the surroundings must be found. If the vehicle has no means of regaining the emitted charge, then its potential will gradually rise until the surface charging unit reaches a potential at which it can no longer deposit (sufficient) charge. The vehicle will require a means of gathering the deposited charge after the charge leaves the useful region below the attraction plate or the vehicle must in some way be grounded.

If the surface is even only moderately conductive, conduction may suffice to enable the electric field of the attraction plate to hold the surface charge in place beneath it. In this case the setup will function more like the design in section 4.1 with two

oppositely charge conductive plates. While the slightly conductive surface can now be used as a means of grounding for the vehicle, this is no longer necessary as in this case not the potential of the surface charging unit, but the potential difference between the charged plate and the surface is determining.

This technology therefor will work both on insulators and on conductors. As long as enough surface charge can be applied on the insulating surface (a test setup is suggested in section 7.2), the attraction force can be expected to be similar to that of the parallel capacitor design independently of the conductivity or dielectric constant of the surface material.

Also with respect to the dependency of the maximum possible attraction force on the separation distance (i.e. the air-filled ground clearance), this configuration has the same characteristics as the parallel capacitor setup from section 4.1, as long as sufficient surface charge can be applied. This means that for air gaps of multiple millimeters the force is limited by the theoretical maximum of $39.8N/m^2$ and increases by multiple orders if the gap is closed and the surface are brought into contact. The problem here with the use of residue surface charge is that the surfaces can (partially) discharge each other when brought into contact. Therefor it is not appropriate for in-contact attraction.

5 The effect of the attraction gap on the achievable force

The main question to this first set of experiments is: What is the limitation on the force introduced by the characteristics of air and other media in the gap?

There are many statements on achieved attraction forces for in-contact electroadhesion, some of which can be found in the previously referenced papers [11][17][15][22] that will in part be looked into in more detail in section 6. In descriptions of the electroadhesive effect it is often stated how important smooth surfaces are, so that a high proportion of surface contact can be achieved. However why surface contact itself is beneficial for electroadhesion is not well described. Surface roughness keeps a large proportion of the surfaces separated by a small distance as only the surface peaks come into contact, but as shown in section 3.1.1 the distance itself in between the electrodes is not a limitation to the force. In fact keeping a larger overall distance in between the electrodes would reduce roughness-induced inhomogeneities in the electric field, which otherwise can lead to losses through partial discharges. In the reviewed reports no connections are made to the physical limits due to the surrounding air.

Materials with high breakdown strength that allow for electric fields of high intensity are used to insulate the electrodes of typical electroadhesives. This prohibits discharges between the electrodes. However as long as these high intensity electric fields extend into the surrounding air beyond the insulation they nevertheless lead to ionisation of the air due to its low breakdown strength. This section targets this effect. The experiments described in the following give a clearer picture of the dependency of the achievable force on the media that fill the attraction gap. Also water is introduced as it plays an important role in the cleaning process.

5.1 Procedure

An experimental setup is designed and built (see appendix A.1), with which experiments for the attraction over a larger air gap of multiple millimeters are conducted. It is important that the experimental setup gives general insight into the effect that air (and later water) has on the attraction forces independently of the type of electrostatic attraction device. For this reason the configuration with the least complex electric field and simplest means of potential generation is chosen, which is the parallel capacitor design from section 4.1. In this manner additional parameters such as the more complex electric field of multi-electrode dielectric devices (section 4.2) or the quality of surface charge distribution of the proposed surface residue charge attraction technology (section 4.3) are excluded.

The experimental setup is used in three variations to compare the attraction forces respectively achieved between two non-insulated electrodes, between one insulated and one non-insulated electrode, as well as between two insulated electrodes (see appendix A.2). The setup is shown in figure 15. With it the attraction forces are measured for the three configurations of electrode insulation. The experimental findings are then compared to and supplemented by simulations of the system in COMSOL, which are consistent with the experimental results. An impression of the model is shown in figure 16 and for details see A.2.4.

Finally water droplets are introduced into the air gap as these are typically abundant during the robotic cleaning process.



Figure 15: Overview of the components of the experimental setup

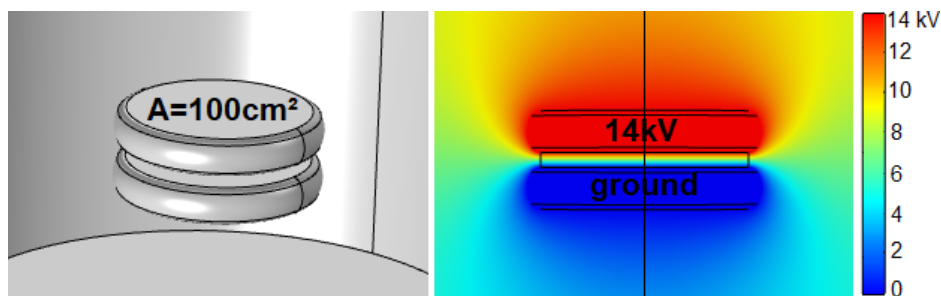


Figure 16: An impression of the electric field around the simulated model of the experimental setup

A further experiment (see appendix A.2.5) uses a similar setup to the first one, in which the insulated electrodes are, however, brought into contact with each other. This configuration shows the effect of minimizing the air gap to allow for electric fields multiple orders higher than across larger air gap.

This setup also serves to compare the effect of water on in-contact adhesives to non-contact electrostatic attraction situations as those demonstrated above.

5.2 Results and conclusions regarding cleaning robots

It is confirmed by the above described procedure that it is not directly a good surface contact that allows for high forces, but rather the absence of air or at least the increase in breakdown strength of the air at small distances in the attraction gap.

More generally it is the consequential absence of any fluid or gaseous material in the gap, that itself makes perfect contact with the solid surfaces, but is capable of conducting charge to some extent, while it cannot transfer mechanical stress.¹⁰

1. The limitation over large air gaps:

In section 4.1 the limit of $39.8N/m^2$ on the electrostatic pressure over a larger air gap was first brought up. It is found that in these experiments the theoretically possible electric field intensity in air is not reached. The highest percentage of the theoretically possible force generated over an air gap was achieved at a distance of $2mm$, at which an electric field of $3.9kV/mm$ is possible going by Paschen's law for air at atmospheric pressure. The measured value of $310mN$ equates to an electrostatic pressure of $33N/m^2$, which is 49% of the theoretical maximum force and therefore 69% of the theoretical maximum electric field intensity at this distance.

Some effects found to limit the achievable attraction force additionally to the limitation given by the theoretical breakdown strength of air are (details in appendix A.2):

- maximum field intensity in air could not reach the respective values given in literature (e.g. $3kV/mm$ at a gap length of $10mm$) (*)
- buildup of space charge (also for non-insulated electrodes)
- accumulation of opposite surface charge on insulated electrodes
- water droplets as a catalyst for charge transport

(*)It is remarkable, that the typical maximum field intensity for atmospheric air was not reached in any of the experimental setups before areal breakdown occurred.

¹⁰This is because the forces are developed at the surface interfaces and not within the bulk of the fluid in which the electric field is reduced or nullified due to its conductivity (see section 3.1.4 for details). In contrary if hypothetically this medium would become solid its conductivity would then increase the attraction between two insulated surfaces, because of its capability of transferring mechanical stress.

The experiments show that a realistic attraction force of $\approx 1/3 \dots 1/2$ of the theoretical maximum in air can be achieved over a distance of multiple millimeters.

The second experimental setup that achieved good surface contact shows that by minimizing the air gap (optimally eliminating it) far higher forces are achievable: An electrostatic pressure of $799 N/m^2$ is measured. This value is within the level of average in-contact electroadhesives presented in literature. By using insulating material with higher breakdown strength higher electric fields are feasible and a force multiple orders higher becomes possible (see section 6).

2. The effect of water on non-contact and in-contact attraction:

The addition of water droplets in the attraction zone of a non-contact attraction device significantly reduced the attraction force by nearly $\frac{1}{2}$.

In-contact adhesion devices benefit from the drastic increase in breakdown strength of air (and gases in general) at increasingly small distances so that attraction forces multiple orders higher can be achieved (for examples and details see section 6). The consequence of the relationship stated at the beginning of this section is, that the addition of non-purified water to the interface of an in-contact electroadhesive fully eliminates the electric field due to its conductivity. Thereby the electrostatic attraction force between the two electrodes is also nullified.

3. Conclusions regarding cleaning robots:

A consequence of this is that for cleaning robots that make use of water, in-contact electrostatic adhesion is only safely realizable if a fail-safe method is found to keep the attraction zone dry, while electrostatic attraction across an air gap is only weakened and can partially be sustained.

At the same time the forces possible with non-contact electrostatic attraction are prohibitively low for traditional cleaning robots and lighter designs would have to be developed.

6 Design criteria for an in-contact solution

From the preceding investigations it has become clear that in-contact adhesion is able to reach far higher attraction forces than the electrostatic attraction over a significant air gap can, due to the breakdown strength of air. To this respect it seems desirable to develop a design that enables the vehicle to move across the surface while its electrostatic attraction device is in contact with the surface, despite the fact that this brings forth the aspect of having to design a more complex mechanism that enables this form of motion. As stated in the introduction, the previously preferred attraction device that is effective over an air gap could otherwise be a rigid plate on the underside of the vehicle, which would combine high robustness with simplicity.

Another important factor regarding cleaning robots and outdoor applications is the sensitivity to being exposed to water. As the preceding experiments showed, an in-contact adhesive will become fully effectless if water is allowed to enter the contact zone, because water will act as a conductor here and shield the electric field.

Despite these drawbacks for the application of in-contact adhesion, the following section will detail what can be achieved with this technology as its force characteristics are promising. It can be used as a guide for the reader interested in following this path.

The most versatile and practical design approach for in-contact electrostatic attraction is the use of the multi-electrode dielectric attraction principle (section 4.2). The parallel capacitor option would only work on conducting surfaces (section 4.1) and the surface residue charge attraction (section 4.3) could suffer from discharging itself when brought into contact, although the latter can be reduced by roughness on well insulating charged surfaces. Because of the complexity in the construction and optimization of this type of electrostatic adhesive and since multiple examples are available in literature, this section primarily concentrates on understanding and analysing some existing setups, after which an approach to optimizing the design for the attraction of glass is made and the main aspects for the application of this technology on cleaning robots are summarized.

6.1 Summarized guidelines

The literature on multi-electrode electroadhesives that was reviewed often concentrates on finding an effective electrode pattern (see B.1). By comparing the results for different patterns it is concluded, that it is not the overall pattern but the effective electrode width and electrode spacing that is of relevance. Therefore any electrode design can simply be represented by an equivalent pair of infinitely long parallel electrodes, a method that has been used by some. This reduces design parameters and

computation effort.

It is also found that despite the fact that this technology relies on the principle of dielectric attraction, the maximum attraction force for given material characteristics, i.e. maximum breakdown strengths, is independent of the separation distance of the electrodes to the attracted object (see B.2). This is derived from the circumstance that the geometric parameters as well as the electric potential can be scaled up or down together. This means that the thickness of the electrical insulation material can be varied without influencing the attraction force if the electrode measurements and supply voltage are adapted appropriately. This is advantageous when adapting the adhesive design to function on rougher surfaces.

Previously published examples, which are quoted in detail in appendix B.3, show that on conductors adhesive pressures in excess of $10000\text{N}/\text{m}^2$ can be achieved (e.g. [22][11]) provided that insulation materials with extremely high breakdown strength are used and a clean and optimized surface contact is realized in which air and other contamination are excluded to a high degree. On glass an adhesive pressure of $8400\text{N}/\text{m}^2$ has been achieved[11], although here no details on the dielectric constant of the attracted glass or the electroadhesive design itself are given.

6.2 Risks for in-contact electroadhesives on cleaning robots

The problem with in-contact electrostatic attraction is that any form of contamination in between the two opposing surfaces can have a strong negative effect on the adhesion force. Any non-conductive grit will increase the surface separation and the amount of air within the gap. Any contamination with low breakdown strength or fluid contamination (i.e. now inherent stiffness) with even a slight conductivity will lead to a reduction up to nullification of the electric field intensity across the gap in between the surfaces (see section 5.2). The nullifying effect of water entering the gap is demonstrated in appendix A.2.5. Therefore, wherever this technology is deployed measures must be taken to ensure a clean and dry contact region for the electroadhesive. Regarding industrial cleaning robots this is difficult to realize with respect to two aspects: cleaning water and water from environmental sources, primarily rain and dew. The more controllable of the two is the water used in the cleaning process. The cleaning mechanism must be capable of drying the surface directly after cleaning so that it leaves behind a clean and dry surface that is adequate to enable electrostatic adhesion. The more difficult to deal with is rain, which is not an unlikely event as these machines are not only deployed during fair weather and a cleaning session can not be postponed or given up simply due to a change in weather. For small indoor cleaning robots satisfying this aspect is far more feasible, since these do not necessarily

use water at all and environmental influences from weather are often not given. Even when these gadgets are used on the outer side of windows, they will usually only be deployed during good weather.

Another potential risk with in-contact electroadhesives is that if they are separated from the attracted surface while activated (powered up), the high field intensities lead to ionization of the surrounding air and accumulation of opposite charges on the insulating surfaces covering each electrode, thus partly neutralizing the fields (see appendix A.2.3 and A.2.5). This can lead to a force reduction at re-engagement with the surface. These surface charges on the attraction device must therefore be neutralized as best as possible for example with grounding brushes before they are brought back into contact with the surface.

6.3 An approach to optimizing an interdigital electrode adhesive for glass

This thesis aims to evaluate the usefulness of electroadhesives for the described cleaning robots. For this reason besides the overall characteristics of each electrostatic attraction technology an estimation of what forces can be achieved by each of these is required. In this section a design customized for the attraction of glass is therefore developed.

1.Method:

Regarding the maximum possible attraction force that can be achieved by a multi-electrode design, there are two main topics for optimization. The first one is the electric field distribution to maximize the divergence of the electric field across the attracted object and the second one lies in prohibiting electrical breakdown in the vicinity of the electroadhesive.

The optimization of the electric field distribution executed here (for details see appendix D.1) follows the aim of achieving the highest possible electric field at the material interface, which results in the highest possible attraction forces, while regarding the breakdown strength of the chosen insulation material which is polyimide foil.

The optimization is performed by simulating one half period of the straight, parallel and infinite-in-length electrodes in multiple iterations, while adjusting one geometric parameter at a time (main iteration steps are displayed in figure 18).

In the course of the second field of optimization (for details see appendix D.2) it is found that due to the high breakdown strength of the available insulation materials; specifically PI foils, the electric field induced within the attracted glass body exceeds its

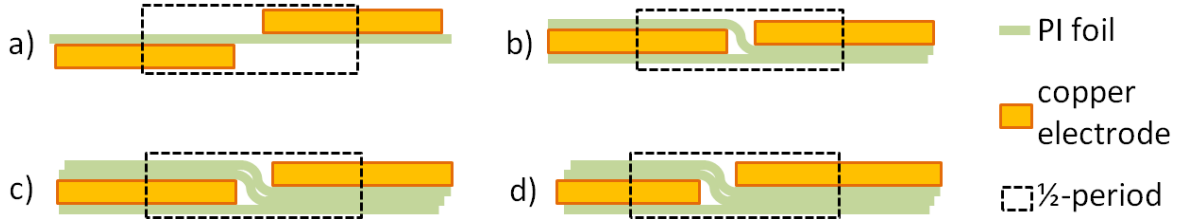


Figure 17: design iterations of electroadhesive layout: a) electrodes placed on opposite sides of insulator foil, b) adding frontal insulation and flattening, c) improving insulation in between the electrodes compared to the insulation toward surroundings, d) optimizing frontal- to backing-electrode width ratio (for detailed explanation see appendix D.1), $\frac{1}{2}$ -period is used for the simulations.

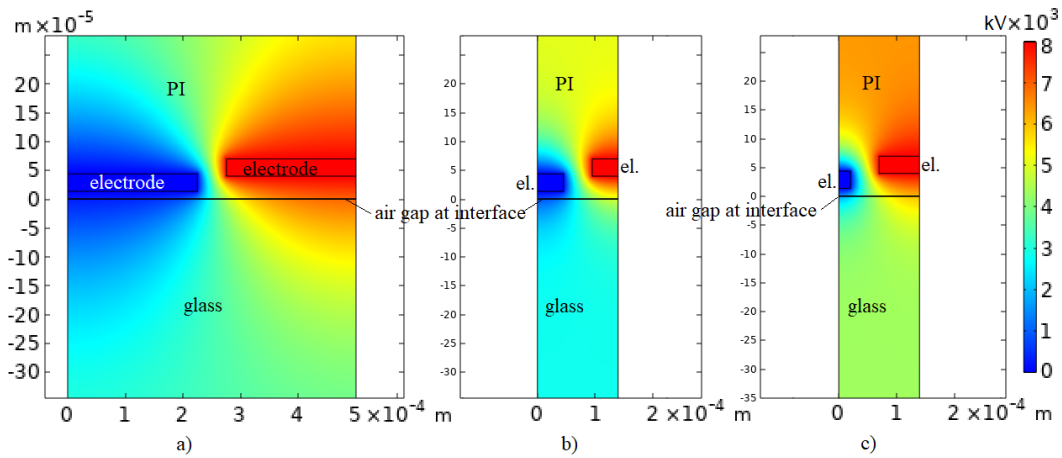


Figure 18: electrode width optimization from simulation results of one half period of infinitely long, parallel electrodes: a) implemented first guess of half period, b) optimized half period, c) optimized frontal- to backing-electrode width ratio, details on iterations given in appendix D

breakdown strength. Thus the limiting factor becomes the breakdown strength within the attracted object.¹¹ The potential that is applied to the electrodes is therefore limited to a value that will not induce failure of the glass.

Apart from monitoring the limitations given by deliberate surrounding materials the latter field of optimization also includes minimizing the amount of air and other contaminants that are trapped in the contact interface. This is discussed shortly at the end of appendix D.2, however this specific topic is left to be done as a separate piece of research (see latter part of "3.Further optimization possible" below).

A remark on the used permittivity for glass: The permittivity of glass can differ

¹¹This introduces a new known and fixed parameter to the optimization, which could open up improved methodologies for optimization.

strongly. The design is optimized for low permittivity glass, as higher permittivity glass will suffer less from breakdown if it has the same breakdown strength, due to the lowered electric fields within it. At the same time it will achieve a higher attraction force, even if the electroadhesive design is optimized for low permittivity glass. This is why it makes sense to optimize the design for the lowest expected permittivity, rather than some averaged permittivity.

2.Result:

By systematically adjusting parameters a powerful electroadhesive that is specialized for attracting glass is found. In simulation it achieves an electrostatic pressure of $2860N/m^2$ on low permittivity glass, while all involved breakdown strengths and permittivities are taken into account and a high level of additional electric insulation is included due to the reduction of the applied potential (see appendix D.2).

Being optimized for glass, on this dielectric it achieves $\approx \frac{1}{5}$ of the attraction force as on conductors. This can be judged as a close to optimal design based on the findings described in appendix B.1, in which the force of a multi-electrode electroadhesive on conductors is compared to the force on material with a relative permittivity of $\epsilon = 5$.

The attraction of this design on a conductor can also be further increased by using a higher electric potential on the electrodes, because the breakdown strength of glass must no longer be considered. In this case the limiting factor is the breakdown strength of the insulation material. In simulation a force of $670600N/m^2$ is achieved, as a result of taking the electric field to the highest material limit available ($315kV/mm$ of Polyimide foil [25]). This is by far higher than practically verified attraction forces found in literature (e.g. [22][11]), however the found examples do not make use of Polyimide foil.

The attraction pressure of $2860N/m^2$ on glass is also higher than what is achieved by most published designs. The only found pad design reported to have exceeded this electrostatic pressure on glass is the one by H. Prahlad et al.[11] that is claimed to have achieved approximately three times this pressure on glass. However no information was found on the permittivity of the glass used in the test, or on the specifications of the design that achieved this attraction.

3.Further optimization possible:

Further optimization on the above developed design can still be done. Some directions of optimization are the reduction of insulation due to the reduced potential and the reduction of the copper plating thickness. Both of these steps can bring the

electrodes closer together and thus further reduce the inactive portion of the adhesive area. Another direction is up-sizing of the pattern, which is possible as long as the attracted body does not become too thin for the range of the generated electric field. This direction of optimization becomes more interesting the rougher the attracted surface is expected to be, as it allows to introduce a thicker layer of soft coating for better contact on rougher surfaces. It may also simplify production due to a less fine electrode structure. For the soft coating it is important to choose a material that has a relative permittivity that is as low as possible and a breakdown strength that is high enough to not introduce a new lower limit to the electric field. Silicone for example is attractive, because of its elastic properties and its high dielectric strength.

6.4 Applying in-contact adhesion to cleaning robots

It was mentioned in the introduction that it would be preferable to realize an attraction across a larger air gap so that the force can be applied permanently without the electroadhesive having to be incorporated in the tracks of the robot. As the distance dependence of the breakdown strength of air prohibits high attraction forces over larger distances, in-contact electroadhesives are the superior technology to this respect.

For this technology to be implemented on industrial cleaning robots some challenges still have to be overcome. If the electroadhesive is incorporated in the tracks the power supply to the electrodes requires special attention. In order to prohibit the accumulation of shielding charges on the surface of the tracks from areal breakdown, only the electrodes in the parts of the tracks that are in contact with the surface may be powered up. Before each section separates from the glass surface the electrodes must be discharged. Additionally, conducting brushes can be used to help neutralize the inevitable level of accumulated surface charge that collects during adhesion.

Instead the idea of implementing electroadhesion to increase the safety of these robots could be reduced to an anti-slip-off device in the form of an electroadhesive plate underneath the robot's body that is brought into contact with the glass surface and powered up in the case that the robot loses its traction and begins to slip off. This would fully eliminate the challenge of moving, open contacts for the high voltage supply to the electrodes and also the need for powering up different sections of the electroadhesive at a time.

In both cases additional precautions must be taken to ensure that the surface on which the electroadhesion is meant to take place is kept dry at all times, as fluid water will nullify the electroadhesion due to its conductivity. This is challenging considering that the industrial cleaning robots work with water and additionally may be deployed

during wet weather. For small window cleaning robots this is less of a concern as their use can be limited to dry conditions.

7 Design criteria for attraction over an air gap

Even though the attraction over a larger air gap has proven to be very limited the drawbacks of in-contact electroadhesion with respect to cleaning robots make it interesting to have a look at the possibilities given by this second approach.

7.1 Choice of adhesion technology

From the insight gained so far it appears most attractive to analyze the residue surface charge option in more detail when it comes to attraction forces over a larger air gap. As mentioned before in contrast to the residue surface charge approach the parallel capacitor design has no use for this application as it cannot attract dielectrics, while it is advantageous for demonstration purposes due to its simplicity and also is a great solution for robots navigating on conducting surfaces. The multi-electrode dielectric attraction approach is a promising and reliable approach at least for dry, in-contact solutions. However, because it relies on the dielectric constant of an attracted non-conducting material the maximum force is further reduced by this property, because dielectric attraction involves attractive as well as repulsive forces. It is however comparatively well studied and can be implemented even for the attraction over an air gap if required from the information that is collected in section 6 and given in literature by optimizing the pattern for larger distances.

The residue charge approach brings forth a few superior properties for this specific application: It relies on pure attractive forces between opposite charges which for glass results in an approximately 4 fold increase in force compared to the dielectric attraction approach (see appendix B.1) and is less affected by wet and otherwise contaminated surfaces. It seems to be a novel approach for this type of application. Residue surface charge is typically used in industry on particle surfaces in material separation processes or particle dispersion as is described for example by A.D. Moore in "Electrostatics and its applications".[2] It is also used in electrostatic motors and generators, which however have not gained the same power density as their electromagnetic counterparts and therefor are not widely used in industry.

Conclusion:

If it can be shown that surface charge densities on a similar level to those within the parallel capacitor (section 5.2) can be maintained, then for two surfaces that do not come into such proximity to one another that they make contact the technique of surface charge attraction (schematic is repeated in figure 19) is superior to the dielectric attraction method.

Furthermore the direct treatment of the glass surface with a high density of charges is expected to have the strongest effect on aiding the cleaning process (see section 8).

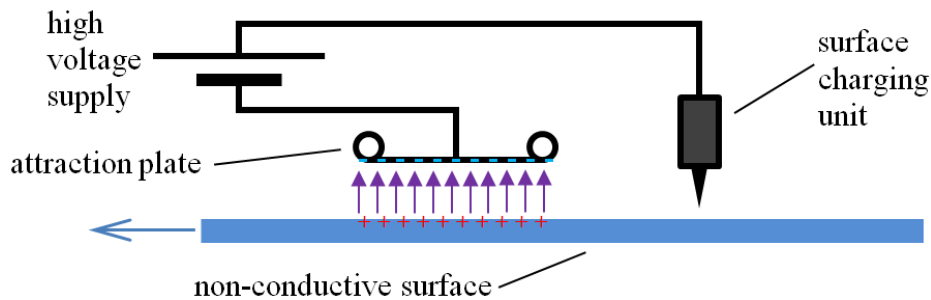


Figure 19: Basic configuration of a surface charge attractor, as is described in section 4.3

7.2 Aspects of residual surface charge

1. The limit to residual surface charge:

In section 4.3 multiple techniques to achieve residue surface charge are introduced. It has proven hard to find comparable information on the capability of different surface charging techniques to achieve high charge densities. This is even more the case if the efficiency or speed of the charging process is to be compared. The information given by B.W. Lee et. al on the triboelectric series [3] gives the impression that with sufficient frictional input any charge density can be achieved, since no limitations are given there. The ultimate limitation in the end would be flashover from exceeding some breakdown strength. In their paper on maximum surface charge density for triboelectric nanogenerators [35] S. Wang et. al state that triboelectrification can only reach a charge density in the region of tens of $\mu C/m^2$ even with their material combination that is specifically chosen for the generation of high surface charge levels through friction, whereas their plasma charging technique can realize $630\mu C/m^2$. However it is made clear that this high value can only be reached due to the fact that in the plasma-charged configuration a thin film was charged that utilized a grounded conductive coating on the back side to carry the opposite charge, thus reducing the electric field within the surrounding air and prohibiting break down.

The highest possible charge density that can be sustained on a surface within air without inducing breakdown can be obtained theoretically. According to the calculation performed in "Electrostatics: Principles, problems and applications" by J. Cross [14] with an electric field that is limited to $3kV/mm$ in air, the maximum surface charge is $26.4\mu C/m^2$. It is further mentioned that this is the mechanism limiting frictional surface charge within air, that otherwise could easily reach far higher values.

If this surface charge value is used for equation 17 for parallel capacitors as the charge on one of the two plates such that $\frac{Q}{A} = 26.4\mu C/m^2$ and the equation is divided by the plate area we obtain:

$$f_{max_surface_charge} = -\frac{1}{2\epsilon} \left(\frac{Q}{A} \right)^2 = -39.4N/m^2 \quad (34)$$

where the "−" marks that it is an attractive force for two oppositely charged plates. This result resembles - apart from a small rounding error - the maximum force that was found earlier on for a capacitor in air.

Concluding:

This value of $26.4\mu C/m^2$ is the actual value relevant for cleaning robots as no grounded backing layer can be introduced, as it was done by S. Wang et. al.[35], which trivially is the same restriction as for any parallel capacitor in air and independent of the surface charging method.

Illustrative side fact: A further derivation in the book of J. Cross [14] shows how little charge a surface charge density of $26.4\mu C/m^2$ actually is. By using the approximate atomic density of a solid surface of $2 \cdot 10^{19}$ atoms per m^2 it is shown that approximately only eight out of every million atoms on the surface carry the charge of a single electron.

2.Applied to cleaning robots:

As it is the breakdown within the surroundings of the charged surface that is ultimately limiting the surface charge density, it can be expected that the maximum charge density does not primarily depend on the mechanism used to achieve it and that the achievable initial charge density on the surface of an insulator will not significantly differ from what is possible on a parallel capacitor with conducting plates.

For the implementation on a battery powered machine it is of further interest to also establish the efficiency of different surface charging methods as a further parameter to decide on which technique to use. Little information was found on this topic.

The challenge could be to counteract the dissipation of charge over time that can occur from low level conductivity:

An experiment was executed to give a first impression on how well surface charge lingers on a clean glass surface (Appendix E.1). It showed that on a dry surface a significant amount of charge resides for a period in the order of minutes (see figure 20), which is a positive outcome for the use during surface attraction beneath a moving

robot. The forces achieved on this setup are lower than what is found for the parallel capacitor in section 5, which suggests that the maximum charge possible until areal breakdown (see part 1 of this section) is not reached during the used charging process.

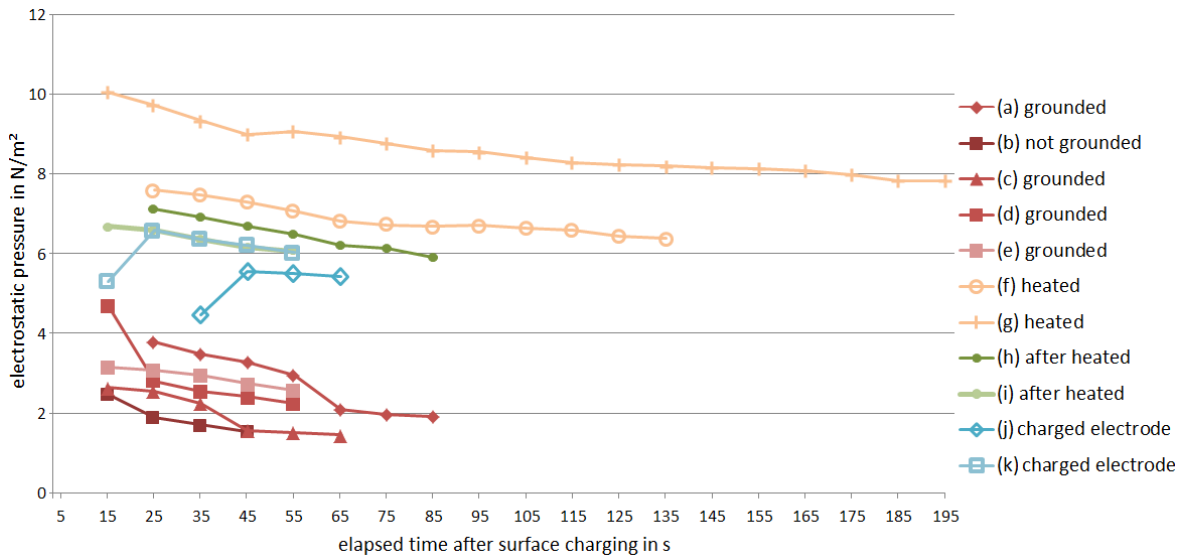


Figure 20: Force data from the glass surface charging experiment, the measurements were conducted in alphabetical order and are described in appendix E.1.

The design for a further test setup is suggested (see Appendix E.2) that demonstrates the attraction force on a wet and contaminated glass surface during exposure to an electric field. The setup is depicted in figure 21. Due to the conductivity of the wet contamination the principle is similar to that of the parallel capacitor design (see section 5) and therefore similar results are expected.

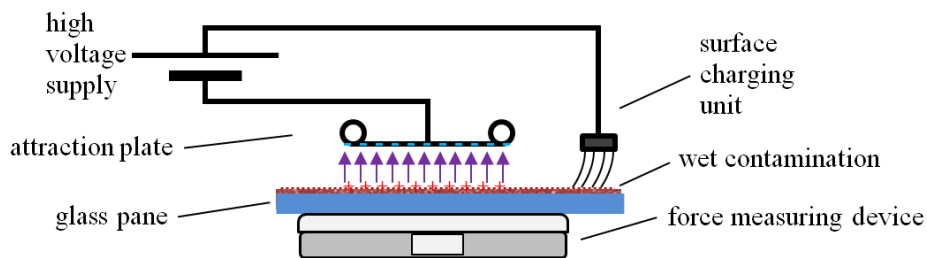


Figure 21: Suggested design of experimental setup for measuring the attraction force on the contaminated surface of an insulator

Conclusion:

It is expected that residue surface charge can achieve similar attraction forces as the parallel capacitor setup from section 5 if the charge can be sustained, which remains to be shown with a setup such as the one depicted in figure 21.

8 Plasma aided surface cleaning

This section treats the effects of introducing charged particles to the surface cleaning process. To date the robotic cleaning of glass roofs, windows and solar arrays is done with brushes and supported by applying water.

8.1 The combination of surface attraction and surface cleaning

All the forms of electrostatic attraction include strong electric fields which will leave behind some level of surface charge. Surface charges in turn attract polar molecules such as those of water, thus increasing the wettability and the speed of wetting of the charged surface.¹² Therefore this aspect is of great interest in combination with the previously described attraction mechanisms. The strong electric fields involved in the electrostatic attraction process induce multiple mechanisms that lead to the accumulation of charges on the surface of insulators. Firstly the fields propel existing charged particles in the direction towards the opposite charge so that such particles are accelerated and accumulate on object surfaces that they collide with if the charge is not conducted to ground. Additionally, if the electric field intensity exceeds the breakdown strength of the surrounding air or other media, then the resulting discharges will generate an avalanche of ions and lead to a fast flow of charges that subsequently can accumulate on insulating surfaces of materials with higher dielectric strength. In the case of deliberate surface charging that is used for the residue surface charge attraction such ionisation of the air is brought about intentionally and the produced ions are guided to the substrate surface by an electric field that is applied for just this purpose.

The high voltage and charge producing technology that is on board the cleaning robot for attraction purposes can be extended to additionally aid the cleaning process as best as possible. Firstly this would include additionally applying surface charge before the cleaning process, rather than solely during the surface attraction, which should preferably take place after the respective region has been cleaned. Secondly the charges would be applied over the entire cleaning width rather than just in the zone where the attraction shall occur.

¹²A detailed examination of the influence of surface charges on the wettability and wetting kinetics of a titanium-dioxide surface was done by L.S. Puah et al.[24]

8.2 Plasma treatment of surfaces in general

For the experimentation cold plasma is chosen as a safe and ready-to-use source of surface charge treatment.

Low pressure plasma has been used for a while for thorough cleaning of sparsely contaminated surfaces in laboratory and industrial processes. A new and growing sector is the use of atmospheric pressure plasma for surface treatment and cleaning. According to suppliers of this technology this reduces the complexity of the tools and therefor the involved costs by eliminating the vacuuming equipment.[32] This is even more the case if simply air rather than a special gas or gas mixture is used as the ionized medium. These developments are allowing plasma treatment to become more available and useful to industrial processes.

Tools for the safe and reliable production of cold plasma are readily available, which is why this technology is chosen as the source of ions for the surface cleaning experiments.

High frequency electric fields are used to excite the air particles until some of them become ionized. This low level ionization of gases is termed cold plasma. It contains a sufficient amount of excited charged particles, which are highly reactive, to induce reactions on the treated surface. The ionized particles carry similar energy levels to those of organic chemical bonds and thereby can vaporize small amounts of organic matter by breaking up such bonds.

These effects are however too weak and slow to be used for the decontamination of grimy surfaces such as roofs and solar arrays. During the search for suited plasma applications for this experimental setup also plasma applications of higher power were encountered, but the use of these tools on surfaces that shall stay intact is explicitly not recommended by the manufacturers, as these tools are meant for the removal of surface material. For this reason plasma treatment alone cannot replace the mechanical cleaning process, but it is expected to have a measurably positive effect on the cleaning process. While the treatment with charged particles can help to break up bonds, the residue surface charge can increase the wettability, i.e. reduce the contact angle of water on the surface and therefor increase the effectiveness of the water in washing away particles.

8.3 Testing plasma aided cleaning

In this section a model system is proposed that can quantify the cleaning progress. The effectiveness of cleaning with and without cold plasma treatment is measured.

The experimental process is designed to give a first evaluation on whether the application of charges in the cleaning process produces significant benefits on the cleaning

result.

The contamination of the glass surface will be evaluated by measuring the surface roughness with confocal microscopy and by comparing the contact angles of water droplets on the clean and the contaminated glass surface. Furthermore the surface data from the confocal microscope will be used in an attempt to quantify the reduction in contamination volume on the surface.

1. Producing the model contamination:

To be able to do experiments on the decontamination of glass surfaces that have collected grime from being exposed to weather, first a practically useful form of contaminated surface must be found. It should be practical but close to the realistic case.

For the experimental method developed for this purpose it is chosen to contaminate the surface of microscope slides that are made of a clear white glass (low iron content) just as the glass that is used for photo-voltaic solar panels.

The constituents of the contamination on the surfaces in question are specific to what is deposited by rainfall and wind. Therefore it is chosen to directly collect the contamination off a surface that has been exposed to such an environment.

The preparation of the samples is described in detail in appendix F.1. Figure 22 gives an impression of the steps involved.

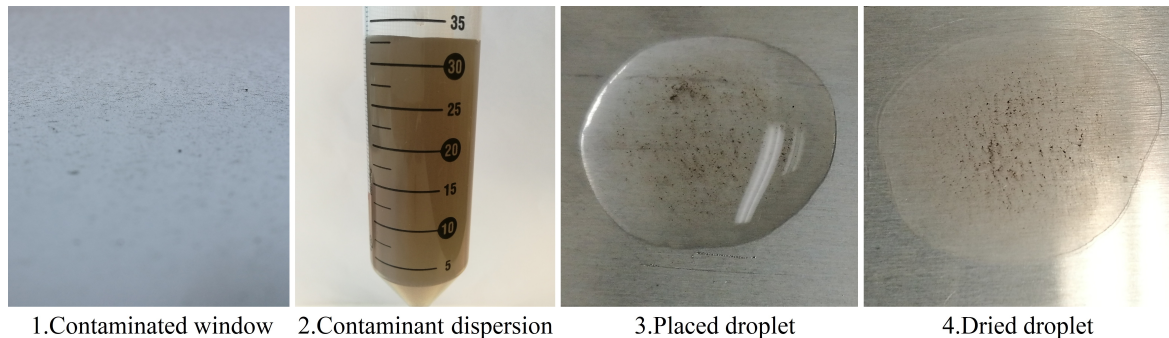


Figure 22: preparation stages of contaminated specimens

A single batch of contamination fluid is produced at a specified concentration that corresponds to the surface area from which the contamination was collected and the area of the dried droplet.

When observing the produced specimens it becomes clear that there exists a strongly contaminated region in the centre of each dried droplet and an outer less coarsely contaminated region. These are treated separately in the results analysis.

Via confocal microscopy and contact angle measurements the contamination states

of the different regions are specified. The different contamination states are clearly distinguishable from one another using the chosen measuring devices, while the results between specimens are consistent across the batch (see appendix F.2).

The roughness and contact angle measurements in the non-contaminated regions of the contaminated specimens are compared to the originally not contaminated specimens, reassuring that handling the specimens has not introduced further unintentional contamination to the surface.

These three aspects point to a model system with repeatable and meaningful i.e. distinguishable results.

During the cleaning process it is also of interest how effectively the volume of the deposited contamination is reduced. For the attempt to quantify the contamination volume one further area directly on the edge of the contaminated region is scanned. The clean part of the scanned area is then used as a height reference. A typical result of such a scan is shown in figure 23. The large contamination volume directly at the edge and low volume contamination further into the contaminated zone make this volume measurement less dependent on the exact proportion of contaminated area compared to clean area of the scanned region. After the height values are corrected by using the clean region as reference, the height values of all measured points are added to yield the volume.

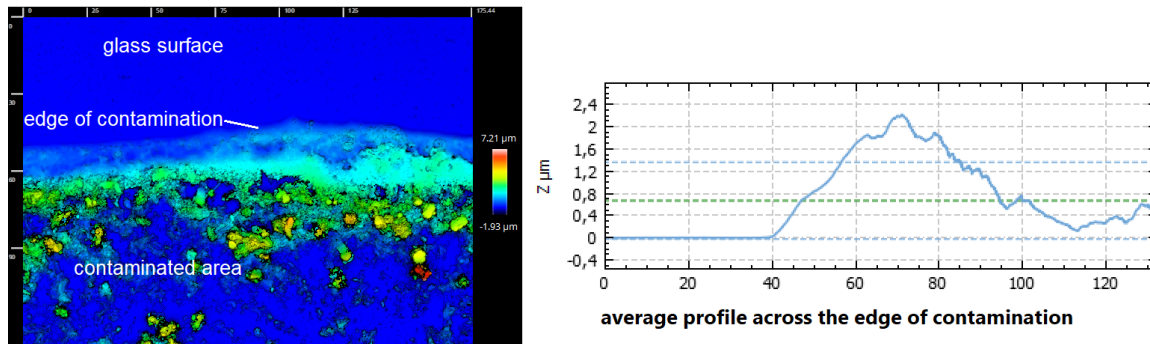


Figure 23: An example of the contamination height profile at the edge of the contaminated area

2.Removing the model contamination:

After the non-contaminated and contaminated states have been specified as described above, the contamination is removed with different methods so as to compare their effectiveness.

The classical cleaning case as it is done by the cleaning robots involves water as a solvent and a mechanical component in the form of scrubbing brushes. To make the

cleaning process reliably repeatable for the experiment the mechanical component is realized by ultrasound rather than a brushing mechanism to better control the energy input. The contaminated samples are suspended at a specified position and orientation in a beaker of distilled water that is hung into an ultrasound water bath.

It was found that a few seconds ($\approx 10s$) of this treatment suffice to remove the large individually visible particles, while a few minutes ($\approx 5min$) of treatment are necessary to visually remove the white crust from the glass' surface. Merely dipping or soaking the sample in water without adding mechanical work does not have a visible cleaning effect. This is also not expected, because this type of contamination is normally deposited by rainfall.

This experiment aims at finding out if the cleaning process is faster if the specimens are first treated with cold plasma (piezobrush PZ3) before they are cleaned. To be able to distinguish between the cleaning result of the ultrasound bath without pretreating the specimens with plasma, to the result of the ultrasound bath on specimens that have been pretreated with plasma, the cleaning duration is reduced below the above stated time spans. Furthermore, to generate information on the cleaning effectiveness with respect to the easily removed larger particles as well as the finer more recalcitrant contamination a two-stage cleaning and analysis process is chosen:

Two-state cleaning process without plasma:

First the contaminated samples are placed into the ultrasound bath for 5s and then retrieved, left to dry and scanned with the confocal microscope. Then they are placed back into the ultrasound bath for a further 60s before repeating the drying and the confocal surface analysis. In a last step the contact angle on the cleaned glass is determined.

Repetition of two-state cleaning process with plasma:

The just described procedure is then repeated with another set of specimens that are treated with cold plasma directly before each cleaning cycle.

In total four specimens are chosen for the cleaning comparison. Two receive no plasma treatment, while the other two do.

In appendix F.3 it is described how an appropriate plasma treatment duration is found. A plasma treatment duration of 10s is chosen as an acceptable time factor compared to the effectiveness. It is also found that the effect of the plasma treatment on the contact angle remains over the time span of half an hour. This means

that during experimentation slight variations in the time between the plasma surface treatment and the cleaning process should not have an effect on the results.

8.4 Results from plasma aided cleaning test

The cleaning of all samples and the surface measurements were conducted over the course of one day to reduce effects of changing surrounding parameters. The roughness analysis and the contamination volume analysis have been used to quantify the cleaning efficiency, and they show similar results with differing information content.

The roughness measurements, the average values of which are displayed in table 3, give more insight into which regions of the contaminated spots clean in which manner. Regardless of the cleaning treatment with or without plasma the most coarse contamination is removed effectively within the first seconds. Also the contamination by the edge of each droplet is hardest to diminish in both cleaning scenarios.

Differences between the two cleaning scenarios are visible in all regions: The treatment with plasma results in an increased cleaning effectiveness in all regions of the contaminated spots although not to an outstanding degree. The clearest difference lies within the outer region of contamination. This fine contamination shows to be the most resistant against the ultrasound cleaning process, while combined with the plasma pretreatment this region becomes the one that is cleaned most effectively. The degree of cleanness reached by this cleaning procedure in this region is close to the pristine uncontaminated surface: Measured by roughness it is an S_q value of $0.0125\mu m$ that is achieved by cleaning compared to an uncontaminated roughness value that was measured to be $0.0093\mu m$ on the clean regions of both the plasma-treated and non-plasma-treated specimens. Therefor almost the roughness of the uncontaminated glass surface is reached.

averaged S_q roughness values in μm	without plasma pretreatment			with plasma pretreatment		
	original	short bath	long bath	original	short bath	long bath
centre of contamination	1.75	0.17	0.03	2.38	0.15	0.02
outer contamination	0.52	0.25	0.04	0.50	0.05	0.01
edge of contamination	0.87	0.47	0.04	0.82	0.28	0.03

Table 3: The development of the surface roughness during both cleaning processes is displayed, with red, yellow and green colouring marking the reducing roughness.

The contamination volume gives more precise information on the actual progress on the removal of contamination. Table 4 shows the averaged results from the measured edges of the contaminated region. Each measurement was performed on a single rectangular scanning region of $175\mu m$ by $132\mu m$ to reduce scanning time. Furthermore

it was not always possible to relocate to the originally scanned section. In all cases an approximately representative section for the respective specimen was chosen. The accuracy and reliability of the results could be increased by scanning the entire contaminated region. This procedure, however, would have required too much time for the current situation. Nevertheless the results give quite clear indications.

After the first short ultrasound bath a difference is already visible in the portion of contamination that is removed. While the plasma treated specimens lost 75% of their contamination the untreated ones lost 59%. After the second long ultrasound bath the untreated specimens remain contaminated by approximately 9 times as much deposited material as the plasma treated ones.

contamination in edge region	volume in μm^3			percentage of contamination removed		
	original	short bath	long bath	original	short bath	long bath
no plasma treatment	13675	5593	340	0	59.1	97.5
plasma treatment	12498	3122	38	0	75.0	99.7

Table 4: The development of the averaged volume of contamination within one scanned area of $175\mu\text{m}$ by $132\mu\text{m}$ after the successive cleaning steps is displayed on the left, while the right hand side shows the respectively removed percentage of contamination compared to the original contamination.

The actual volume reduction values enable the calculation of a half life for the cleaning process. Beginning with the decay formula:[29]

$$P(t) = P_0 e^{-\lambda t} \quad (35)$$

with the original proportion of contamination being $P_0 = 100\%$ and $P(t)$ being the remaining proportion of contamination at time t , rearranging yields the time constant as

$$\lambda = \frac{\ln \frac{P_0}{P(t)}}{t} \quad (36)$$

The half life is defined as:

$$t_H = \frac{\ln 2}{\lambda} \quad (37)$$

resulting in

$$t_H = \frac{\ln 2}{\ln \frac{P_0}{P(t)}} t \quad (38)$$

The proportion of contamination is known at three points in time. These are t_0 before cleaning, $t_1 = 5\text{s}$ after the short ultrasound bath and $t_2 = 65\text{s}$ after the long ultrasound bath. These yield four half lives from the two different cleaning procedures and the two measuring points (see table 5). The large difference in the calculated half lives for

the two different time points respectively indicates that there are indeed at least two different cleaning processes occurring: one being the dislodging of large solid particles and the second being the removal of fine, possibly partly soluble contamination. Both processes overlap.

Remarkably, in both of the stages of the cleaning process that were observed the plasma treatment resulted in a reduction in cleaning-half-life of 36%.

halftime in s	short bath	long bath
no plasma treatment	3.9	12.2
plasma treatment	2.5	7.8
reduction by	36%	36%

Table 5: The four half lives from the two different cleaning procedures and the two measuring points respectively; the numerically identical reduction in cleaning-half-life for both time points of 36% is more coincidental than owing to the preciseness of measurements.

Conclusion:

As the duration of 10s required for the plasma treatment itself is low compared to the cleaning period of approximately 1min that was required to gain a relatively clean surface with this setup, the reduction of 36% in cleaning time for the same cleaning result appears attractive. In the case of a faster cleaning process the duration of the charge treatment may have to be shortened too.

Remark on residual contamination:

During the cleaning process no contact angle measurements were taken. The contact angles measured after the cleaning process show that the effect of the plasma treatment barely wears off during the cleaning process in the ultrasound bath. The contact angle on the two plasma treated specimens remained at 14° and 19°, which is only just above the contact angle of around 10° directly after plasma treatment. In contrast to these low contact angles the angles measured on the two non-plasma-treated specimens are decisively high at 60° and 70°. This indicates that a smooth, i.e. not rough, hydrophobic residue contamination was left on the glass after cleaning. For comparison the non-contaminated specimen was subdued to the contact angle measurement before and after having been treated in the ultrasound bath. This yielded an average contact angle of 39° and 42° respectively, confirming that the ultrasound bath itself does not unintentionally have a significant effect on the contact angle of the clean sample.

9 Final conclusions

It remains to evaluate what the examined technologies yield for cleaning robots and in which directions further investigation seems useful. The next parts treat both of these points.

9.1 Usability of the attraction forces for cleaning robots

This section refers back to the robot dimensions defined in the introduction in section 2.1. Here the found attraction forces are put into relation with the aim of increasing the gradeability of the described robots.

1. Attraction over an air gap:

The investigation including the gradeability calculations in appendix G has shown that the originally favoured idea, to place a solid attraction panel underneath the robots body that induces the attraction force over an air gap of multiple millimeters (see section 2.1), is not feasible for the described cleaning robots (increase in gradeability $\leq 1^\circ$). It was shown that theoretically the attraction force of such a device could not exceed $39.8N/m^2$ due to the breakdown strength of air (first mentioned in section 4.1). Furthermore the performed experiments gave the insight that the practically achievable force is considerably lower (section 5). One factor with a considerable influence is the effect of water droplets in the attraction area. The experiments show that a realistic attraction of $\approx 1/3 \dots 1/2$ of the theoretical maximum in air can be achieved over a distance of multiple millimeters for the case that the surface can be optimally charged. It remains to be shown that such a charge can be sustained on the contaminated surface of an insulator (see appendix E.2 for the suggested experimental setup).

While the attraction over a gap turns out to be not useful for traditional cleaning robots, it may remain interesting for situations in which water on the attracted surface can not be avoided, but a super lightweight design in comparison to the attraction area is feasible. For example at a gradeability of 45° an attraction area of $\approx 0.4m^2$ per kg of weight is necessary, that could be realized with an adapted large lightweight panel design.

2. In-contact electroadhesion:

The in-contact electroadhesion is promising for increasing the gradeability of robots from the force point of view. Multiple examples in literature show that useful forces can be achieved practically (see appendix B.3). The interdigital electrode design optimized

for glass in section 6.3 showed an electrostatic pressure of $2860\text{N}/\text{m}^2$ in simulation, while all breakdown strengths of the included materials were taken into account. It depends on the quality of contact that is achieved by a practical design and the cleanness of the contact area (appendix D.2), how well this force can be achieved in practice. This form of strong attraction is only possible on surfaces that are not contaminated with materials with low breakdown strength or with conductive fluids. These can reduce or eliminate the electrostatic attraction.

The calculations show that the gradeability of industrial cleaning robots increases from 25° to 39° with the electrostatic pressure from above (appendix G), which is a significant increase that can extend the working range of these robots.

For small scale cleaning robots this electrostatic pressure exceeds the robots typical weight (appendix G), allowing it to hang up side down if appropriate mechanical measures against gradual peel off are taken.

This means that for a mobile and constantly active electroadhesion approach it is inevitable to find a commercially feasible caterpillar track design that incorporates the electroadhesion modules. Furthermore measures must be taken to ensure that the surface on which the tracks run is clean and dry.

The suggested alternative use of an electroadhesive on industrial cleaning robots, as a safety mechanism that is only brought into contact with the surface to break the robots slip, is also feasible with respect to the achieved attraction force. However in the case of uncontrolled slipping, guaranteeing that the adhesion area below the robot is clean and dry becomes more challenging.

9.2 Usability of surface charge treatment for the cleaning process

The original question regarding the cleaning process is if it makes sense to combine the surface charge effects of electroadhesion technology with a new grade of cleaning equipment that profits from residue surface charge.

The conducted experiments show that treating the surface with cold plasma can reduce the cleaning halftime by 36% (section 8.4). This may or may not be sufficient motivation to implement this technology on glass roof, solar array and window cleaning robots depending on the emphasis in product design.

Firstly in the case that high voltage equipment is set up on board the robot for surface adhesion purposes, it is a smaller step to extend this equipment to deliberately deposit surface charge on the to-be-cleaned area. Presumably the most straightforward

technique to distribute charged particles, once a high voltage supply is on board the robot, is to utilize corona discharge from sharp metallic tips (section 4.3).

Secondly cleaning velocity is a strong argument in the cleaning industry so that implementing this technology could become feasible even without combining it with electroadhesion technology.

9.3 Ideas and recommendations for further research

This thesis has looked closely at the different options available for electroadhesion and gives information on how to optimize the design of interdigital electrode adhesives as the most promising electroadhesive technology for cleaning robots. It has also found that electrical treatment of the contaminated surface accelerates the cleaning process. Below the most pressing questions in four research direction are outlined.

1. Quality of surface contact in practice:

While the parameters affecting the quality of contact: surface roughness, material stiffness and surface cleanness, have been named and their effects in the contact zone explained, it has not been treated in detail how well practically a nearly air-free contact zone can be realized. For real-world usability of a certain adhesive design the sensitivity of the electrostatic pressure to certain types of residual surface contamination should be analyzed.¹³

2. Other aspects of implementation:

Apart from optimizing the electroadhesive itself some peripherals need to be considered in more detail, too. For the implementation of in-contact electroadhesives in situations that can involve water or other fluid and conductive surface contamination, engineering solutions must be found to prevent the zone that is used for adhesion from being wetted. To be able to implement in-contact electroadhesives for industrial cleaning robots, overcoming this challenge is a necessity.

It may also be interesting to investigate further on the attraction from a distance via surface residue charge on contaminated surfaces. However applications for this have yet to be found.

3. Effectiveness of surface charging methods for enhanced cleaning:

Regarding surface-charge enhanced cleaning it should be of interest to determine

¹³For example a small number of large grains dispersed on an otherwise smooth surface will have a stronger effect on an electroadhesive with a thin stiff frontal coating, than on a design with a thicker and more compliant coating.

the effectiveness and speed of different surface charging methods such as cold plasma generators and corona discharge units and their individual benefits on the cleaning process. Specifically charging speeds must be achieved that compare well with the current brush-cleaning velocity. Then the feasibility given by the reduction in cleaning time compared to the technical costs can be evaluated.

4.Safe grounding:

Lastly a safe, reliable manner of grounding such a robot that is working with high voltages and deposition of charges must be provided as well as further safety mechanisms to deactivate all high potential sources once the robot is not in regular operation. The robot must be uncharged before it can be touched or handled manually.

A Details of experiments on attraction forces over an air gap

The following sections give details on the experimental procedure for the evaluation of the effect of air and other contamination in the attraction interface in section 5.1. It is important to have an experimental configuration that gives results that can be applied as best as possible to all versions of electrostatic attraction devices. A design is chosen that will generate the best possible charge on the two surfaces that face each other and that does not depend on some form of optimization such as the maximization of charge density on an insulator's surface (residue charge attraction) or an electrode pattern that itself would be dependent on the separation distance (multi electrode dielectric attraction). Instead of such a pattern of oppositely charged electrodes, simply two opposing plane electrodes are used, forming a traditional parallel capacitor. To begin with these electrodes are left bare, without any form of electrical insulation. While a setup with non-insulated electrodes on both poles is not very practical for a real application, because of its ability to short circuit, its advantage for gaining an understanding of the principles is that attracted opposite charges will not accumulate on the electrodes surfaces.

In this manner an electrostatic attraction configuration with optimally charged counterparts is used to find values for the forces that are maximally possible in air. This (optimal charge) is not necessarily the case for the residue charge configuration nor for multi-electrode adhesives in general, but it will produce an insight into the given upper limits, independently of the technology used.

The idea is that within the medium air, it is not possible to generate forces above a certain limit, due to the breakdown field strength of atmospheric air at approximately $E_{max_air} = 3kV/mm$ and that non-insulated electrode surfaces are capable of sustaining the highest forces for a given configuration (in size and separation distance) due to their capability of neutralizing attracted charges on their surface rather than accumulating them.

Equation 33 is repeated here as it is the theoretical limit to the following experiments:

$$f_{max_air} = \frac{1}{2}\epsilon E_{max_air}^2 = 39.8N/m^2 \quad (39)$$

A remark on the execution of the experiments: The setup-build and experimentation for this section were executed entirely in private premises. Avoiding laboratory and workshop visits on the one hand made the process very efficient, eliminating complications and delays due to the corona pandemic regulations. On the other hand it

put restrictions on the manufacturing possibilities and available equipment. Nevertheless the desired experiments could be conducted to a satisfactory degree and a lot of useful experience was gained on the practical work with high voltages in electrostatic applications.

A.1 Build of experimental setup to test non-insulated and insulated electrodes

The setup consists of two powered electrodes that form a parallel capacitor. Their distance to one another is adjustable and the attractive force is measured.

To gain an estimation of the output potential of the used high voltage power supply, the maximum flashover distance in air is found. To reduce the effects of sharp corners that promote ionisation of the air due to local peaks in the electric field, the contacts are connected to spheres of about $20mm$ in diameter that are covered in aluminium foil to get closer to a uniform field. The maximum flashover distance for the bare contacts was at $12mm$ and the minimum separation of the ball electrodes for which no flashover occurred was at only $x = 5mm$. The large difference in distance shows that the ball-electrodes have contributed strongly to the reduction of spikes in the electric field. Assuming a breakdown strength in air of $E_{max,air} \approx 3kV/mm$, the high voltage supply unit generates:

$$V_{supply} = E_{max,air} \cdot x \approx 3kV/mm \cdot 5mm = 15kV \quad (40)$$

It can be expected that due to the spherical electrodes the actual voltage is close to $15kV$, but more likely slightly below that, as the radius of the ball-shaped electrodes is still in the order of the distance between the spheres, so that the electric field in between will not have been uniform.¹⁴ Following from this finding, to begin with, the electrodes of the experimental setup are positioned with a separation of around $5mm$ to one another.

The force measuring device used is a weighing scale with a resolution of $0.01g \approx 0.1mN$ and a scale up to $200g \approx 2000mN$. An appropriate capacitor plate size is chosen, to generate forces in the order of the weighing scale's range. Using the maximum force assumption from equation 33 multiplied with the surface area, an area of $A = 100cm^2$ is chosen, resulting in an expected maximum achievable force of:

$$F_{max,setup} = \frac{1}{2} \varepsilon A E_{max,air}^2 = 398mN \quad (41)$$

¹⁴The post simulation of the experiments in appendix A.2.4 leads to the conclusion that the voltage is actually closer to $14kV$.

The experiment involves operating the capacitor close to the breakdown field-strength of air. This brings forth the necessity to avoid protruding sharp corners and edges. Therefore the capacitor plates are chosen to be of a circular shape with a large thickness with rounded edges. Figure 24 shows their construction.

The rounding of the electrode edges makes defining the frontal area difficult: The main attraction will occur in between the closeup, plane surfaces, but also the rounded-off edges will still develop some attraction as well as the extended field beyond the diameter of the discs¹⁵. It was chosen to scale the total projected frontal area to $A = 100\text{cm}^2$, knowing that the resulting mainly-active area is then smaller.

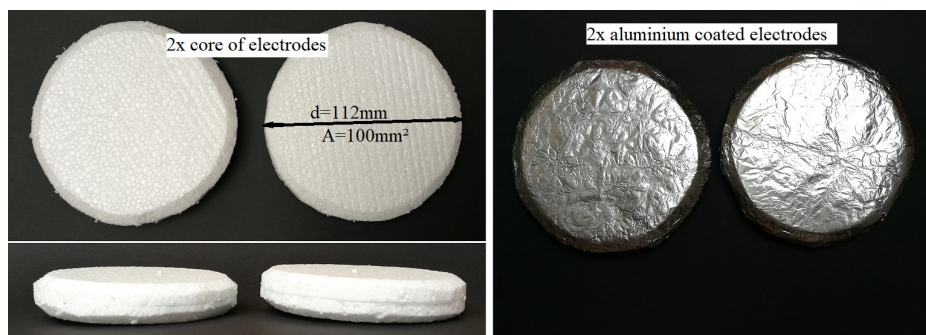


Figure 24: Test electrodes with a frontal area of approximately 100cm^2 ($r_{outer} = 56\text{mm}$), polystyrene cores (left) with aluminium foil finish (right)

The electrodes are constructed of a polystyrene core coated in aluminium foil. This makes shaping them easy and results in light weight electrodes, which is advantageous for the force measurement. The aluminium foil finish is not entirely smooth, but the irregularities are at the least an order smaller than the dimensions of the capacitor including the plate separation distance.

The finished setup (see figure 25) allows the upper electrode to be adjusted in height while the lower electrode is mounted freely on the weighing scale. As both electrodes need to be powered the lower electrode is also connected to the power supply via a flexible wire. The vertical motion of the digital scale due to changes in loading is however negligible so that the stiffness of the wire and changes in plate separation distance can be neglected. On startup the scale resets itself to zero. After that, any attractive force between the plates is displayed as a negative weight.

Experiments are conducted with open, i.e. non-insulated, electrode surfaces and with insulated electrode surfaces. The insulation is added by applying self-adhering plastic foils. The tool on the right hand side of figure 25 is used to neutralize any residual charge on the electrodes between measurement cycles and after operation.

¹⁵More details are given in a post simulation in appendix A.2.4



Figure 25: (left) The complete parallel capacitor force measuring setup, (middle) different electrode surface configurations from top to bottom: conducting-conducting, insulated-conducting, insulated-insulated, (right) electrode surface discharging tool

To increase safety during operation the setup is constructed inside a box and the power switch for the high voltage supply is located out of reach at a distance from the setup. In this manner it is ensured that the system can only be powered up from a safe distance. As long as the power is switched on, an unpleasant high pitch tone is clearly audible that keeps up awareness of the applied high voltage. The system is operated in a ventilated environment to avoid the accumulation of ozone.

A.2 Analysis of the conducted experiments and resulting forces

During the first operation it was found that in between the capacitor plates flashovers would still occur continuously at a distance of 5mm although this was not the case for the spherical electrodes. An explanation for this may be that due to the larger volume in between the plates more charged air particles are able to accumulate until a flashover can occur at a field strength that is lower than $3\text{kV}/\text{mm}$. This effect was sought for but not found in literature. In between the ball electrodes from the first voltage test this would not have been so much the case. Possibly also the irregularities on the plates' surfaces facilitate the production of ions increasing the aforementioned effect. An explanation for the opposite effect, i.e. a breakdown strength in air of above $3\text{kV}/\text{mm}$ during the voltage test with spherical electrodes, was not found. From this standing point there is no reason to expect the applied voltage to be higher than the found value and it remains probable that the actual voltage is somewhat below this value. The same configuration as used in the following experiments was analyzed in a post simulation (see appendix A.2.4). Comparing its results with those from the

first experiment allow for the conclusion that the supplied potential was indeed in the range of $14kV$ rather than $15kV$. Therefore in the following calculations this value will be preferred.

To fully eliminate flashovers the distance between the plates is increased to $7mm$. At this distance no full electrical breakdown of the air occurs. A slight hissing noise from in between the plates can be perceived. This gives the impression that - locally - low level corona discharge is still taking place.

A.2.1 First experiment: Non-insulated electrodes

This first configuration is used to test the setup and the reliability/repeatability of the measured values. Furthermore it gives information on the relation between calculated values and the forces that are actually produced on this setup. Lastly it provides values for the forces possible in air for an electrostatic attraction configuration with optimally charged counterparts.

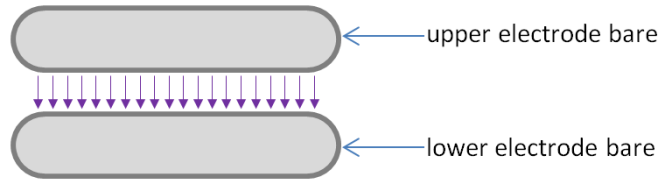


Figure 26

For the distance of $7mm$ the calculated attraction force using the estimated supply voltage is:

$$F_{expected} = \frac{1}{2}\epsilon A \left(\frac{14kV}{7mm} \right)^2 = 177mN \quad (42)$$

Five measurements were taken with an average result of $164mN$ with a maximum deviation between values of only $1mN$ (max: $164.4mN$, min: $163.4mN$). In between every measurement the power supply was switched off and the electrodes' surfaces were brought into electrical contact with each other with the tool displayed in figure 25.

The measured force is stable between measurements. Its level is lower than the calculated value but within a realistic range. There are a few parameters that include uncertainties. The first of which is the electrode area, as is explained in the previous section. If only the actual plane surface area is taken into account the radius is $r_{inner} = 50mm$ which replaces $r_{outer} = 56mm$ in the equation. This small difference has a quadratic effect on A that becomes:

$$A_{plane_area} = \pi r_{inner}^2 = 0.0079m^2 \quad (43)$$

and results in a calculated force generated by the plane electrode area of only

$$F_{plane_area} = \frac{1}{2}\varepsilon A_{plane_area} \left(\frac{14kV}{7mm}\right)^2 = 139mN \quad (44)$$

which is clearly below the measured value. This strengthens the notion that the attraction forces beyond the plane area cannot be fully neglected. In fact the post simulation in appendix A.2.4 gives an answer to this, yielding an equivalent surface area of $A_{equivalent} = 0.0094m^2$ in equation 52.

Also the voltage controls the force quadratically, so it could have had a considerable contribution to the lower force, as it could not be measured precisely. Calculating with the original plate area of $A = 100cm^2$ the measured force would be equivalent to a voltage of $13.5kV$ and calculating with the corrected plate area of $A = 94cm^2$ the measured force would be equivalent to a voltage of $13.9kV$.

Apart from that, inaccuracies within the measured plate distance also affect the force quadratically: Calculating with the original plate area and voltage the measured force would be equivalent to a plate separation distance of $7.3mm$. The uncertainty from reading the distance measurement is lower than this deviation, but it could also have played a role.

The measured force values given above represent only the initial force values. In every cycle the measured force dropped within seconds after switching on. Only the initial, maximum values were around $164mN$. The attraction force would drop by 5.5% to around $155mN$ within about 10s and stabilize there. An explanation for this lies in the generation of ions in between the electrodes. Each electrode produces ions of the same polarity as that of its own charge. This space charge forms a shield in front of both electrodes: the ions repel the electrode that they originate from and are attracted by the oppositely charged ions and opposite electrode, thus part of the attractive forces have been transferred to the air particles and do not contribute to the attraction of the plates to one another anymore. This effect increases until an equilibrium is found between the production and annihilation of ions on the two electrodes' surfaces.

In conclusion the knowledge gained through this experiment gives valuable guidelines for what can be expected from an attractor with non-insulated electrodes. Firstly it confirms that the force cannot exceed the previously calculated maximum value because at higher field intensities electrical breakdown will occur through the air, which however is by no means a surprise. Secondly it shows that realistically the attractive force is even substantially lower than that.

With a voltage of $14kV$, at a minimum separation distance of $7mm$ before electrical breakdown, an electric field of only 2/3 of the maximum electric field intensity in air

according to Paschen's law was achieved. Because the electric field intensity has a quadratic influence on the attraction force, the maximum achievable force per area ends up at $4/9 \approx 45\%$ of the theoretical value i.e. at $17.7N/m^2$ over the plane capacitor plate area. In appendix A.2.4 that discusses the simulation results, leading up to equation 54 it is explained why this is the value over the plane area. This is the same electrostatic pressure as was previously found analytically in equation 42.

It would be instructive to demonstrate the constant adhesion force for multiple distances. However the used power supply does not have the option to alter the output voltage and therefor can not be adjusted for multiple distances. A trial to use an isolated constant charge on the capacitor plates by disconnecting them from the high voltage supply during operation did not work: The charge dissipated too quickly off the plates. In replacement this experiment, too, was simulated, the details of which are given in appendix A.2.4.

Further investigation may be useful with respect to the influence of electrode roughness, air humidity and possibly also temperature. Also scaling effects, such as the one suspected to have influenced the maximum field intensity before electrical breakdown between the spherical electrodes during the voltage test and the plate electrodes of the experimental setup could be investigated.

A.2.2 Second experiment: Semi-insulated electrodes

The only change that was made to the setup in comparison with the first experiment is the addition of an insulating foil on the upper electrode. On the one hand the foil prohibits discharge from this electrode into the air. On the other hand it also blocks the annihilation of oppositely charged ions that are produced by the other electrode.

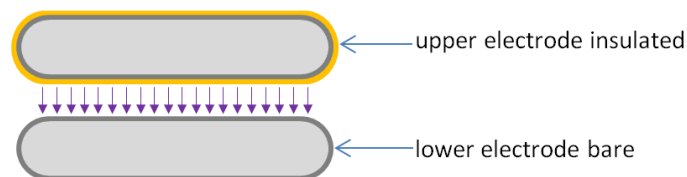


Figure 27

After a short buildup period a few closely succeeding flashovers would occur, even though the distance and voltage had not been altered. After the flashovers the situation stabilizes and an attractive force between the plates of merely $80mN$ is approached. The extreme force reduction after the flashovers is easily explained. Once a flashover is able to occur the air is strongly ionized and the resistance drops dramatically which allows a comparatively large current to flow from one electrode to the other. The open

electrode is able to absorb the displaced charge and transport it away, thus allowing a large amount of charge to flow off. The opposite electrode however is covered in an insulator. The displaced charge can only collect on its surface. This forms a shielding opposite charge directly on the surface of the insulated electrode. The potential between the open electrode and the surface of the insulated electrode has strongly decreased compared to the originally supplied potential.

A sure explanation for why a flashover occurred, rather than a slow and steady accumulation of surface charge on the insulation of the upper electrode - that would inevitably occur over time from ions originating from the air and the surface of the opposite electrode - has not been found. One factor could be that only one electrode can freely produce ions so that only ions of one polarity are generated and space charge can accumulate without opposite ions cancelling each other out within the volume in between the electrodes. The higher overall concentration of ions could then result in a decreased breakdown potential for the given distance.

The only other possible effect that comes to mind is that the insulation reduced the discharge current into the air and in the case that the output potential of the simple high voltage supply unit is strongly current dependent even at extremely low currents, this could have resulted in a slight increase in the supplied potential, thus facilitating a flashover. This could not be verified due to the lack of a potential measuring device. This configuration spectacularly demonstrated the effect of accumulating surface charge on an insulator in an electric field. It draws a dissuasive picture for the use of electrode pairs that are only insulated on one pole: The configuration does not prevent flashover while at the same time it allows for opposite surface charge accumulation resulting in a degradation of the attraction force.

A.2.3 Third experiment: Fully-insulated electrodes

This configuration has both electrodes covered by an insulating foil. Discharge from the electrodes is thus fully prohibited. Initially the force at the original separation distance of $7mm$ is tested. After that the separation distance is reduced to see the effect of an electric field intensity above that of electric breakdown in air. This is possible now, because the electrodes cannot short circuit via flashovers anymore.

Similarly to the first two experiments the initial force, i.e. when switching the power supply on, is the highest. Within seconds the force drops, while a slight crackling sound is emitted from in between the plates, and then it stabilizes at a lower level. For a separation distance of $7mm$ this is around $F_{7mm} = 130mN$. After that a low level hissing sound weaker than that in experiment one is perceivable.

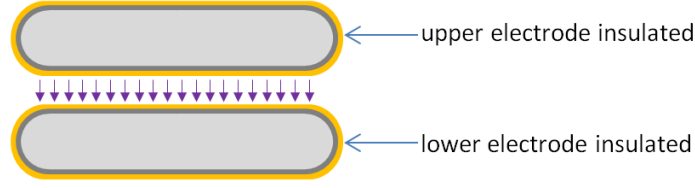


Figure 28

The crackling noise after switching on is a sign of low level breakdown in the air between the electrodes, which results in a fast accumulation of surface charge on the outside of their insulation layer. This again weakens the electric field within the air in between the electrodes until the ionization of the air is reduced to a minimum, for which a balance is found between production and annihilation of charged air particles. The insulation of both electrodes prohibits a full breakdown so that the final force is significantly higher than in the second experiment, but still lower than in the first experiment, because it prohibits the neutralization of ions on the electrodes surfaces. The following test with a reduced electrode separation distance of $3mm$ shows similar behaviour to the previous one, but with an increased initial partial breakdown until a new equilibrium is found for this configuration. The final force was around $F_{3mm} = 240mN$. This increase in force shows that a slightly higher electric field is sustained in between the electrodes. While it was approximately at $E_{max.7mm} = 2kV/mm$ in the first experiment with a separation of $7mm$, now, using a rearrangement of equation 20 shows that it remains at:

$$E_{max.3mm} = \sqrt{\frac{2F_{3mm}}{\varepsilon A_{equivalent}}} = 2.4kV/mm \quad (45)$$

with $A_{equivalent} = 0.0094m^2$ taken from equation 52. $A_{equivalent}$ can also be used to gain the electrostatic pressure sustained over the plane electrode area, as if it were an ideal parallel capacitor:

$$f_{max.3mm} = \frac{F_{3mm}}{A_{equivalent}} = 25.5N/m^2 \quad (46)$$

If it were possible to sustain a potential difference of $14kV$ between the insulator surfaces, then that would result in an attractive force of:

$$F_{3mm_vacuum} = \frac{1}{2}\varepsilon A_{equivalent} \left(\frac{14kV}{3mm}\right)^2 = 906mN \quad (47)$$

which means that a substantial surface charge has built up, reducing the resulting potential difference. Equation 45 multiplied with the separation distance yields a

remaining potential of:

$$V_{max.3mm} = \sqrt{\frac{2F}{\varepsilon A_{equivalent}}} x = E_{max.3mm} x = 7.2kV \quad (48)$$

When the power supply is switched off, both electrodes discharge through the power supply within the order of a second. During this discharge the attractive force first drops and even becomes negative for a moment, before it finally reaches a level of around $70mN$ that then very slowly dissipates within the order of minutes. In the short period of repulsion during discharge the electrodes effectively had the same polarity, either because of a difference in surface charge on the insulators or due to unequal discharge rates of the conducting parts.

The finally remaining force is a result of the remaining surface charge and thus the direction of the electric field has now switched.

The potential difference sustained by the lingering residual surface charge is therefor

$$V_{residual.3mm} = \sqrt{\frac{2F}{\varepsilon A_{equivalent}}} x = 3.9kV \quad (49)$$

which is about

$$\frac{V_{residual.3mm}}{14kV - V_{max.3mm}} \cdot 100\% = 57\% \quad (50)$$

of the potential due to surface charge that was present during operation at $3mm$ distance and sustains an electric field intensity of

$$E_{residual.3mm} = \frac{V_{residual.3mm}}{x} = 1.3kV/mm \quad (51)$$

A repetition of the procedure with an electrode separation distance of $2mm$ which again showed similar behaviour resulted in a sustained attractive force of $310mN$ and a residue charge attraction of $220mN$. These forces, though significantly increased, remain clearly below the theoretical border given by the breakdown strength of air that for a distance of $10mm$ was calculated to be $398mN$ for this setup. They do show again that with a smaller air gap the electric field intensity can further approach the maximum field intensity for atmospheric air defined by Paschen's law. Although at this point it may be remarked that at these increasingly small distances the breakdown strength of air already noticeably increases. At a distance of $2mm$ $E_{brakdown}$ of atmospheric air is approximately at $3.9kV/mm$.

The residue force was seen to reduce by approximately $1mN$ every $20s$. However this rate is expected to be strongly dependent on ambient humidity and other parameters and therefor is not necessarily representative.

separation distance	7mm	3mm	2mm
$F_{operational}$	130mN	240mN	310mN
$F_{residual}$	-	70mN	220mN
$E_{max_operational}$	1.8kV/mm	2.4kV/mm	2.7kV/mm
$V_{max_operational}$	12.4kV	7.2kV	5.5kV
$f_{max_operational}$	13.8N/m ²	25.5N/m ²	33.0N/m ²
$E_{residual}$	-	1.3kV/mm	2.3kV/mm
$V_{residual}$	-	3.9kV	4.6kV
$f_{residual}$	-	7.4N/m ²	23.4N/m ²
$\frac{V_{residual}}{14kV - V_{max_operational}}$	-	57%	54%

Table 6: Comparing the parameters for different separation distances of the insulated electrodes

For comparison the same calculations as for a separation of 3mm are also done for the other two separation distances of 7mm and 2mm. The results are shown in table 6.

The residue charge attraction of the 2mm configuration are a first impression of what may be expected from the plasma charged attractor design. Here the residual charge has shown to sustain approximately 2/3 of the maximum attraction force, and that it does not dissipate quickly. With the fixed voltage supply of this experiment, dependencies on the supply voltage cannot be ruled out, but it is expected that forcing higher surface charge to accumulate on the insulating surfaces at larger distances (7mm or 10mm) via a higher voltage will result in higher residual charge at a level similar to that of the 2mm configuration, with the residual force remaining at about 2/3 of the maximum sustained force during powered operation.

It seems remarkable that the ratio of $\frac{V_{residual}}{14kV - V_{max}}$, i.e. of the potential of the lingering residual charge to the potential due to the insulator surface charge during operation, remains at around 1/2 for both distances that it was evaluated for. It could be interesting to take further measurements and its value should strongly reduce if even higher supplied field intensities are used, as the residual potential ($V_{residual}$) should not be able to exceed the operational potential ($V_{max_operational}$). However the possibilities with this setup are limited: The positioning accuracy is not adequate for separation distances below 2mm as well as the roughness of the electrodes and with the fixed voltage there is not much residual surface charge at large distances such as 7mm or more, because the backward potential that builds up on the insulator surfaces during

operation is low.

Because water is necessarily involved in the process of cleaning outdoor surfaces, it is of interest to test the effect of wetted surfaces. In a further iteration of one of the fully insulated configurations water is sprayed into the gap between the electrodes (see figure 29). Water has a high relative permittivity, but if it is not highly purified, it is a moderately good conductor. The insulated electrodes at a separation distance of 3mm to one another originally produced an attraction force of 240mN . Spraying water in between them strongly reduced the force to 140mN . Sprayed water droplets can transport charge. Especially if they originate from the surface of one of the electrodes, they will leave charge behind due electrostatic induction that leads to the separation of charges within the droplets and the leaving portion of the droplet will become attracted by the opposite electrode. Additionally large droplets significantly reduce the gap in between the electrodes and lead to strong spikes in the electric field so that further discharge can occur. This stage of the experiment shows that care must be taken when water is introduced to an electrostatic attractor, since it is a further factor that can significantly reduce the produced force.



Figure 29: The insulated electrodes at a separation distance of 3mm after water is sprayed into the gap

A.2.4 Comparison of experimental results with simulations

The following simulations were computed in COMSOL Multiphysics using the Electrostatics package. They were conducted to support the data from the experiments one, two and three. One set of simulations is designed to be comparable with the measurements taken on the real setup. Another is configured to compare with the analytical formulation for a parallel capacitor. Together the results allow for conclusions on what exactly each method yields.

It could be shown that the analytical solution yields precisely the same results as the simulation if the simulation is setup in such a way, that only the volume in between the electrode plates is taken into account. This also shows that the FEM used in the simulation can yield very accurate solutions for the field and resulting forces for simple

shapes. It is more useful, however, for finding the solutions on more complex shapes that are harder or impossible to solve analytically.

The Electrostatics package will clearly only take into account the classical mathematical electrostatic relations, so that the simulation does not give any insight into other parameters such as discharge effects. The experimental approach yields of course the most realistic results as it includes all possible physical effects, but that can make it difficult to separate effects, find correct dependencies and thus gain useful answers. Therefor theoretical knowledge, mathematical relations and simulational support are useful tools to supplement those findings. Apart from their complexity, experimental results also include uncertainties from measurements and other approximations.

Firstly a better approximation of the supply voltage of the experimental setup was found. Figure 30 shows the two modeled electrodes inside a larger simulation volume on the left hand side and besides that two resultant potential distributions. Just like the experimental electrodes these have an outer radius of $r = 56.4mm$ resulting in a projected frontal area of $A = 100cm^2$, the plane surface of the electrodes has a radius of $r = 50mm$ with an area of $A_{plane} = 78.5cm^2$ and they are separated by a gap of $7mm$. In table 7 the column "fully in air" contains the simulated attractive forces for the experimental setup as if it were surrounded by perfectly insulating air or space at different voltages. At the maximum electric field intensity of atmospheric air with a voltage of $21kV$ an attractive force is found which is just below the analytically calculated maximal force for a parallel capacitor in air with a surface area of $A = 100cm^2$. This makes sense as the actual area on which this field intensity is acting upon on the electrodes is smaller than $100cm^2$. At the originally estimated voltage of $15kV$ the generated force is still significantly higher than the measured force. It is a voltage of $14kV$ that yields an attraction force that is very close to the measured value. Therefor this voltage is adopted for the calculations in the analysis of the preceding experiments.

Secondly it was of interest to find an equivalent surface area that could more accurately represent these slightly reshaped electrodes in the analytical formulation for a parallel capacitor. By rearranging the formulation for the force given in equation 19 for the area A and inserting the newly defined voltage, assuming the separation distance was measured accurately, the effective parallel capacitor area is found:

$$A_{equivalent} = \frac{2Fx^2}{\epsilon V_{corrected}^2} = 94cm^2 \quad (52)$$

It is insightful that this effective surface area is still significantly larger than the plane surface area of the electrodes which is at $A_{plane_area} = 79cm^2$ which was found in

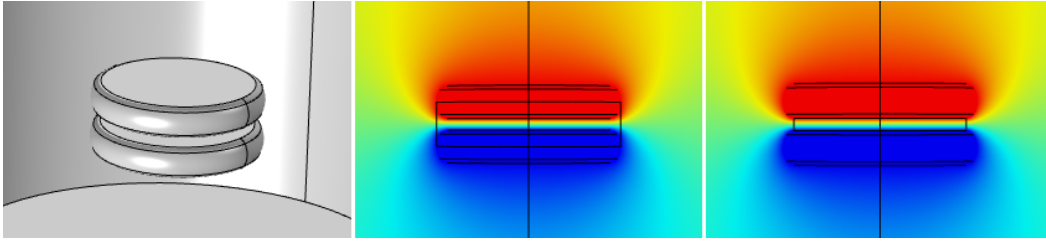


Figure 30: Configuration of the simulation of the experimental setup at a $7mm$ plate separation: (left) the two electrodes inside a larger simulation volume, (middle) an intermediate cylinder limits dielectric permittivity of air to a radius of $r = 56.4mm$, (right) a smaller intermediate cylinder limits dielectric permittivity of air to a radius of $r = 50mm$

voltage \ config.	fully in air	air up to $r = 56.4mm$	air up to $r = 50mm$
$V_{\max_air} = 21kV$	$375mN$	$365mN$	$313mN$
$V_{\text{estimated}} = 15kV$	$191mN$	$186mN$	$160mN$
$V_{\text{corrected}} = 14kV$	$167mN$	$162mN$	$139mN$

Table 7: Results of the simulation of the experimental setup at a $7mm$ plate separation with different voltages: "fully in air" represents the real situation, "air up to $r = 56.4mm$ " only takes into account the forces generated in the volume in between the plates and "air up to $r = 50mm$ " only takes into account the forces generated in the volume in between the plane surfaces of the plates.

equation 43. The last two columns of table 7 contain the simulation results for the imaginary case in which the surroundings of the electrodes are filled with a fictional material that has a dielectric permittivity that approaches zero, i.e. it suppresses the permittivity of empty space. This way only the remaining volume of air or space in between the electrodes can permit (used as an equivalent to conduct) the electric field. If the complete volume in between the electrodes is permissive a reduction to about 97% of the original force is the consequence - independently of the supplied potential. That means that with electrodes of this shape, the electric field responsible for the attractive force extends beyond the diameter of the plates. If only the volume in between the plane surfaces is permissive, the attractive force reduces to about 83%. The attractive forces in this last column are interesting, because if they are divided by the plate area, they represent the attractive force per area calculated via the analytical

formula. Therefor at $21kV$ where the force is $F_{21kV_{r50}} = 313mN$ the fore per area is:

$$f_{21kV_{r50}} = \frac{F_{21kV_{r50}}}{A_{plane_area}} = 39.9N/m^2 \quad (53)$$

which is the maximum attractive force per area that was calculated at the beginning of section 5, and at $14kV$ the force $F_{14kV_{r50}} = 139mN$ per area over the plane surface of the electrodes is:

$$f_{14kV_{r50}} = \frac{F_{14kV_{r50}}}{A_{plane_area}} = 17.7N/m^2 \quad (54)$$

which was the analytically found maximum achievable value for the setup of experiment one in which the minimum possible separation distance was $7mm$.

It now remains to demonstrate how the simulated force between two fully plane plates relates to the solution found by the analytical formula (similar to the reduction of r above) and to use this configuration to simulate multiple electrode separation distances with equal electric field intensity, which was not possible experimentally with the built setup, because only one set voltage was available. Figure 31 shows this model and an exemplary potential distribution.

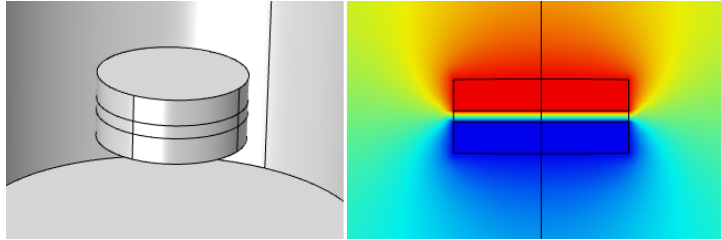


Figure 31: Parallel capacitor with area $A = 100cm^2$ and distance $x = variable$, the apparent body in between the two electrodes is only for modeling convenience and simply has the same characteristics as the remaining surrounding air.

	x = 10mm, V = 30kV	x = 7mm, V = 21kV	x = 5mm, V = 15kV	x = 3mm, V = 9kV	x = 2mm, V = 6kV
F	$395mN$	$396mN$	$397mN$	$398mN$	$398mN$

Table 8: Results of the simulation of a parallel capacitor with a plate area of $100cm^2$ at multiple plate separation distances, each with equal electric field intensity of $3kV/mm$

Despite a five fold change in distance between the plates the computed force only changes by 0.8%. The analytical solution is approached as the plates are brought nearer together. The further the plates are moved apart, the larger the deviation

from the assumption for the analytical formulation becomes, that the plates are of much larger extent than the distance between them. The slight loss in force compared to the analytical solution is a result of the outward spreading electric field at the edges.

A.2.5 Fourth experiment: In-contact, insulated electrodes

This experiment is designed as a concluding opposite to the previously described configurations. It shows that with a similar setup to the previous ones, but with the electrodes are brought into contact, higher forces that are in the order of what is stated in literature for in-contact electroadhesion are achieved. Up to this part this section was devoted to understanding the limits given by an air gap in between opposite potentials. In this part a small setup is tested to demonstrate how nearly excluding air by enabling good surface contact moves this border by several orders of magnitude and allows for greatly increased electric field intensities thanks to the property of gases that is described by Paschen's law.

It is also verified that in-contact adhesion relies on a dry contact zone, as non-purified water will generally eliminate the attraction force.

The configuration consists again of two oppositely charged plane and parallel electrodes. Their composition is detailed in figure 32. The upper electrode has a smooth glass surface. The glass pane with a thickness of 1.7mm is backed by a rectangular sheet of aluminium foil of the size 35mm by 55mm . The opposite electrode of the same dimensions has a plane but also slightly compliant surface so that it can adapt to the surface that it is brought into contact with. The top layer is a shiny smooth plastic foil that stabilizes the thin aluminium foil that it is adhered to and gives it a soft surface with low roughness. This compliant double layer is then glued onto a rubbery foam block that serves as a compliant connection to the rigid carrier. With this design the glass surface can make good contact with the surface of the plastic foil. Figure 33 shows the built electrodes. The remainder of the the setup is similar to that of the previous experiments.

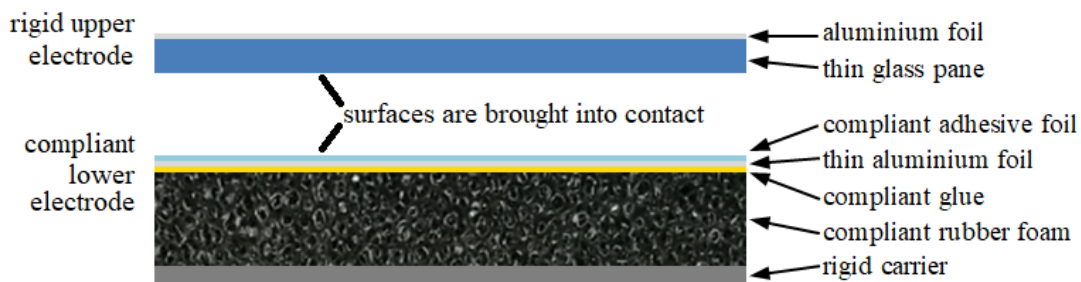


Figure 32: Composition of the two electrodes that are designed for good surface contact

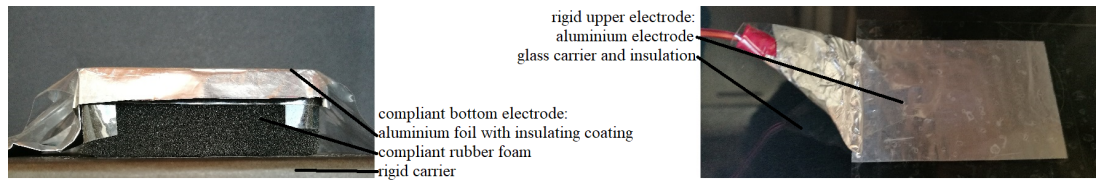


Figure 33: The built electrodes with dimensions 35mm by 55mm : (left) side view of the bottom electrode, (middle) top view of bottom electrode, (right) upper side of top electrode

The experimental procedure involved zeroing the scale, then bringing the surfaces into contact with each other by lowering the upper electrode down onto the bottom electrode, turning on the power and then gradually lifting the upper electrode while monitoring the force until the electrodes would separate.

On separation a clearly audible crackling is generated by numerous small breakdowns within the air coating the insulated surfaces in charge that is opposite to that of the electrodes. If the supply is then switched off and the surfaces are brought back into contact, a weaker adhesion force is sustained by lingering surface charge, although the contacting surfaces partially neutralize each other again while omitting a slight crackle.

The maximum adhesive force that was measured with the procedure described above approached 1.5N . Dividing this force by the electrode area yields an electrostatic pressure of $f = 779\text{N}/\text{m}^2$, which is already around twenty times the maximum achievable attraction over a larger air gap (equation 33). This electrostatic pressure implies that an electric field intensity of $E = \sqrt{2f/(\epsilon_0\epsilon_{air})} = 13.3\text{kV}/\text{mm}$ in between the two facing surfaces could be sustained. According to the experimentally gained Paschen curve for air that is displayed in "Electrical breakdown of gases" by J.M. Meek et. al [21] on (p.542), this electric field intensity if interpreted as the maximum field intensity before breakdown corresponds to a gap length in the order of $40\mu\text{m}$. The two specifically chosen smooth contacting surfaces of this experiment will have had a far smaller average separation or asperity width, which would allow for higher electric fields to be sustained according to Paschen's law. Therefore further effects have negatively influenced the pull-off force. One contributing factor is likely a not perfectly uniform detachment of the entire surface at once. The compliant surface is able to deform and peel-off beginning at the edges, thus increasing the pull-off distance and decreasing the force.

The achieved force is also very dependent on the quality of contact that is made before the power is turned on. A short contact period with low pressure resulted in forces as

low as $0.3N$.

To approximate the electrostatic pressure for a perfectly airless contact i.e. the maximum possible force per area of this setup, the used glass is assumed to have a relative permittivity of $\varepsilon_{glass} = 5$, although values for glass vary strongly. The thickness of the plastic foil and of the diminished air gap are neglected. The sought force is the sum of forces acting upon all layer interfaces of either of the electrodes up until the air gap (see section 3.1.4). For the glass covered electrode these are the interface between the aluminium foil and the glass pane and the interface of the glass pane to the air gap. For the plastic coated electrode these are the interface between the aluminium and the plastic foil and the interface of the plastic foil to the air gap. Since the sum of the forces on the multi-layer electrode up to the air gap is equal to the force of the uncoated electrode facing an air gap and the thickness of the plastic foil is so low that it does not significantly influence the electric field intensities over the rest of the layers the formula for this second electrode simplifies.

For a visualization see figure 9 in section 3.1.4, where layer 1 will be regarded as the glass pane and layer 2 shall be the air gap. We have the values:

$$\varepsilon_{glass} = 5, \quad l_{glass} = 1.7mm, \quad \varepsilon_{air} = 1, \quad l_{air} \rightarrow 0$$

Because of $l_{air} \rightarrow 0$, D simplifies to:

$$D = \frac{\varepsilon_{glass}\varepsilon_{air}V}{l_{glass}\varepsilon_{air} + l_{air}\varepsilon_{glass}} = \frac{\varepsilon_{glass}V}{l_{glass}} \quad (55)$$

with which the electric field intensities E_{glass} and E_{air} equate to:

$$E_{glass} = \frac{D}{\varepsilon_{glass}} = \frac{V}{l_{glass}} \quad (56)$$

and

$$E_{air} = \frac{D}{\varepsilon_{air}} = \frac{\varepsilon_{glass}V}{l_{glass}\varepsilon_{air}} \quad (57)$$

The force on the electrodes can now be calculated. Calculating the force of the second electrode on the air gap is equivalent to calculating f_{56} from figure 1. The equation now reads:

$$f_{airless} = -\frac{1}{2}\varepsilon_0\varepsilon_{air}E_{air}^2 = -7503N/m^2 \quad (58)$$

For this force to be realized the electric field in the gap E_{air} reaches $41kV/mm$. This is approximately the breakdown strength of air at the Paschen minimum, implying that the contact zone should not have regions larger than $7\mu m$ so as to avoid areal breakdown. The negative sign on the force value indicates that the force is acting in the negative direction, relating to figure 1 that is to the left. The force could of course

just as well be calculated from the other side using the sum of the forces on the two interfaces of the other electrode (aluminium-glass and glass-air), which are equivalent to f_{12} and f_{34} in figure 1. The force is then acting in the positive direction.

Despite the uncertainty in the used permittivity for the glass pane it can be said that the result shows clearly that the quality of the contact can be further improved to allow a significantly higher force.

Compared to the attraction forces from the non-contact experiments the magnitude of the electrostatic pressure measured in this experiment is closer to the values stated in literature about successful electroadhesion prototypes, as these generally treat in-contact situations, but still is about an order of magnitude lower than some. An example with especially high values is the versatile soft gripper developed by J. Shin-take et. al [22] for which adhesion pressures of up to $13000N/m^2$ are claimed. To achieve this the gripper used an even higher field intensity exceeding $50kV/mm$.

The forces generated here and also those quoted correspond to what is possible for an electroadhesive attracting a conductor. In the discussion of figure 35 in appendix B.1 an example is given of how the forces that can be expected when attracting a dielectric such as glass relate to those generated when attracting a conductor. In that example the dielectric with a relative permittivity of $\epsilon_r = 5$ produces an attraction of about one quarter of what is possible with a conductor.

Again the effect of water on the force is of importance, especially with such a narrow gap. Therefore in a further step water is introduced into the gap in between electrodes. The surface tension of the water pulls it in, fully replacing the air. While water has a high relative permittivity, it also - as has been mentioned previously - is a moderately good conductor if it is not purified.

The pull-off force found for the experimental setup with water in between the electrodes is $550mN$. However this force was independent of the applied voltage: It could be measured with or without applying an electric potential. The entire force therefor must have been due to the water meniscus that forms at the edge of the electrode. Consequentially, water in between the electrodes fully eliminates the electroadhesive force.

Within ideal conductors no electric field can exist. From the above result it is concluded that in a non-alternating electric field water acts as a sufficiently good conductor to achieve this state, thus eliminating the electric field that is required to generate an electrostatic force.

A.3 Summary of results

1. Limit to attraction force in air:

Within the medium air it is not possible to generate forces above a certain limit, due to the breakdown field strength of air, regardless of the use of electrical insulation on the electrodes. The original hypothesis that non-insulated electrode surfaces are capable of producing the highest forces for a given configuration could be confirmed by experiments at a separation distance of $7mm$. Because of the fixed supply voltage, no comparison was made at other distances.

2. Further force-reducing effects and achieved percentage of theoretical forces:

The experiments revealed some effects that additionally limit the achievable attraction force. These are:

- maximum field intensity in air could not reach the respective values given in literature (e.g. $3kV/mm$ at a gap length of $10mm$)
- buildup of space charge (also for non-insulated electrodes)
- accumulation of opposite surface charge on insulated electrodes
- water droplets as a catalyst for charge transport

It is thought remarkable, that the typical maximum field intensity for atmospheric air was not reached in any of the experimental setups. It ranged from $1.8kV/mm$ (60% of $3kV/mm$) for insulated electrodes at a separation of $7mm$ up to $2.7kV/mm$ (69% of $3.9kV/mm$) for insulated electrodes at a separation of $2mm$. While possible explanations for this are given, these are still of a somewhat speculative character and should be treated that way. Finding further information on this, either in literature, or by means of further experiments may be of interest. In the referenced book "Electrostatics and its applications" by A.D. Moore [2] it is mentioned that a "realistic" electric field intensity in air is at 80% of the maximum, which nonetheless is not reached by any of these configurations.

The maximum sustained electrostatic force generated during these experiments was $310mN$ equating to $33.0N/m^2$, which is 49% of the theoretically possible force at that separation distance of $2mm$, where an electric field of $3.9kV/mm$ should be sustainable. However it is probable that non-insulated electrodes with the appropriate supply voltage would have resulted in a slightly higher force, due to their capability to neutralize attracted ions at their surface. An overview of the achieved percentage of the maximum possible force for each configuration is given in table 9.

Configuration	7mm non-insulated	7mm insulated	3mm insulated	2mm insulated
breakdown field intensity	3kV/mm	3kV/mm	3.6kV/mm	3.9kV/mm
maximum theoretical force	375mN	375mN	540mN	634mN
measured force	155mN	130mN	240mN	310mN
percentage of maximum	41%	35%	44%	49%

Table 9: Achieved percentage of theoretically possible attraction force for each of the non-contact configurations, the maximum theoretical force is calculated with the equation $F = \frac{1}{2}\varepsilon A_{equivalent} E^2$

3. Resulting distance dependency of force: Even though the force is not distance dependant for a constant electric field intensity, the slight distance dependency of the breakdown strength of air at these distances and the increase of the achieved percentage of that limit at decreasing gap lengths that was found in these experiments reintroduces a distance dependency to the achievable attraction force.

4. In-contact: higher forces, more vulnerable to contamination: The fourth experiment rounds off the investigation by demonstrating the opposite effect: Excluding air as best as possible from the region in between the electrodes makes use of the non-linearity of the breakdown strength of gases, thereby pushing the boundary on the field strength and thus allowing for far greater forces. At the same time it makes the system vulnerable to conductive, fluid surface contamination such as water, which can eliminate the adhesion force.

B Details of research on in-contact electroadhesives

The following sections give details on the derivation of the summarized information given in section 6.1.

B.1 Current state of the art of dielectric attraction

A comparatively extensive comparison of different electrode patterns for an in-contact electroadhesive is done by J. Guo et. al.[17] Nine different patterns are compared in simulations and then three of these that yield good theoretical results are manufactured and tested. The nine selected patterns appear to have been chosen ar-

bitrarily and no argumentation is given on why certain patterns are chosen for this comparison between one another. The electrode width and pad area are the same between most of the pattern variations. The nine patterns are similar to the five presented in figure 34 with further variations or combinations of these.

In the paper it is concluded that different patterns yield differing attraction forces. After attentive consultation of the results though, it becomes apparent that it is after all more an "effective" electrode width, rather than the overall pattern that effects the adhesion force and leads to differences in the respectively achieved results that are presented there. This conclusion is not made in the paper however. At the same time a few inconsistencies in the electroadhesive pad design, such as slight variations between the specimens in total electrode area, differing electrode widths (for example pattern "e" in figure 34) and one design with varying electrode width (similar to pattern "c" in figure 34) as well as another design in which neighbouring electrode digits have equal polarity (similar to pattern "d" in figure 34) remain uncommented. Two electrode digits beside each other with the same polarity, each with the width d , effectively produce approximately an electrode with a width of $2d + g$, where g is the gap in between the electrodes. Furthermore the dependency of the force on the electrode width is not even mentioned. The patterns with "double" electrodes or wider electrodes yield significantly weaker forces, while the designs with the thinnest electrodes yield the best results.

A conclusion that is drawn in this paper though is that the simulated results are a valid tool to pre-evaluate which design will perform better as a real setup.

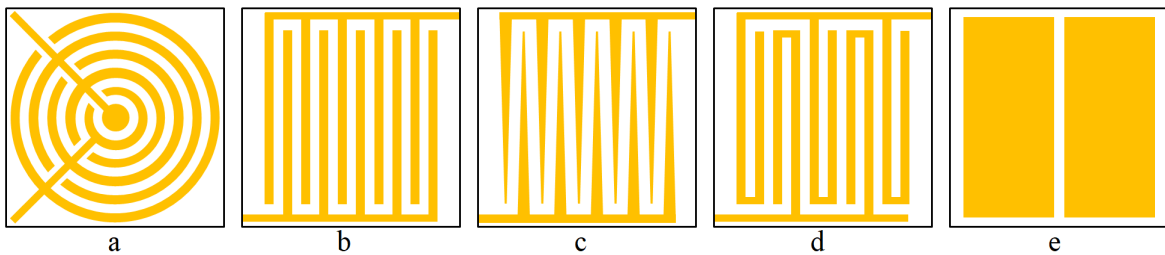


Figure 34: Examples of pattern types compared in [17]

Another paper on the design and fabrication of interdigital-electrode electroadhesives is presented by J. Fessler et. al [20] which nicely shows that an optimal electrode width for a given distance between the electroadhesive and the substrate that is to be attracted exists. 2D simulations are performed that yield the adhesion force as functions of multiple design parameters. One of these is the distance between the electrodes and the attracted object consisting of the insulator coating thickness and the air gap distance. Further parameters are the attracted object's thickness and the

electrode potential difference. A certain design is then manufactured and the test results are shown to correspond very well with the predicted forces. However it is not explained how the air gap distance was estimated and chosen to be at $195\mu m$ which is a strikingly large gap.

The optimized solutions found there are nevertheless specific to the used spacing in between the electrodes and the relative permittivities of the materials used. Further optimization is necessary to find the best gap width with respect to the involved material permittivities and electrode potentials. As these and the aforementioned parameters are all interdependent that is a cumbersome endeavour.

A mathematical basis for calculating the attraction force on a segment of an interdigital-electrode adhesive is given by C. Cao et. al.[4] It treats the segment idealized as a portion of an infinitely extensive pad of straight parallel electrodes. The normal force on a segment of width L and unit length then breaks down to

$$F_N = \frac{1}{2}\varepsilon_0 \int_0^L (E_y^2 - E_x^2) dl \quad (59)$$

where E_y and E_x are the electric field components at the interface with the attracted dielectric object in normal and in "L" direction respectively, but this formula still relies on an unknown electric field distribution that is dependent on all the physical properties of the setup. C. Cao et. al further discuss this function and present graphs revealing the dependencies of this function with respect to the major physical parameters for a few specific design cases. A set of functions to generate such dependencies is not given.

The following paragraphs and next section will give an impression of what the attraction force of a device that relies on the multi-electrode dielectric attraction specifically depends on.

The above mentioned paper by J. Fessl et. al, in which the optimal electrode widths are found for a few specific configurations[20], does not state any achieved electrostatic pressures or the area on which the presented forces were produced. For this reason a simple simulation model is setup here as an example. On an area of $40mm$ by $40mm$ parallel electrodes are arranged approximately in accordance with the found optimum from this paper for a separation distance between electrode and substrate of $0.2mm$. The electrodes therefor have a width of $0.8mm$ at a spacing between the electrodes of $0.4mm$. This is the optimum that was found for the attraction of PLA with a relative permittivity of $\varepsilon_r = 3.6$. This value is near but not identical to the relative permittivity of glass that will be used in the following simulation. Further deviations

from the quoted optimized setup are that the additional insulating layers with their individual permittivities are omitted to simplify the setup and thus reduce the number of variable parameters. The configuration is displayed on the left hand side of figure 35.

If the attracted object is chosen to be made of a conductor it will allow for complete rearrangement of the charges within it. The voltage between the electrodes is set so that the resulting electric field strength is $3kV/mm$, which is what was chosen as the maximum electric field strength in the previous evaluation of the parallel capacitor¹⁶, so that it is comparable. The required voltage for this case is $1200V$ because the separation distance of $0.2mm$ must be taken into account twice: once from one electrode to the surface of the attracted object and once again from the object's surface back to the next electrode. The resulting electrostatic pressure from this simulation is $25.0N/m^2$ ($40.0mN/1600mm^2$), which is close to two thirds of what a parallel capacitor produces (see section 4.1), which again makes sense as only two thirds of the electroadhesive's area are actually electrode area. If the attracted object is chosen to be made of glass with a relative permittivity of $\epsilon_r = 5$, then the electrostatic pressure drops to $11.6N/m^2$ ($18.6mN/1600mm^2$), which is achieved by a strong polarization within the glass that could be regarded as an incomplete separation of charges that depends on the relative permittivity of the material.

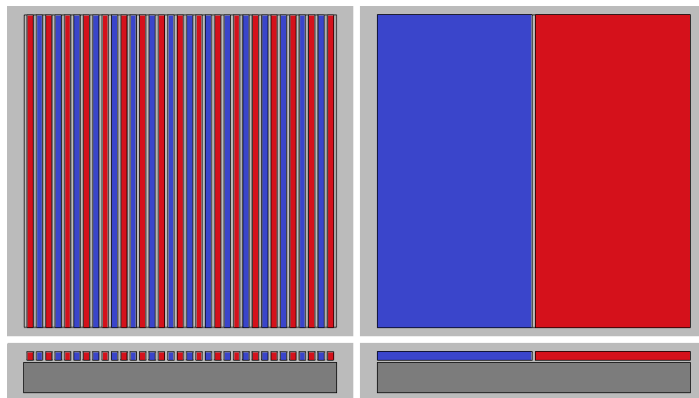


Figure 35: Idealized $40mm$ by $40mm$ electrode configurations of dielectric attractors: (left) close to optimal electrode width and spacing for attracting a weak dielectric (glass, $\epsilon_r = 5$) from a distance of $0.2mm$, (right) simplest configuration which is optimal for the attraction of conductors but feeble at attracting dielectrics, red and blue represent opposite potentials, dark grey is the attracted object.

Although this electrostatic pressure is merely around a quarter of what is possible for the same field strength on a conductor, this is a high value, thus confirming the

¹⁶This however is only truly limited at this value for large air gaps

setup to be optimized to some extent. Other less optimal configurations that were simulated ended up one or two orders of magnitude lower for the attraction of glass. The following example gives an impression of this. The optimal configuration for the attraction of a conductor, which effectively has infinite permittivity, is the largest possible area per electrode so that as little area as possible is lost on the spacing in between the electrodes. For an attractor that includes both polarities within its surface plane the minimum number of electrodes is two. A reconfiguration of the setup described above so that it has only two electrodes (see right hand side of figure 35) yields an electrostatic pressure of $39.4N/m^2$ for conductors, which if the $0.4mm$ wide space between the electrodes is subtracted, corresponds perfectly with the value for a parallel capacitor, as the result then is $39.8N/m^2$. For an object with a relative permittivity of 5 the electrostatic pressure however is only $0.77N/m^2$. This difference will become still more pronounced if the two-electrode design is applied to a larger attraction area. The attraction of dielectrics occurs mainly near the adjacent edges of the two oppositely charged electrodes as here the electric field and the divergence over the volume of the attracted object are strongest. For this exemplary simulation the thickness of the attracted object was chosen to be $4mm$, which is realistic for a pane of glass and large compared to the gap length between electrode and substrate surface so that the strong region of the diverging electric field is largely within the object's volume.

Reasoning from the point of view that a larger separation of charges (due to higher relative permittivity with the upper limit being at infinity for conductors) must lead to stronger attractive and weaker repulsive forces within each molecule of the attracted object, the attractive force on a dielectric insulator cannot exceed the attractive force on a conductor for any electrode configuration.

This notion has so far been confirmed by all conducted simulations and not contradicted by any found literature except for the paper on geometric optimization by J. Guo et. al [17] who find higher forces on the tested dielectric, which is glass, than on a conductor. An explanation for this is not given in the paper and has not been found unless it is a mistake.

A further rule of thumb that becomes apparent from these observations is that at any given separation distance a higher relative permittivity of the attracted object requires wider electrodes for optimal attraction. The higher permittivity allows for better charge separation over longer distances, which increases the divergence of the electric field in the volume of the attracted object, while wider electrodes result in fewer spaces in between the electrodes so that a larger proportion of the area is ac-

tively used. The exact relation between electrode width and distance to the attracted substrate depend on multiple factors, such as the spacing in between the electrodes and the relative permittivities of the insulating layers used on the electroadhesive.

B.2 Distance dependency of dielectric attraction forces

At this point a note is made on the distance dependency of dielectric attraction. Even though this technology relies on the divergence of the electric field (in contrast to a parallel capacitor for example) and diverging fields remind of the interaction between point charges, this principle also turns out to be independent of the separation distance.

A simulation was performed that can be directly compared to the one done for the design displayed on the left hand side of figure 35, which was optimized for a separation distance of $0.2mm$. For this new configuration the design is optimized for a separation distance of $0.1mm$. The electrode width is chosen to be $0.4mm$ based on the optimization results from J. Fessl et. al [20]. Following the requirement of maintaining the same electric field intensity across the gap that is mentioned in the text leading up to equation 20, the voltage between the electrodes is decreased from $1200V$ to $600V$, thus maintaining the electric field intensity of $3kV/mm$ from the electrodes to the attracted substrate¹⁷. This halved potential difference consequently allows for the reduction of the electrode spacing from $0.4mm$ in the previous example to $0.2mm$, which stands in contrast to the procedure by J. Fessl et. al [20] in which the electrode separation is always kept constant at $0.4mm$. By doing so the ratio between the actively used electrode area and the passive spacing area is maintained, thus keeping a further parameter constant. The number of electrodes is not increased so that the dimensions of the simulated attractor shrink to $20mm$ by $40mm$. The resulting electrostatic pressure that was computed for this setup is again $11.6N/m^2$ ($9.3mN/800mm^2$), which is identical to the pressure found above for the original simulation with a separation distance of $0.2mm$. Physically it is the same field distribution and therefor attraction situation scaled down two half the spacial dimensions but with the same field strengths, which accordingly leads to the same electrostatic pressure.

¹⁷Again this specific maximum field intensity is maintained for comparability with the foregoing configurations. The linear dependency of the breakdown voltage to the separation distance does not apply to gases at such short gap lengths.

B.3 Forces achieved with in-contact dielectric attraction

So far the derived force values have been limited by the low electric field intensity of $3kV/mm$ that was used to remain directly comparable with the previous examples that assumed a large air gap in between the electrodes and the attracted substrate. As this section and the quoted literature treat in-contact attraction, thus named adhesion, this section would be incomplete without treating the practically achieved adhesion forces for the case of bodies put into contact with the electroadhesive.

Contact however is relative and more like the closest proximity that is possible, which depends on the surface roughness and compliance of the materials that are brought into contact. Rougher surfaces as well as a higher stiffness of the materials in contact will result in fewer points of contact at the highest peaks on the rough surfaces and larger distances between the remaining surface area. An important factor for electroadhesion that is affected by the degree of surface contact is the presence of air or any other substance in between the facing surfaces. This was addressed in the introduction of section 5 and in appendix A.2.5.

Depending on how good the contact is or - to be more precise - how good the exclusion of air (and other weak media) within the contact region is, much higher electric field intensities are possible. In the following a few examples of the forces that can be expected from this type of setup are discussed.

J. Guo et. al state in their comparison of electroadhesives[17] that the best configuration experimentally achieved a force of $1.7N$ on glass. On aluminium apparently a force of only $0.5N$ was achieved. As mentioned above, it is peculiar that the conductor should have been attracted less than the dielectric, so possibly these values are interchanged.¹⁸ Following from the specified adhesive dimensions of $176mm$ and $228mm$ the active area is $0.04m^2$, so that the maximum electrostatic pressure that was achieved is $42.5N/m^2$ and $12.5N/m^2$ on the dielectric and conductive substrate respectively. While these electrostatic pressures are slightly higher than those found above for the attraction across an air gap (i.e. $E_{max} = 3kV/mm$), they are still very low compared to the results of other in-contact electroadhesives. If the electrode width optimization by J. Fessl et. al [20] is used as an orientation, the electrode width of $1.8mm$ and even more so the spacing of $4mm$ are, however, far from optimal.

J. Shintake et. al present an effective gripper[22] that makes use of in-contact electroadhesion that achieves impressively high but plausible results for the attraction of a metallic body on a force sensing head. For the attraction of a conductor the

¹⁸A simulation of a section of an electroadhesive with the characteristics of this configuration was conducted and is documented in appendix C.1.

electrostatic pressure reaches values of up to $13000N/m^2$ for the most effective combination of insulator thickness on the electrodes and applied voltage, that results in a field intensity approaching $50kV/mm$ over the attraction distance. The designed electroadhesive has a visibly smooth surface and is thin and flexible so that it can make good contact with the surface of the attracted object. The electrode digits are wide (effectively around $2mm$) with a coating thickness of merely $0.05mm$. The spacing between the electrodes of $0.5mm$ is quite small compared to the electrode width so that little area is left passive. This configuration is relatively good for the attraction of conductors, but - if again the width optimization by J. Fessl et. al [20] is taken as a reference - it is not optimized for common dielectrics, as the electrode width is far too high. No measurement results are given for the attraction of dielectrics. Some exemplary objects are however lifted by the gripper, most of which are dielectrics. Their weights are documented and lifting them requires at the most only about a tenth of the force that was achieved on a conductor. The fact that these objects are being lifted however, does not necessarily present the maximum capability of the adhesive. Being dielectrics, though, naturally means that the electrostatic pressure exerted on them is lower than on conductors.

For verification the $1cm^2$ -sized design used by J. Shintake et. al [22] was replicated in a simulation model. This model achieved comparable results for the attraction of a conductive substrate, confirming that such high attractive forces can be generated with this design in the absence of air or any other medium with low breakdown strength. If the attracted conductive object is replaced by a dielectric with a low permittivity of $\epsilon_r = 5$ representing glass, the force even drops to merely 0.2% of the previous value¹⁹. Any form of optimization of the electrode-widths for the used insulator-thicknesses and the permittivity of the attracted materials is not mentioned in this paper. Peculiarly the developers chose to compare the previously described design to a double layered electrode configuration in which one electrode covers the complete area of $1cm^2$, while the second electrode is placed behind the first electrode and also covers the full area. An extreme increase in adhesion force is found between this design and the interdigital design from above. This is not a very useful comparison as the double layer electrode design clearly can only produce marginal attraction to any external object as most of the electric field is confined to the thin volume in between the two electrode layers.²⁰ Dielectrics will only develop slight attraction along the borders of the electrode and

¹⁹The simulation is documented in appendix C.2.

²⁰This feature however does have a purpose in the overall gripper design, where it is used to clamp/pressurize a stretchable elastomer membrane in between the two electrodes to evoke an actuated motion of the asymmetric multi-layer foil.

conductors can additionally be weakly attracted over the surface area if the conductor is grounded or extensive in size and brought into very close proximity to one of the two electrodes.

A further example of an in-contact interdigital-electrode electroadhesive is the pad presented by H. Prahlad et al.,[11] which is claimed to achieve $42400N/m^2$ on steel and $8400N/m^2$ on glass. No information was however found on the specifications of this electroadhesive pad design.

C Simulation of known electroadhesives

This section contains the simulations for appendix B.3.

C.1 Simulation of electroadhesive from reference [17]

This simulation replicates the electroadhesive design that was used in the force measurement done by J. Guo et. al [17] to generate the forces quoted in appendix B.3. The electrode width is stated to be $1.8mm$ with a spacing gap in between the electrodes of $4mm$. The electrode "pattern" is idealized to an infinite array of straight and parallel electrodes with alternating polarity. This way a single period of the opposing electrodes can be simulated in 2D to allow for the computation of finer details, such as a thin air gap at the contact interface. This air gap is necessary if the simulation includes a solid (i.e. material that can build up stresses) dielectric in the gap that has a relative permittivity of a value other than one. The air gap width is set to $1\mu m$, which is in a realistic order of magnitude for these smooth surfaces and still large enough for sensible meshing and computation times. At such low thickness values compared to the total gap its exact thickness has a small influence on the force results.

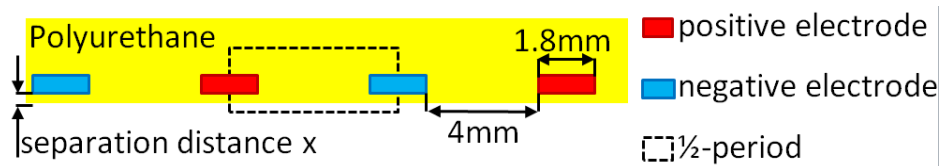


Figure 36: Sketch of infinite array of straight and parallel electrodes with alternating polarity of which $\frac{1}{2}$ -period is simulated

As no information is given on the thickness of the insulating electrode-coating, multiple different separation distances were simulated. The relative permittivity of the medium surrounding the electrodes is set to the value that is given for the coating material Polyurethane which is $\epsilon = 3.6$. The potential difference between the electrodes

is $3.2kV$.

In all simulations this configuration clearly showed the expected behaviour: The conductor is attracted significantly stronger than the dielectric.

As an example the results from the attraction across a thickness of $0.1mm$ and $0.2mm$ are given here. The force on the glass surface at these distances is in the order of magnitude of the measured forces, but both achieve far higher (two orders of magnitude) attraction forces for conducting objects. However these distances are nevertheless rather large: The coating used is sprayed Polyurethane that will likely be thinner.

Parameters:

$width = 1.8mm$,

$spacing = 4mm$,

$\epsilon_{r_coating} = 3.6$,

$x_a = coating\ thickness = separation\ distance = 0.1mm$,

$x_b = coating\ thickness = separation\ distance = 0.2mm$,

$V = 3.2kV$

Resulting forces:

for $x_a = 0.1mm$

glass with $\epsilon_r = 5$: $f = 38.83N/m^2$

metal (conductor): $f = 4557N/m^2$

for $x_b = 0.2mm$

glass with $\epsilon_r = 5$: $f = 30.3N/m^2$

metal (conductor): $f = 1206N/m^2$

Both forces increase with decreased coating thickness. In the case of a metallic object this increase is approximately the square of the change in distance, as due to its "infinite" permittivity it is the volume directly below the electrodes in which the significant attraction occurs. Die dielectric coating creates a small deviation from this behaviour.

The low forces reported from the practical experiment can hardly be explained. One factor could be strong areal breakdown despite contact, possibly due to a non-planar surface of the coated electroadhesive. The electrode spacing itself is large enough to prevent breakdown in air without an object placed in front of the electroadhesive, but with an object with increased permittivity in front of it the electric field intensity in the zone where the electrode faces the object increases. This happens even more so

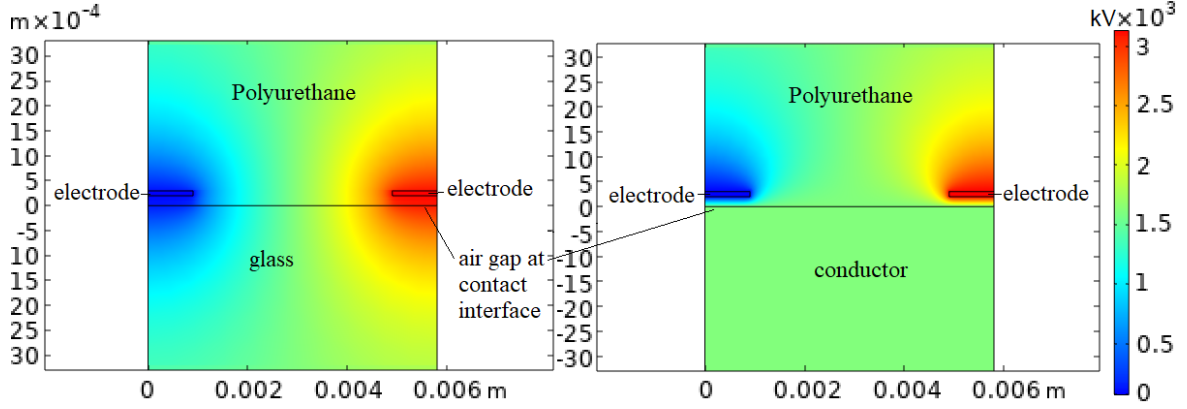


Figure 37: 2D electric field distribution of the described electroadhesive attracting a glass object with $\epsilon_r = 5$ and a conducting object on the left and right hand side respectively.

for the conducting object, so that here the reduction in force due to breakdown is naturally higher.

Another factor that can strongly reduce the pull-off force is a gradual peel-off due to the compliance of the materials used in the contact zone.

As a simple validation of the simulation the attraction of the conducting object is calculated analytically for the distance of 0.2mm using the method described in section 3.1.4:

$$D = \frac{\epsilon_{r_coating}\epsilon_{air}V}{x_b\epsilon_{air} + air_gap \cdot \epsilon_{r_coating}} \quad (60)$$

$$E_{air} = \frac{D}{\epsilon_{air}} \quad (61)$$

$$f_{conductor} = \frac{1}{2}\epsilon_0\epsilon_{air}E_{air}^2 = 3577\text{N/m}^2 \text{ of electrode} \quad (62)$$

To gain electrostatic pressure over the area of the electroadhesive the non-active area in must be taken into account, so that:

$$f_{conductor} = \frac{1.8\text{mm}}{5.8\text{mm}}3577\text{N/m}^2 = 1110\text{N/m}^2 \quad (63)$$

This electrostatic pressure is close to, but a little below the simulated result. Due to the large distance of the electrodes to one another and the large gap to the attracted object compared to the electrode width, the simple analytical equation becomes inaccurate: It does not take fringe effects into account. In this case that means that the additional attractive force induced by the spreading electric field at the electrode edges is neglected.

C.2 Simulation of electroadhesive from [22]

This simulation gives an insight on the relation between the attraction of a conductor and a dielectric for the electroadhesive design used on the versatile gripper from J. Shintake et. al.[22]

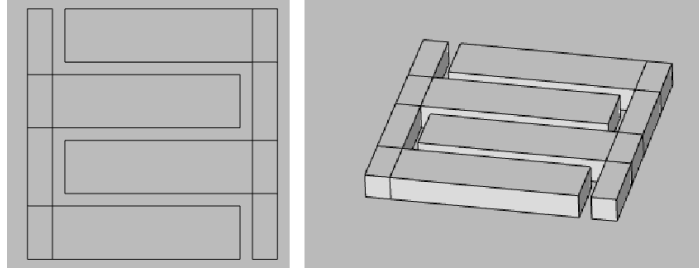


Figure 38: 2D and 3D view on the modeled 1cm^2 electrode pattern of the versatile gripper

This electroadhesive has a total area of 1cm^2 . Its pattern is displayed in figure 38. The coating material is silicone, for which a relative permittivity of $\varepsilon = 4$ is used. The voltage and thickness parameters used for the simulation correspond to those that delivered the strongest force in the paper, which reports an experimental pull-off force of 1.3N for the metallic substrate, which equates to an electrostatic pressure of $13000\text{N}/\text{m}^2$.

Originally the simulation model was designed in 3D as depicted above. As this model could not include a thin air gap at the contact interface because of the necessary increase in meshing fineness a 2D model was created, in which far higher mesh densities are possible. The field distributions are displayed in figure 39.

Parameters:

$$\varepsilon_{r_coating} = 4,$$

$$x = \text{coating thickness} = \text{separation distance} = 0.05\text{mm},$$

$$V = 5\text{kV}$$

Resulting forces:

$$\text{metal (conductor): } f = 125093\text{N}/\text{m}^2$$

$$F = 3.857\text{N}$$

$$\text{glass with } \varepsilon_r = 5: f = 1133\text{N}/\text{m}^2$$

$$F = 0.007\text{N}$$

The theoretically achievable attraction force on a conductor found for this setup is

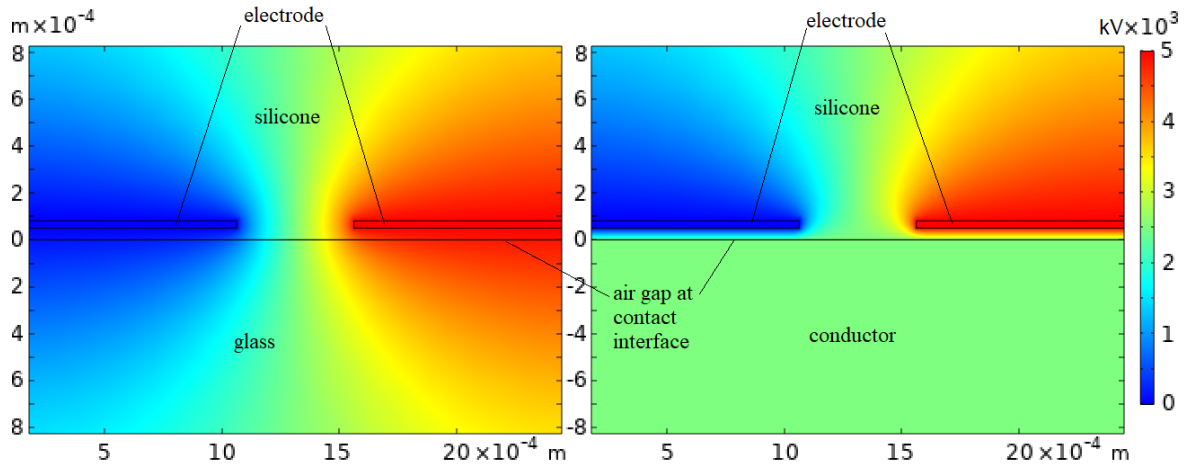


Figure 39: 2D electric field distribution of the described electroadhesive attracting a glass object with $\epsilon_r = 5$ and a conducting object on the left and right hand side respectively.

about an order higher than the experimentally found pull-off force. A higher theoretical force is not surprising as it does not take into account any losses due to discharges within the surrounding air and inhomogeneities in the contacting interface.

Here the attractive force on the dielectric glass with a permittivity of $\epsilon_r = 5$ is only 0.9% of that on metal, showing that its design with approximately 2mm wide electrodes is inappropriate for the attraction of low permittivity dielectrics.

However the large difference between the theoretical and practical attraction of a conductor suggests that there is a lot of potential being lost when adhering to a conductor. This may be not so much the case when adhering to a dielectric, because the electric field strengths in the contact zone are far lower due to the decreased dielectric permittivity. Therefore in practice dielectrics with $\epsilon_r = 5$ could well achieve a higher percentage of the attraction of conductors that in theory.

As stated in appendix B.3 it appears that the dielectric objects that were lifted required about one tenth of the measured attraction on conductors, which fits to the findings described above.

If the gap to the attracted object is instead filled with a medium with low relative permittivity, i.e. a low permittivity coating is used, with for example $\epsilon_r = 1$, then this has an interesting effect on the attraction forces:

$$\text{metal (conductor): } f = 8760N/m^2$$

$$F=0.964N$$

glass with $\epsilon_r = 5$: $f = 606N/m^2$

$F=0.052N$

Now the attractive force on the glass is 6.9% of that on metal. This is due to the fact that with silicone as the coating medium, the dielectric permittivity of the coating is close to that of the attracted dielectric object (glass), so that a large portion of the diverging electric field is diverted toward the opposite electrode before it even penetrates the object that is meant to be attracted.

Consequently for the attraction of dielectrics it is better to have a coating that has a low relative permittivity and high breakdown strength, while for conductors it is advantageous to have a coating with high relative permittivity and high breakdown strength. The objects are attracted less in this second configuration because the lower permittivity of the coating increases the electric field intensity across the coating, thereby reducing the electric field within the contact interface (this is treated in section 3.1.4). Therefore, if the breakdown within the air gap was the limiting factor before then now the applied potential could be increased.

To increase the grippers capability of attracting dielectrics the electrode width should be decreased. The optimization by J. Fessler et. al [20] suggests that at this coating thickness an electrode width in the region of $0.3mm$ will deliver the best results for low permittivity objects such as glass.

D Optimizing an in-contact electroadhesive for glass

This section details the process chosen to find an effective electroadhesive design that is described in section 6.3. The optimization consists of two main topics.

D.1 Optimizing the electric field distribution

The highest electric field intensities occur within the electroadhesive near the electrode edges and - if an insulator with a relative permittivity above one is used - also in the gap at the interface between adhesive and attracted body due to the lower dielectric permittivity in this region. The material with the highest breakdown strength that was found is a PI foil with a thickness of $12.7\mu m$ and a breakdown strength of $315kV/mm$, as stated in the material properties collection in section 3.2. This allows for a potential of $4.0kV$ per layer of foil. This high breakdown strength is not achieved by the bulk of the material PI itself. It is only this high for thin foils, so that this restriction has to be accounted for in the electroadhesive design. The electrodes must

be insulated toward the surroundings, i.e. materials that they come into contact with, as well as to one another.

In appendix B.1 it is shown that the force is increased by minimizing the passive spacing in between the electrodes. Therefore it is of highest interest to optimize the breakdown strength of the material separating the electrodes from one another. This can be realized by placing the electrodes of opposite polarity on opposing sides of the insulating PI foil as is figure 40 a). To give it a plane frontal surface and insulate the remaining electrodes a further foil is added in front of the configuration and the first PI foil can be pressed into a wavy shape to fill in the voids as best as possible, which is shown in figure 40 b). In this way the two electric poles are separated from one another by one layer of PI foil, while to the surroundings the potential difference is insulated via three layers in total. This is an inconvenient ratio. To improve the ratio it is suggested to add a second PI layer separating the opposing poles: They are then separated by a double layer of foil while the potential difference is insulated toward the surroundings by four layers as it is shown in figure 40 c). This will allow for a potential difference between the electrodes of up to $8kV$, while an average distance of the electrodes to the attracted object of only $25.4\mu m$ is allowed. It may be advisable to connect the frontal electrodes to a grounded pole, while the backing electrodes are held at a high potential as these are insulated towards the frontal surface by an additional redundant foil layer. The back side of the electroadhesive layup can be arbitrarily well insulated without having to minimize insulation thickness.

Next the minimum spacing in between the electrodes and the optimal electrode width must be found. The electrode width is optimized in two stages: First an optimal average electrode width is found, then the ratio of the electrode widths used on either pole is altered: The frontal electrodes are made thinner while the backing electrodes become wider, as shown in figure 40 d), because the electrodes have differing distances to the attracted material.

A typical thickness for copper-plating on PCBs is $0.035mm$. This plating was also used for the electroadhesives tested by C. Cao et. al [4]. It is expected that at minimum a gap of four times the foil thickness equating to approximately $0.05mm$ will be required to allow the double foil layer to follow the height difference from one electrode to the next as it is shown in figure 40 c) and d).

The optimization of the electrode widths done by J. Fessl et. al [20] is used as an orientation, although it must be extrapolated to lower coating thicknesses. However, since no information is given on the effect of reducing the electrode spacing, a correction for this narrower electrode spacing introduces a large uncertainty in the first guess.

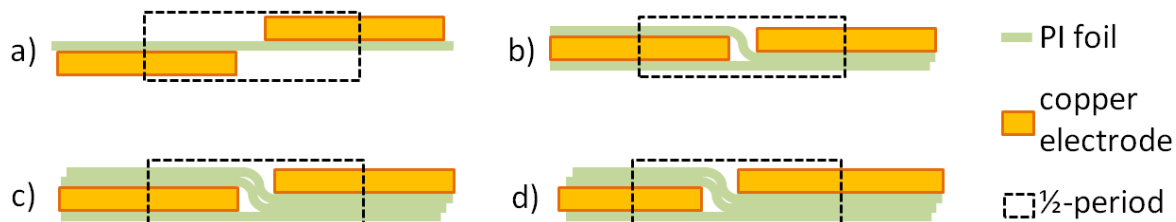


Figure 40: design iterations of electroadhesive layup: a) electrodes placed on opposite sides of insulator foil, b) adding frontal insulation and flattening, c) improving insulation in between the electrodes compared to the insulation toward surroundings, d) optimizing frontal- to backing-electrode width ratio, $\frac{1}{2}$ -period is used for the simulations.

This first guess yields an electrode width of 0.45mm for the previously found spacing of 0.05mm between the electrodes and average distance of 0.025mm of the electrodes to the attracted body.

This guess is implemented in a 2D simulation model over half a period of the alternating electrodes to give it symmetrical boundaries as is depicted in figure 41 a). The model includes the designed electrodes incorporated in a simplified bulk of dielectric with the average relative permittivity of PI of $\epsilon_r = 3.325$. This assembly is facing a low permittivity glass with $\epsilon_r = 5$ over an air gap of $1\mu\text{m}$. When facing a clean glass surface this air gap should likely become far smaller. To reduce simulation effort it is kept at this value, because multiple simulation iterations are necessary to approach the optimal design. The iterations yielded an over twofold increase in attraction force until the peak at an electrode width of 0.09mm was found. Including the electrode spacing of 0.05mm this yields a half period length of 0.14mm . This is depicted in figure 41 b). After this period length is found the ratio between the frontal and backing electrodes is varied, yielding a further increase by 12% until the frontal electrodes are shrunk to 0.05mm and the backing electrodes have a width of 0.13mm , which is depicted in figure 41 c).

The simulated model of this optimized design achieves an attractive force of $135500\text{N}/\text{m}^2$ on glass. On a conducting object it develops an attractive force of $670600\text{N}/\text{m}^2$ which is about five times the force on glass. This shows that the design is well optimized for attracting this dielectric. In appendix B.1 it was found that a close to optimal electrode design could attract glass one quarter as strongly as it could attract a conductor if it uses an insulating material with a relative permittivity of $\epsilon_r = 1$. In this case, which is additionally optimized for functioning with high intensity electric fields, the PI insulation introduces a relative permittivity above one, which slightly reduces the

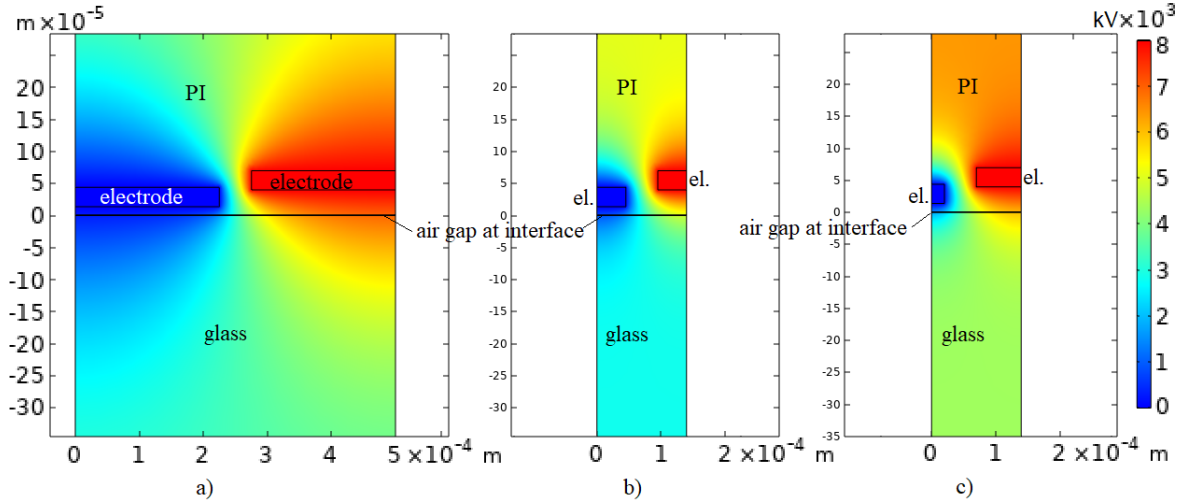


Figure 41: electrode width optimization from simulation results: a) implemented first guess, b) optimized half period, c) optimized frontal- to backing-electrode width ratio

attraction of dielectrics compared to the attraction of conductors, as it promotes the divergence of the electric field before this reaches the attracted dielectric object.

This optimized design is also maintained when all parameters are scaled up or down together. For example doubling all size parameters will yield an electroadhesive with the same capabilities, i.e. same electric field intensities, if also twice the electric potential is applied to the electrodes. While having to apply even higher potentials can be seen as a drawback, scaling the pattern up may be useful for production simplicity and it also decreases the influence of variations in the air gap on the attraction force. A thinner air gap will slightly increase the attraction force, as there is less distance over which the electric field is applied, therefore increasing the field intensity. For example a tenfold reduction of the originally implemented $1\mu\text{m}$ air gap down to an $0.1\mu\text{m}$ air gap increases the attraction from the above stated $135500\text{N}/\text{m}^2$ by 14% to $154600\text{N}/\text{m}^2$. Also the above described double size design that will have the same characteristics for a doubled air gap reaches $147900\text{N}/\text{m}^2$ with a $1\mu\text{m}$ air gap.

D.2 Prohibiting breakdown in the vicinity

The second field of optimization of this electroadhesive design lies in minimizing breakdown in its surroundings. This applies especially to the surface facing the attracted body. Breakdown can occur within the remaining air trapped in asperities and any other form of contamination within the gap as well as within the attracted body itself.

The maximum electric field intensity in the gap at the material interface is $\approx 300\text{kV}/\text{mm}$

for this configuration that realizes an attraction of $135500N/m^2$. The breakdown strength of air increases strongly at low distances and reaches a value around $70kV/mm$ for gaps below $5\mu m$. [38] Below this distance the breakdown characteristics are not well defined in the viewed literature. It is stated that at smaller gaps electron field emission from the involved surfaces takes over and the Paschen curve is no longer valid. The data that was found to be available for breakdown over very small gap distances applies, however, to non-insulated conducting surfaces, i.e. typical electrodes made from different metals that were used in the experiments. As this vacuum breakdown is an effect that depends on the electrode materials, only a dedicated experiment on electron field emission of PI and glass or similarly good insulators will give adequate results for the estimation of breakdown at the interface of this electroadhesive. Up until the breakdown strength of the insulators it is expected, however, that the breakdown will approximately continue to follow Paschen's law which at $1\mu m$ would reach a value of $30MV/mm$.

The maximum field intensity within the insulating material is $240kV/mm$. It is lower than the electric field in the interface gap due to the higher relative permittivity of the insulation material. The real electroadhesive design will have higher values that are closer to the material limit here, because it is built of foil layers with voids in between, rather than a bulk filling.

The maximum field intensity within the attracted glass only reaches up to $62kV/mm$, but this is still too high compared to the typical breakdown strength of glass around $10kV/mm$. Therefore it is chosen to reduce the applied potential on the electrodes. A potential of $1.15kV$ is found to induce a maximum field intensity of $9.7kV/mm$. With this reduced potential the electroadhesive yields a remaining attraction of $2860N/m^2$. The maximum electric field within the insulation is thereby reduced to $30kV/mm$ and within the interface gap to $43kV/mm$ which is still within the range of areal breakdown resistance for gaps up to about $7\mu m$. In this case it becomes less urgent to analyze the electron field emission of PI and glass for high electric field intensities.

The permittivity of glass can differ strongly. At the beginning of this section it is remarked that the design will be optimized for low permittivity glass. Higher permittivity glass will suffer less from breakdown if it has the same breakdown strength, due to the lowered electric fields within it. At the same time it will achieve a higher attraction force, even if the electroadhesive design is optimized for low permittivity glass. This is why it makes sense to optimize the design for the lowest expected permittivity, rather than some averaged permittivity.

A further part of this second field of optimization lies in the exclusion of contamination between the contacting surfaces. The assumed low gap distances can only be realized with smooth and clean surfaces. It is important that no large grit particles are deposited on either of the surfaces, as each particle will create a large zone in its surroundings that is held at an increased distance. The surfaces of glass and PI themselves are very smooth. The roughness that was found quoted by PI foil manufacturers for this product is $Ra = 0.01\text{--}0.03\mu\text{m}$ (e.g. DuPont [7]) and the glass surfaces that were analyzed for the later section of glass cleaning were found to have an $Sq = 0.03\mu\text{m}$. Both these values are smooth enough by a safe margin. To enable a good contact over a large area, however, the electroadhesive should have a certain degree of compliance. Especially if occasional irregularities such as glass pane borders - in the case of glass cleaning robots - are to be overcome. An additional soft compliant layer on the surface of the electroadhesive can help to achieve a better surface contact despite punctual irregularities. Such an additional coating will however inevitably increase the distance of the electrodes to the glass surface. This increase could be combined with a general up-scaling of the electrode pattern and applied electric potential. The necessary coating thickness and compliance depend on the level of cleanness that can be achieved on the glass and electroadhesive before contact.

E Experiments for residue surface charge attraction

This section contains the experiments for section 7.

E.1 Surface charging of glass

There are some reports covering surface charging of glass. H. Kitabayashi et. al measured the surface potential of a glass substrate that is immersed in different types of plasma (Ar, O₂, SF₆) while a parallel plate electrode configuration creates AC and DC electric fields.[10] It is concluded that the gas species and power source have a considerable effect on the surface charge. Specifically it is shown experimentally that DC fields and higher potentials lead to higher surface charge values on the substrate. In another paper X. Tian et. al discuss the results from computer simulations and experiments on the surface potential of glass and other dielectrics positioned within a hydrogen plasma and an electric field.[39] It is found that the residual potential on the dielectric remains lower than - but rises linearly with - the applied potential and that the factor between the two potentials is about 2/3 for the used configuration. For this project it is of interest to find specifically how well surface charge is retained

on a glass surface in a non-plasmatic air environment. No specifications were found on this case except that the break down strength of air naturally limits the electric field intensity that can be obtained from the residue surface charge. Therefore first of all an experiment is conducted to test the residence of surface charge on glass under a few circumstances. This shall serve as a first indicator of the feasibility of this approach. The glass surface is charged via a corona discharge needle that is moved across the surface while an electrode of opposite polarity is placed behind the glass (see figure 42). After the entire surface has been treated, which took about 10s, the power is turned off and the glass is taken from the charging setup and placed above a grounded conducting plate that is mounted on the force measuring setup. The separation distance between the two facing surfaces can be adjusted. It is set to 10mm for all the following experiments.

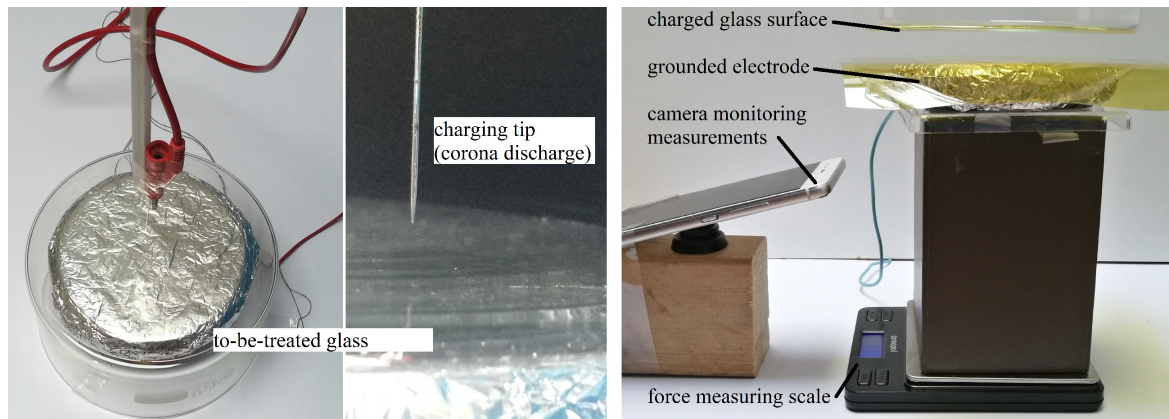


Figure 42: The two stages of the glass charging experiment: (left) glass charging setup in which the glass pot is placed up side down over a circular electrode while a sharply pointed opposite electrode is moved across the surface leaving behind residue charge from the corona discharge, (right) the charged glass surface is suspended above the grounded metallic surface, the attraction of which is measured by the weighing scales and recorded by the digital camera.

From the point at which the glass surface is securely mounted above the metal surface the actual measurement begins. Due to this procedure a certain time span is lost between the end of the surface charging process and the beginning of the measurement. This time span lay typically at 15s but sometimes also took up to 25s. This is also displayed in the collected data, for which time zero is set to the point at which the charging process was terminated. The measured force values are displayed in figure 43. It is assumed that a significant portion of charge can be lost during the first seconds as here the potential is the highest. This loss may be prohibited or reduced if the surface

charge and an electric field can be applied during the force measurement.

The weighing scales have a measurement-dependent timeout, so that the force data is not collected over the same duration for each experiment. The measurements were repeated eleven times and a few alterations were made in between some of the measurements. Measurements (a) to (e) were conducted as described above, except for (b) for which the conducting plate was disconnected from the grounding wire to check how much effect the grounding has. Measurement (b) is the lowest of all, but because there was not an outstanding difference it was not repeated. Before the surface charging of measurement (f) and (g) the glass surface is heated with hot air. This treatment, especially when repeated obviously has a strong effect on how much charge the surface can retain. Also the measurements (h) to (k) conducted after the heat treatment remain elevated, but to a decreasing level. Measurements (j) and (k) stand out, because the opposite potential that was originally used on the underside of the glass during the charging process is applied to the attracted conducting plate. The upward step in the measured force marks the point at which the potential was applied. These two show that in this case an opposite potential that is attracting the charged surface can increase the force, but does not necessarily restrain the surface charge from decreasing over time. This gives a hint that the loss of surface residue charge on the glass occurs largely over the air rather than across the glass' surface and from there to ground via the mounting setup. This is concluded from the fact that the charge on the glass is attracted by the powered plate and should remain there, unless it has a means of traveling even closer to the electrode. The most direct way it can do so is across the separating air gap.

The plate and charging-electrode surface area used here are identical to that used in the previous experiments in section 5. Also the potential source is the same. In this experiment a slightly larger distance was used for the same potential and only one side is actively charged, while the maximum force that was measured is at $95mN$.

The experiments show that a significant amount of charge can be sustained for a period in the order of minutes. This is a positive first outcome for the application of residue charge attraction.

E.2 Attraction forces on a contaminated glass surface

To render the surface charge approach superior to other methods for this application it would remain to be shown to which extent the charge can be maintained on a contaminated and wet surface.

Such a surface contamination will increase the conductivity to a level that may sig-

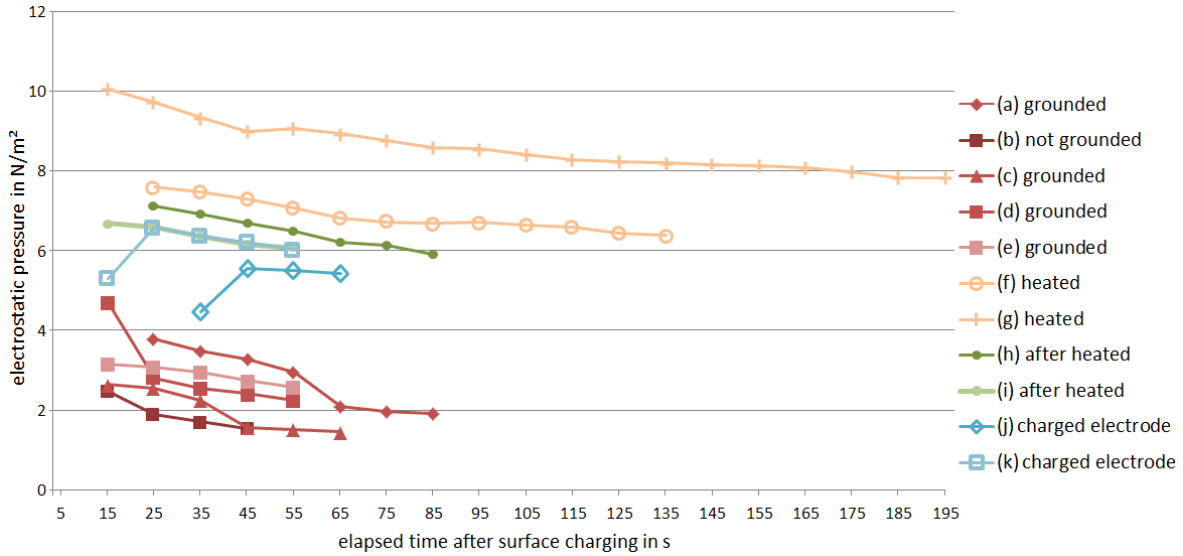


Figure 43: Force data from the glass surface charging experiment, the measurements were conducted in alphabetical order.

nificantly effect the movement of charges on this surface. If applied to the surface as done in the experiment of appendix E.1 then the charge can flow off to ground at a far higher rate then it did during that experiment. However, the electric field created by the attraction plate could have the effect that it prevents the charges from flowing off by attracting these. For this effect to occur the attraction plate would have to maintain a certain potential in relation to the charged surface. Therefor repeating the previous experiment with a contaminated surface would not yield a representative result. The setup must be altered slightly.

Furthermore the slight conductivity may allow the electric field to cause charges to accumulate underneath the attraction panel even independently from a surface charge source. The surface charging unit, for example a corona discharge needle, would merely serve as a grounding for the high voltage unit on board the robot that allows the attraction panel to be charged by giving of charge to the environment and thus establishing the elevated potential of the panel compared to the attracted surface. In this form the surface charge configuration has close resemblance to the parallel capacitor design.

This would also simplify the surface charging unit. A corona discharge would be realisable without having to provide an oppositely charged electrode, because the marginally conductive contaminated surface that is facing the attraction plate acts as an opposite electrode that attracts the charges. A corona discharge over a distance however adds an - in this case avoidable - voltage drop. Here the surface charging unit should take on the form of contact brushes reducing the voltage drop within the charge transfer from

electrode to surface and thereby becoming nearly identical to the parallel capacitor design.

An experimental setup to test this functionality is schematically displayed in figure 44. It allows for the attraction force to be measured while the surface is charged from one point and the attraction plate generates the opposite pole for the electric field.

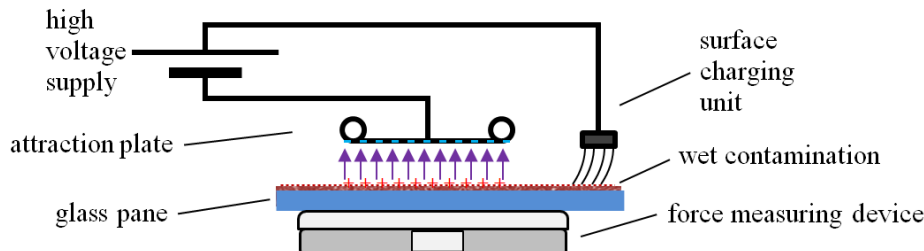


Figure 44: Design of experimental setup for measuring the attraction force on the contaminated surface of an insulator

Due to regulations, unfortunately, it was not possible to realize such a setup within the scope of this thesis.

A difficulty with attracting a charged contaminated surface may be that charged particles on the surface can be attracted too strongly and end up passing the air gap and accumulating on the underside of the panel. This would at least present a nuisance by strongly contaminating the underside of the machine if not even diminishing the attraction force by weakening the electric field. This will depend strongly on the electrical insulation chosen for the attraction panel. A conductive panel would be able to transport opposite charges away and maintain the electric field strength, while a full electrical insulation will have no means of neutralizing the attracted charges.

F Detailed steps taken for plasma aided cleaning test

The following sections give details on the preparation of the plasma aided cleaning test described in section 8.3.

F.1 Method of preparing contaminated samples

Rather than engineering a surrogate contamination the specific contamination for the cleaning samples is chosen to be collected from a glass surface that has been exposed to realistic conditions. The surface in this case is a slanted roof window that has collected grime for approximately half a year over the summer months. A photo of the glass before and after collecting the contamination is displayed in figure 45.

A small amount of purified water is used to help remove the grime from the glass surface with a squeegee. The highly concentrated mixture is collected and the surface from which it was collected is measured and noted as well as the resulting amount of fluid. In this case the surface has the dimensions $750mm$ by $450mm$ and the resulting amount of contaminated water is $5ml$.

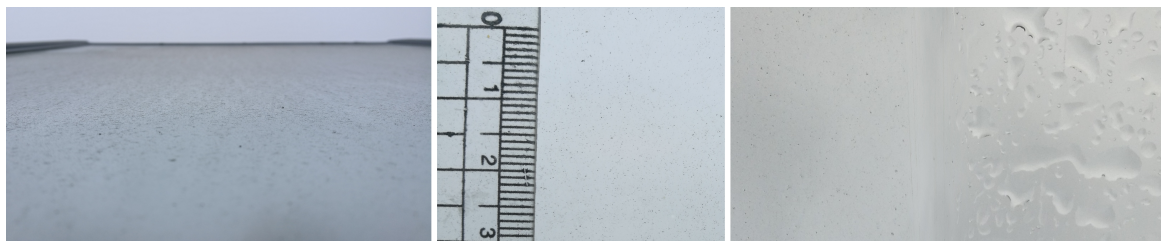


Figure 45: (left) contaminated window glass, (middle) scale impression of contamination, (right) section of window before and after collection of the contamination with rain water on it

Next the spreading area of a specifically sized droplet on the surface of a cleaned microscope slide is identified.

The pre-cleaning of the slides is done in two steps by first treating them with acetone and wiping them with a paper cloth and then by treating them with 2-propanol and again wiping them with a paper cloth. Finally the slides are blown with pressurized air to remove any new dust particles before placing them inside plastic storage containers.

It is found that a droplet with the volume of $0.25ml$ results in an adequate spreading area with a diameter of approximately $18mm$, which gives a contaminated area of $254.5mm^2$. From this volume-to-area ratio an adequate concentration for the contamination liquid can be derived.

The concentration of the collected contamination sample is found to be 66.3 times more concentrated than is needed for deposition on the microscope slides. It is chosen to deposit double the contamination dose per unit area as was found on the roof window to approximately represent a surface that has been exposed to weather and not cleaned for one year. Therefore the sample must be diluted to 33.2 times its volume. $32.2ml$ of purified water are added to $1ml$ of the collected sample yielding $33.2ml$ of twofold concentrated contaminator fluid. The different mixtures are displayed in figure 46.

A batch of cleaned slides is prepared with the procedure described above. Then all but 2 of these are contaminated each with $0.25ml$ of the previously prepared contaminator fluid. The droplets are then dried in a vacuum oven (Binder VD 23 Vac Drying Oven)

at 60°C and 0.2bar . The placed and dried droplets are displayed in figure 47.



Figure 46: (left) concentrated collected contamination, (middle) 32.2ml of purified water, (right) resulting 33.2ml of twofold concentrated contamination fluid

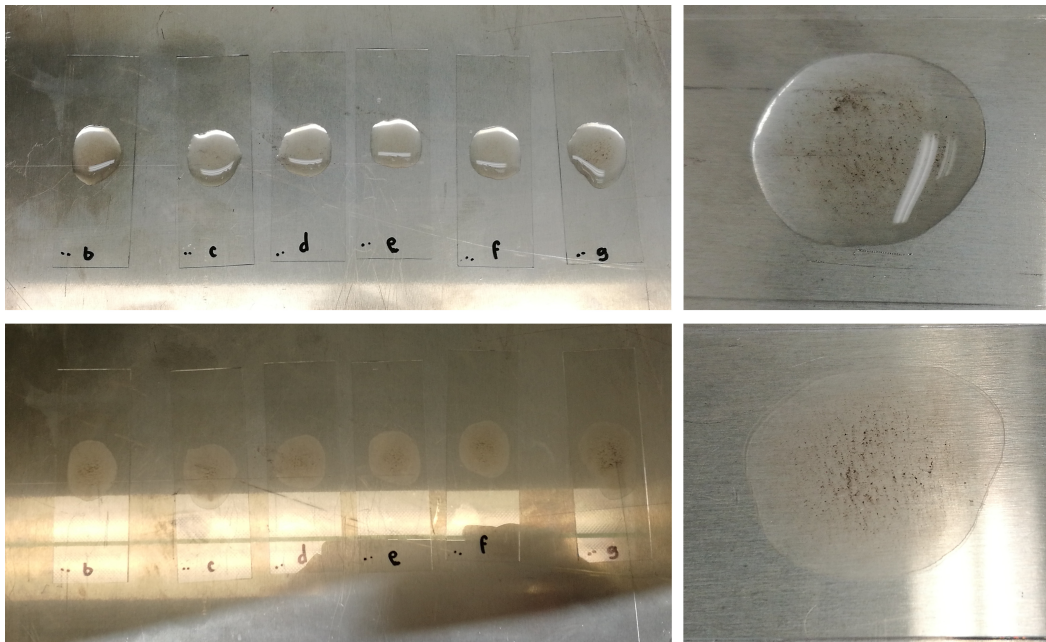


Figure 47: (top) freshly placed droplets of microscope slides, (bottom) after drying in vacuum oven at 60°C and 0.2bar , sample "a" was left uncontaminated in all batches

It is visible that the droplets tend to concentrate larger particles near the middle, while the outer region is coated with very fine contamination.

F.2 Specifying contaminated and non-contaminated states

Five measuring points are chosen along the microscope slide to include the non-contaminated end regions as well as the middle of the contaminated zone and the outer region of the contaminated zone (see figure 48 as reference). The five points will

be numbered "1" through to "5" starting from the point furthest from the inscription. By including the non-contaminated end points 1 and 5, a change of the surface properties from handling the slide can be detected.

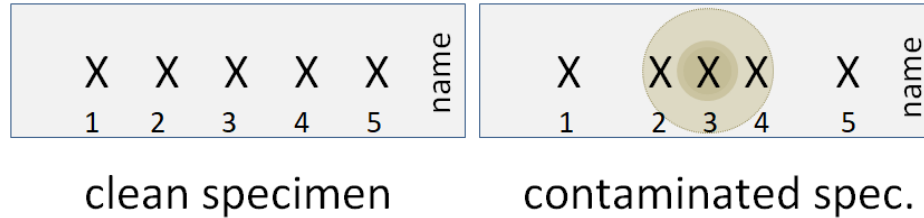


Figure 48: Five points along the specimen are chosen for measurements. They are numbered "1" through to "5" starting from the point furthest from the inscription. On contaminated samples the three inner points are chosen such that they lie in the outer and middle regions of the contaminated zone.

A selection of the samples is then analysed in terms of the surface roughness and the contact angle of water droplets on the surface.

The roughness is determined via confocal microscopy (Sensofar S Neox) in multiple points on the samples (see figure 48). First of all the non-contaminated specimen is scanned in point "3", i.e. the center, at multiple magnifications. The result from scanning with a magnification of 100x is displayed in figure 49. Then multiple randomly selected contaminated specimens are scanned in multiple points. As an example, results from one specimen are displayed in figure 50. The root mean square height, Sq , on the non-contaminated areas was found to be around $0.05\mu m$ when measured at 20x magnification and $0.01\mu m$ when measured at 100x magnification.

The Sq values show that the higher resolution and smaller region of the 100x magnification gives a higher differentiation between the roughness in the different regions than the results from the 20x magnification images. Therefore it is chosen to use the 100x magnification to later evaluate the level of cleaning.

The Sq roughness of each zone, i.e. non-contaminated, outer contamination and centre of contamination, is approximately an order apart and therefore easy to distinguish: The coarse contamination in point "3" has an Sq value in the mid μm range, the finer contamination in points "2" and "4" has an Sq value in the mid $\frac{1}{10}\mu m$ range and the clean points "1" and "5" have an Sq value in the lower $\frac{1}{100}\mu m$ range.

The roughness of the clean sample and of the clean zones of the contaminated samples were not distinguishable, i.e. no additional rough contamination was unintentionally deposited during handling of specimens.

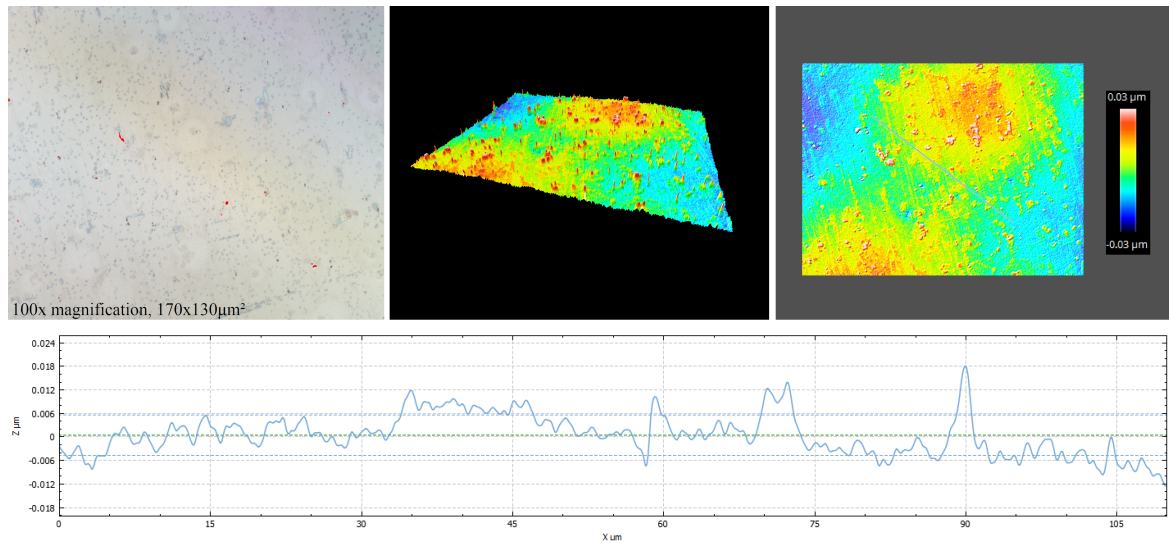


Figure 49: Example of a non-contaminated glass surface at 100x magnification and with confocal height information, in this area $S_q = 0.01\mu m$

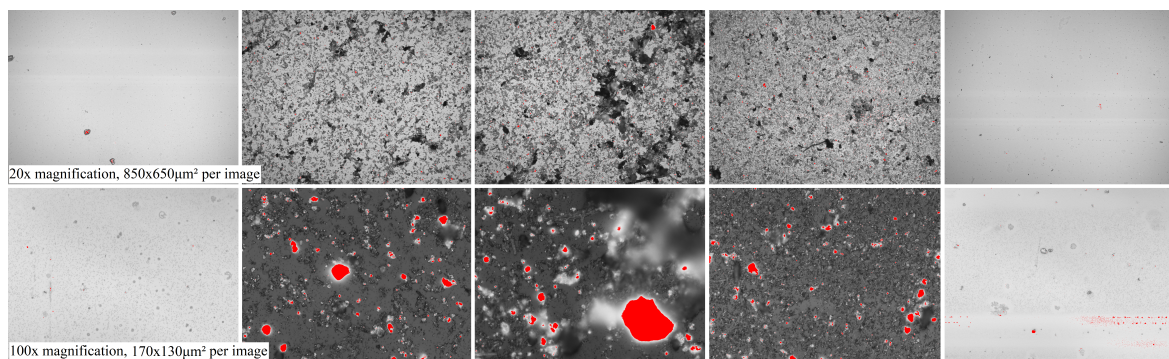


Figure 50: Optical microscope images of points 1 to 5 along a contaminated microscope slide at 20x and 100x magnification, the measured S_q roughness values on these areas are: $0.13\mu m$, $0.55\mu m$, $1.91\mu m$, $0.62\mu m$, $0.03\mu m$ and $0.01\mu m$, $0.75\mu m$, $4.09\mu m$, $0.48\mu m$, $0.01\mu m$ for the 20x and 100x images respectively.

The contact angle is then found by placing droplets of $10\mu l$ each onto the specimens' surfaces. The positions of the droplets are displayed in figure 51 for reference. An image of the droplet's profile from which the contact angle can be measured is then taken shortly after it has made contact with the surface. An example of a typical droplet's profile on a clean and on a coarsely contaminated region are displayed in figure 52.

The contact angle on the contaminated zones averages at 64.6° with values varying between 61.7° and 67.1° . The contact angle on the clean zones averages at 34.0° with values varying between 31.7° and 35.6° . The increase in contact angle due to the contamination indicates that the surface energy has been lowered. The angle on

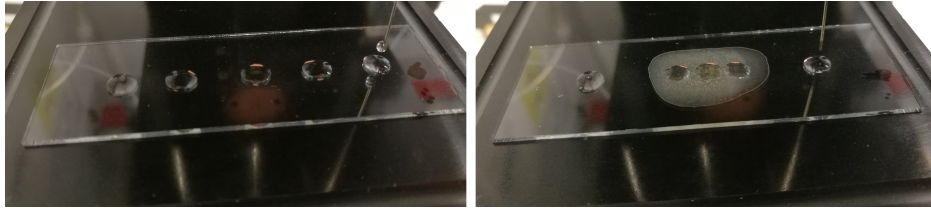


Figure 51: Droplets for contact angle measurement in positions 1 to 5

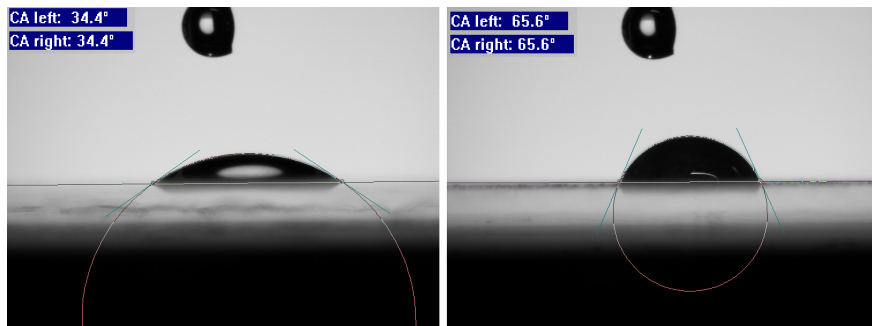


Figure 52: Two examples of the contact angle: (left) on clean surface, (right) on coarsely contaminated surface in position 3

the clean specimen is not distinguishable from the angle on the clean zones of the contaminated specimens. This confirms that handling of the contaminated slides has not added further unspecified or random contamination to the surface, so that later measurements on the contaminated regions capture the pure deliberate contamination.

F.3 Characterization of piezobrush PZ3 plasma treatment

The plasma treatment is done with the plasma pen piezobrush PZ3. For the treatment of the specimens it is held directly onto the area that is to be treated. This ensures a constant distance and angular orientation of the pen between treatments. On clean microscope slides it was found that a cold plasma treatment over 5s would effectively reduce the contact angle, while longer treatment will slightly further decrease the contact angle, while becoming comparatively time consuming. This stands in contrast to a treatment with hot plasma, which is capable of reducing the contact angle of water to zero within the order of a second. Figure 53 displays the resulting averaged contact angles depending on the treatment duration with the plasma pen. A plasma treatment duration of 10s is chosen as an acceptable time factor compared to the effectiveness.

It is also found that the effect of the plasma treatment on the contact angle does not wear off within minutes, which is displayed in figure 54. This means that during

experimentation slight variations in the time between the plasma surface treatment and the cleaning process should not have an effect on the results.

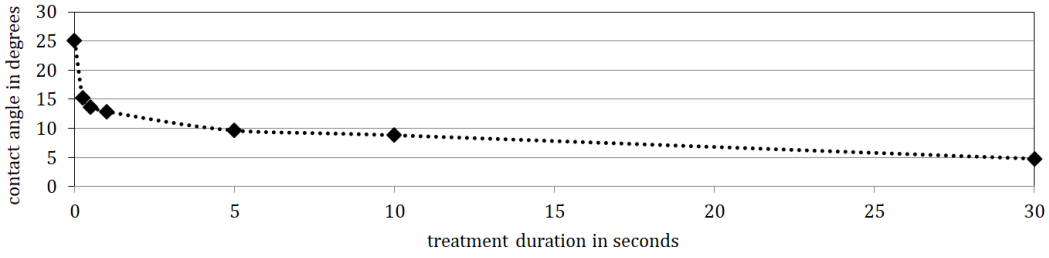


Figure 53: Graph of the contact angle of water droplets on clean microscope slides after treatment with the plasma pen for different time periods. The contact angle measurements were taken approximately 20s after the end of each plasma treatment.

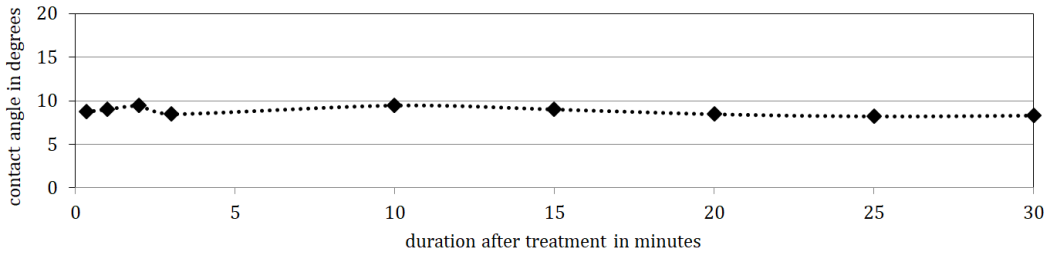


Figure 54: Graph of the contact angle of water droplets on clean microscope slides after different time periods after the treatment with the plasma pen for 10s.

G Mathematical derivation and examples of increased gradeability

This section supplements section 9.1 which concludes on the usability of the attraction forces for cleaning robots.

The original gradeability of $\alpha = 25^\circ$ of the industrial caterpillar track robots indicates that the current friction coefficient is:

$$\mu = \tan(\alpha) = 0.47 \quad (64)$$

To evaluate the capability of the attraction techniques it is of interest which area of electrostatic attraction per vehicle weight is necessary to achieve a certain gradeability at a given slope angle α and friction value μ . The following dependencies are given:

$$F_t = F_g \sin(\alpha) \quad (65)$$

$$F_n = F_g \cos(\alpha) + F_{attraction} \quad (66)$$

where F_t and F_n are respectively the tangential and normal force of the vehicle on the surface derived from the vehicles weight force F_g on the slope at angle α and the electrostatic attraction force $F_{attraction}$. Further the traction limit requirement is

$$F_n = \frac{F_t}{\mu} \quad (67)$$

with which the minimum required normal force, before slip-off occurs at a certain tangential force and friction coefficient, is defined.

The weight force F_g and the electrostatic attraction force $F_{attraction}$ are found by

$$F_g = m_{vehicle} g \quad (68)$$

$$F_{attraction} = A p_{el.stat.} \quad (69)$$

where A is the area of the electrostatic attractor and $p_{el.stat.}$ is the electrostatic pressure that is achieved by the used attraction technology.

With these dependencies the relations

$$\frac{F_{attraction}}{m} = g \left(\frac{\sin(\alpha)}{\mu} - \cos(\alpha) \right) \quad (70)$$

which is the required attraction force per vehicle weight and

$$\frac{A}{m} = \frac{g}{p_{el.stat.}} \left(\frac{\sin(\alpha)}{\mu} - \cos(\alpha) \right) \quad (71)$$

which is the required attraction area per vehicle weight are found.

For an attraction over a gap it is assumed in accordance with section 5.2 that half the theoretical maximum force is reached. With this attraction of $\approx 20N/m^2$ equation 71 shows that to achieve a gradeability of 26° the robot is required to have an attractive area of $\approx 0.02m^2$ per kg of weight. In this case an industrial cleaning robot with a weight of $50kg$ would require approximately $1m^2$ of attractive area. The previously defined available area of $(0.4m)^2 = 0.16m^2$ on the other hand only allows for a slope of 25.16° , which is a negligible improvement to the original gradeability. The force generated over this area is $3.2N$.

For the small window cleaning robots it is assumed that 50% of the area underneath the robot can be utilized for attraction purposes, either as an underbody panel or on the drive tracks. As the weight to area ratio on the small cleaning robots in this case is more favourable than on the industrial cleaning robots the available attraction area just suffices for a gradeability of 26° , but it remains debatable whether this increase of 1° is worth the technical effort, especially on the small scale robots that are mainly

designed for private use.

For in-contact attraction the interdigital electrode design optimized for glass in section 6.3 showed an electrostatic pressure of $2860N/m^2$ in simulation. With this electrostatic pressure a gradeability of 45° can be achieved with an attraction area of $0,0028m^2$ per kg of vehicle weight. For the described industrial cleaning robots it means that the area on standard sized caterpillar tracks ($0.1m^2$) suffices for a gradeability of 39° . This is a significant increase that can extend the working range of these robots. For small scale cleaning robots this electrostatic pressure suffices to hang upside down from a horizontal surface with a large safety margin if appropriate mechanical measures against gradual peel off are taken. With 50% of the underbody area of the exemplary small cleaning robot described in the introductory section 2.1 equating to $0.02m^2$, the designed electroadhesive achieves an attractive force of $57.2N$, while the robots weight is around $1kg$.

For the industrial cleaning robots the suggested alternative use for the electroadhesive effect is a deployable underbody mechanism for securing the robot in the case that its tracks begin to slip. This would be a solid adhesion plate that is brought into contact with the surface, when it is activated. The underbody area is larger than the contacting area of the caterpillar tracks and thus suffices to introduce a larger adhesion force capable of breaking the vehicle's slip. However in the case of uncontrolled slipping it becomes even harder to guarantee that the adhesion area below the robot will be clean and dry.

References

- [1] A. Belkind ; S. Gershman. "plasma cleaning of surfaces". https://www.researchgate.net/publication/284486745_Plasma_cleaning_of_surfaces, 2008, last accessed 1st March 2021.
- [2] A.D. Moore. "Electrostatics and its applications". John Wiley & Sons, 1973.
- [3] B.W. Lee ; D.E. Orr. "the triboelectric series". <https://www.alphalabinc.com/triboelectric-series/>, Last accessed 16th October 2020.
- [4] C. Cao ; X.Sun ; Y. Fang ; Q. Qin ; A. Yu ; X. Feng. "theoretical model and design of electroadhesive pad with interdigitated electrodes". *Materials & Design*, Volume 89, 2016.
- [5] D. Gatti et al. "the dielectric breakdown limit of silicone dielectric elastomer actuators". *Applied Physics Letters* 104, doi: 10.1063/1.4863816, 2014.
- [6] D.J. Griffiths. "introduction to electrodynamics". Pearson Education, Inc., 1989.
- [7] DuPont. "polyimide film". <https://www.dupont.com/content/dam/dupont/amer/us/en/products/ei-transformation/documents/EI-10172-Kapton-EN-A-C-Y-Z-Data-Sheet.pdf>, 2020, last accessed 29th December 2020.
- [8] E. Seran ; M. Godefroy ; E. Pili ; N. Michielsen ; S. Bondiguel. "what we can learn from measurements of air electric conductivity in 222rn-rich atmosphere". *Earth and Space Science*, Vol. 4, Issue 2, 2017.
- [9] G.D. Schmidt et al. "formelsammlung". Cornelsen Schulverlage GmbH, 2013.
- [10] H. Kitabayashi ; H. Fujii ; T. Ooishi. "electrification of glass substrate surface by plasmas". *Journal of Electrostatics* 40 & 41, 1997.
- [11] H. Prahlad ; R. Pelrine ; S. Stanford ; J. Marlow ; R. Kornbluh. "Electroadhesive robots — wall climbing robots enabled by a novel, robust, and electrically controllable adhesion technology". *IEEE International Conference on Robotics and Automation*, DOI: 10.1109/ROBOT.2008.4543670, 2008, last accessed 1st September 2020.
- [12] Herbert A. Poh. "theoretical aspects of dielectrophoretic deposition and separation of particles". *J. Electrochem. Soc.: NEWS AND REVIEWS*, Vol. 115, No. 6, 1968.

- [13] J. Carter. "the best robotic window cleaner". <https://www.gearhungry.com/best-robotic-window-cleaners/>, 2018, last accessed 1st March 2021.
- [14] J. Cross. "electrostatics: Principles, problems and applications". IOP Publishing Limited, 1987.
- [15] J. Guo ; J. Leng ; J. Rossiter. "electroadhesion technologies for robotics: A comprehensive review". IEEE, Journal Article, Volume: 36, Issue: 2, 2020.
- [16] J. Guo ; M. Tailor ; T. Bamber ; M. Chamberlain ; L. Justham ; M. Jackson. "investigation of relationship between interfacial electroadhesive force and surface texture". IOP Publishing Ltd, Journal of Physics D: Applied Physics, Volume: 49, Number: 3, 2015.
- [17] J. Guo ; T. Bamber ; T. Hovell ; M. Chamberlain ; L. Justham ; M. Jackson. "geometric optimisation of electroadhesive actuators based on 3d electrostatic simulation and its experimental verification". IFAC-PapersOnLine 49-21, pp.309-315, 2016.
- [18] J. Rumble. "crc handbook of chemistry and physics - 101st edition". Taylor & Francis, 101st Edition, 2020.
- [19] J. Shintake ; V. Cacucciolo ; D. Floreano ; H. Shea. "soft robotic grippers". Advance Materials, Vol. 30, Issue 29, 2018.
- [20] Jan Fessl ; František Mach ; Jiří Navrátil. "design, fabrication and testing of electroadhesive interdigital electrodes". De Gruyter, Open Physics 16(1), pp.430-434, 2018.
- [21] J.M. Meek ; J.D. Craggs. "electrical breakdown of gases". John Wiley & Sons, 1978.
- [22] Jun Shintake ; Samuel Rosset ; Bryan Schubert ; Dario Floreano ; Herbert Shea. "versatile soft grippers with intrinsic electroadhesion based on multifunctional polymer actuators". WILEY-VCH Verlag GmbH & Co. KGaA, Weinheim, 2015.
- [23] Lenntech. "water conductivity". <https://www.lenntech.com/applications/ultrapure/conductivity/water-conductivity.htm>, Last accessed 25th September 2020.

- [24] L.S. Puah ; R. Sedev ; D. Fornasiero ; J. Ralston ; T. Blake. "influence of surface charge on wetting kinetics". *Langmuir*, Volume 26, Issue 22, pp. 17218-17224, DOI: 10.1021/la103351t, 2010.
- [25] M. Hendrick. "why dielectric strength of kapton® film matters". <https://www.dupont.com/content/dam/dupont/amer/us/en/products/ei-transformation/documents/DEC-Kapton-HN-datasheet.pdf>, 2015, last accessed 25th September 2020.
- [26] M. Javid ; P.M. Brown. "field analysis and electromagnetics". New York, McGraw-Hill, 1963.
- [27] M Ozdemir ; C.U. Yurteri ; H. Sadikoglu. "physical polymer surface modification methods and applications in food packaging polymers". *Critical Reviews in Food Science and Nutrition*, Volume 39 Issue 5, pp. 457-477, doi.org/10.1080/10408699991279240, 1999.
- [28] National Research Council. "plasma processing and processing science, ion implantation and surface modification". Washington, DC: The National Academies Press. <https://doi.org/10.17226/9854>, 1995.
- [29] Nipun. "how to calculate half life". <https://pediaa.com/how-to-calculate-half-life/>, 2015, last accessed 1st March 2021.
- [30] Omnexus. "key features & applications of pi". <https://omnexus.specialchem.com/selection-guide/polyimide-pi-plastic#properties>, Last accessed 25th September 2020.
- [31] Prof. Dr. H. Föll. "3.3 frequency dependence of the dielectric constant". https://www.tf.uni-kiel.de/matwis/amat/elmat_en/kap_3/backbone/r3_3.1.html, Last accessed 27th November 2020.
- [32] relyon plasma. "advantages of atmospheric pressure plasma technology". <https://www.relyon-plasma.com/technology/?lang=en>, Last accessed 1st March 2021.
- [33] relyon plasma. "surface activation (plasma activation)". <https://www.relyon-plasma.com/plasma-technology/surface-activation/?lang=en>, Last accessed 1st March 2021.
- [34] Robert J. Stokes ; D. Fennell Evans. "fundamentals of interfacial engineering". Wiley-VHC, Inc., 1997.

- [35] S. Wang ; Y. Xie ; S. Niu ; L. Lin ; C. Liu ; Y.S. Zhou ; Z.L. Wang. "maximum surface charge density for triboelectric nanogenerators achieved by ionized-air injection: Methodology and theoretical understanding". *Advance Materials*, Vol. 26, Issue 39, 2014.
- [36] TG hyLIFT. "hycleaner black solar facelift". <https://hycleaner.eu/en/produkte/hycleaner-black-solar/>, Last accessed 1st March 2021.
- [37] TG hyLIFT. "tg hylift". <http://tg-hylift.com/en.html>, last accessed 1st March 2021.
- [38] V. Babrauskas. "arc breakdown in air over very small gap distances". *Conference: Interflam 2013*, Volume 2; pp. 1489-1498, 2013.
- [39] X. Tiana ; R. K.Y. Fua ; J. Chena ; P. K. Chua ; I. G. Brown. "charging of dielectric substrate materials during plasma immersion ion implantation". *Nuclear Instruments and Methods in Physics Research B* 187, 2002.
- [40] Z. Losonc. "calculation of electrostatic forces in presence of dielectrics". <http://www.energythic.com/view.php?node=209>, Last accessed 7th October 2020.